Department of Cardiology, Angiology and Intensive Care Medicine
Deutsches Herzzentrum der Charité (DHZC)
Charité Universitätsmedizin Berlin, Germany

The impact of gut microbial imidazole propionate on endothelial regeneration and the development of atherosclerosis

Inaugural-Dissertation
to obtain the academic degree
Doctor rerum naturalium (Dr. rer. nat.)

submitted to the Department of Biology, Chemistry, Pharmacy
of Freie Universität Berlin

by
Vanasa Nageswaran
from Berlin

Berlin, 2023

The doctoral thesis was conducted between 2019 and 2023 at the Charité Universitätsmedizin Berlin (Deutsches Herzzentrum der Charite) under the supervision of PD Dr. med. Arash Haghikia.

1st reviewer: Prof. Dr. med. Arash Haghikia
Deutsches Herzzentrum der Charité
Department of Cardiology, Angiology
and Intensive Care Medicine
Charité-Universitätsmedizin Berlin
Campus Benjamin Franklin
Hindenburgdamm 30
12203 Berlin, Germany

2nd reviewer: Prof. Dr. rer. nat. Petra Knaus
Freie Universität Berlin
Institute of Chemistry and Biochemistry
Signal Transduction
Thielallee 63
14195 Berlin, Germany

Date of defense: 21. March 2024

„மலையே வந்தாலும் தலையே சுமக்கணும். “

- அம்மா

Declaration of Independence

I, Vanasa Nageswaran, hereby declare that I have written my dissertation independently and have used no sources or aids other than those specified by me.

The dissertation has not been accepted or rejected in any previous doctoral procedure.

Berlin,

_____

(Vanasa Nageswaran)

I Table of Contents

II List of Figures

III List of Tables

IV List of Abbreviations

ABC	avidin-biotin complex
ACVD	atherosclerotic cardiovascular disease
AEC	3-amino-9-ethyl-carbazole
AMPK	AMP-activated protein kinase
AMPs	antimicrobial peptides
Apoe$^{-/-}$	apolipoprotein E knock out
BAs	bile acids
BME	basement membrane extract
BMI	body mass index
BSA	bovine serum albumin
CAD	coronary artery disease
CBP	CREB-binding protein
CD106	cluster of differentiation 106
CD54	cluster of differentiation 54
CD62E	cluster of differentiation 62E
CI	carotid injury
CVD	cardiovascular disease
CVDs	cardiovascular diseases
DAPI	4′,6-diamidino-2-phenylindole
DCM	diabetic cardiomyopathy
DiI	1,1’-dioctadecyl-3,3,3’,3’-tetramethylindocarbocyanine
DNA	deoxyribonucleic acid
ECs	endothelial cells
EDTA	ethylene-diamine-tetraacetic acid
EGM-2	endothelial growth medium-2
eNOS	endothelial nitric oxide synthase
ERK	extracellular signal-regulated kinase
EtBr	ethidium bromide
FACS	fluorescence-activated flow cytometry
FCS	fetal calf serum
FGF	fibroblast growth factor
FHD	FOX DNA-binding domain
FMOs	fluorescence-minus controls

FOXO	forkhead box O
FPLC	fast-performance liquid chromatography
GPCRs	G-protein-coupled receptors
HAECs	human aortic endothelial cells
HATs	histone acetyltransferases
HDL	high-density lipoprotein
HE	hematoxylin/ eosin
HFD	high fat diet
HM	hydrophobic motif
HUVECs	Human Umbilical Vein Endothelial Cells
ICAM-1	intercellular adhesion molecule- 1
IDL	intermediate-density lipoproteins
IGF-1	insulin-like growth factor 1
IKK	I kappa B kinase
IL-1	interleukin-1
IL-1β	interleukin-1 beta
IL-6	interleukin-6
ImP	imidazole propionate
IRS	insulin receptor substrate
JNK	c-Jun N-terminal kinase
LCA	left carotid artery
LDL	low-density lipoprotein
MAPK	mitogen-activated protein kinase
mTORC2	mammalian target of rapamycin complex-2
NES	nuclear export sequence
NGS	next generation sequencing
NLS	nuclear localization signal
NO	nitric oxide
ORO	Oil Red O
oxLDL	oxidized low-density lipoprotein
PBS	phosphate-buffered saline
PDGF	platelet-derived growth factor
PDK1/ 2	phosphoinositide-dependent kinase-1/ -2
PDK4	pyruvate dehydrogenase kinase 4

PFA	paraformaldehyde
PH	pleckstrin homology
PHLPP	PH domain and leucine-rich repeat protein phosphatase
PI(3,4)P2	phosphatidylinositol-3,4-bisphosphate
PI3K	phosphoinositide 3-kinases
PI3KC2α	phosphatidylinositol-4-phosphate 3-kinase C2 domain-containing subunit alpha
PI3P	phosphatidylinositol 3-phosphate
PIP2	phosphatidylinositol-4,5-bisphosphate
PIP3	phosphatidylinositol-3,4,5-trisphosphate
PKB	protein kinase B
PP2A	protein phosphatase 2A
PTEN	phosphatase and tensin homolog
RNA	ribonucleic acid
ROS	reactive oxygen species
RT	room temperature
RTKs	receptor tyrosine kinases
SCD	standard chow diet
SCFA	short-chain fatty acids
Ser	serine
siRNA	small interfering RNA
SIRTs	sirtuins
SOD	superoxide dismutase
T1D	type 1 diabetes
T2D	type 2 diabetes
TAD	transactivation domain
TAE	Tris-acetate-EDTA
TGF-β	transforming growth factor-beta
Thr	threonine
TMA	trimethylamine
TMAO	trimethylamine N-oxide
TNF-α	tumor necrosis factor alpha
UHP-LC	ultra-high-performance liquid chromatography
UV	ultraviolet

VCAM-1	vascular cell adhesion protein-1
VEGF	vascular endothelial growth factor
VLDL	very low-density lipoprotein
VSMCs	vascular smooth muscle cells
WHO	World Health Organization

V Abstract

Background/ aims: Growing evidence suggests a critical role of distinct gut microbially produced metabolites in developing cardiometabolic and -vascular diseases. The amino-acid-derived metabolite imidazole propionate (ImP) is increased in patients with pre- and type 2 diabetes. However, its impact on endothelial cell physiology and vascular disease has not been examined so far. Here, the effects of ImP were studied on endothelial cell function and inflammatory activation, as well as on endothelial regeneration after injury and development of atherosclerosis in atheroprone *Apoe*$^{-/-}$ mice.

Methods/ results: Cell culture experiments, next-generation sequencing, western blotting, and immunostaining were performed to identify the potential underlying mechanism of ImP-mediated effects on primary human aortic endothelial cells (HAECs). Transcriptomic profiling of HAECs revealed altered regulation of several genes involved in angiogenesis in ImP-treated cells. In particular, decreased PI3K/ AKT signaling was found upon pre-treatment of ImP, followed by insulin receptor stimulation with IGF-1, which led to an increase in FOXO1 protein expression as well as nuclear accumulation of FOXO1 in HAECs. Consequently, ImP impaired migratory and angiogenetic properties of endothelial cells assessed by scratch wound healing and Matrigel tube formation assay. Moreover, ImP promoted inflammatory activation of endothelial cells, leading to increased expression of pro-inflammatory cell adhesion molecules (VCAM-1, ICAM-1, and E-selectin) and, finally, to increased adhesion of monocytes under flow conditions. In an *in vitro* rescue experiment, the ImP-mediated pro-inflammatory phenotype was abrogated by targeted gene silencing of FOXO1 in endothelial cells. Vascular regeneration *in vivo* was analyzed using a carotid artery injury model (CI) in C57BL/6J mice treated with ImP or vehicle for three weeks via drinking water. Re-endothelialization was determined by Evans blue staining three days post-CI. The results showed that treatment with ImP significantly impaired wound healing compared to control animals. Finally, atherosclerotic plaque formation was analyzed *in vivo* using apolipoprotein E knockout (*Apoe*$^{-/-}$) mice fed a standard chow diet (SCD) or high-fat diet (HFD) and simultaneously treated with vehicle or ImP in drinking water for 6 and 12 weeks. Oil red O staining displayed increased atherosclerotic plaque formation in *en face* aortic arch and aortic root sections upon

ImP treatment. CD68 expression was also enhanced in murine atherosclerotic lesions in response to ImP treatment, indicative of increased macrophage accumulation.

Conclusion: The gut microbially produced metabolite ImP impairs the insulin receptor signaling pathway via PI3K/ AKT/ FOXO1 in endothelial cells, thereby affecting their functional properties such as migration, proliferation and angiogenic capacity. Moreover, ImP promotes inflammatory activation of endothelial cells leading to increased monocyte adhesion. These effects result in impaired vascular healing after injury and increased atherosclerosis in atheroprone *Apoe*$^{-/-}$ mice.

VI Zusammenfassung

Einleitung: Es gibt immer mehr Hinweise darauf, dass bestimmte Bakterien-Metaboliten, welche vom Darm-Mikrobiom produziert werden, eine entscheidende Rolle bei der Entwicklung von kardiometabolischen und -vaskulären Erkrankungen spielen. Der Darm-Mikrobiom abhängige Metabolit, Imidazol Propionat (ImP), wurde als ein neuartiger Metabolit aus dem Histidin-Stoffwechsel identifiziert. Neue Studien haben gezeigt, dass ImP vermehrt im Darm von Patient:innen mit Prä- und Typ-2-Diabetes produziert wird. Die Auswirkungen von ImP auf die Physiologie von Endothelzellen und damit verbundenen Gefäßerkrankungen sind jedoch bislang nicht untersucht worden. In dieser Arbeit wurde der Einfluss von ImP auf die endotheliale Gefäßfunktionen, inflammatorische Aktivierung sowie auf die endotheliale Regeneration nach Gefäßverletzung und die Entwicklung von Atherosklerose in *Apoe*$^{-/-}$-Mäusen näher untersucht.

Methodik/ Ergebnisse: Anhand von Zellkultur-Experimenten und Next-Generation-Sequenzierung konnte ein ImP-induzierten Signalweg in humanen Aorten-Endothelzellen (HAECs) *in vitro* nachgewiesen werden, der die physiologischen Funktionen von Endothelzellen beeinflusst. Die RNA-Expressionsanalyse zeigte eine transkriptomische Veränderung in zahlreichen Genen, die an der Proliferation von Endothelzellen beteiligt sind, in ImP-behandelten Zellen. Mittels Western Blot Analysen und Immunfärbungen konnte gezeigt werden, dass ImP den intrazellulären Signalweg von PI3K/ AKT signifikant hemmt, was zu einer Erhöhung von zytoplasmatischem FOXO1-Proteinexpression sowie der nuklearen Akkumulation von FOXO1 in HAECs führt. Infolgedessen, beeinträchtigt ImP die funktionellen Eigenschaften von Endothelzellen wie Migration und Angiogenese, die mittels eines Scratch- und Tube Formation Assays untersucht wurden. Darüber hinaus, fördert ImP die entzündliche Aktivierung von Endothelzellen, was zu einer verstärkten Expression von pro-inflammatorischen Zelladhäsionsmolekülen (ICAM-1, VCAM-1 und E-Selektin), und schließlich zu einer erhöhten Adhäsion von Monozyten unter Flussbedingungen führt. In einem *in vitro* Rescue-Experiment konnte dieser pro-inflammatorische Phänotyp von ImP durch ein zielgerichtetes Gen-Knockdown von FOXO1 in Endothelzellen aufgehoben werden. Die vaskuläre Regeneration *in vivo* wurde anhand eines Verletzungsmodells der Karotiden bei C57BL/6J-Mäusen drei Wochen nach Behandlung mit ImP oder Vehikel über das Trinkwasser untersucht. Die

Re-Endothelialisierung wurde drei Tage nach Gefäßverletzung durch Evans-Blau-Färbung bestimmt. Die Ergebnisse zeigten, dass die ImP-behandelten Mäuse nach einer Gefäßverletzung eine signifikant schlechtere Wundheilung aufweisen als die Kontrollgruppe ohne ImP-Behandlung. Schließlich wurde die Entwicklung von Atherosklerose *in vivo* bei Apolipoprotein E Knockout (*ApoE*$^{-/-}$) Mäusen, nach Behandlung mit oder ohne ImP und einer zusätzlichen Kontrolldiät (SCD) oder einer fettreichen Diät (HFD) für 6 und 12 Wochen, untersucht. Die Öl-Rot-O-Färbungen zeigen eine erhöhte atherosklerotische Plaquebildung in den Aortenbögen und den Aortenwurzeln nach Verabreichung von ImP. Auch die CD68-Expression war in den atherosklerotischen Läsionen der Mäuse infolge der ImP-Behandlung erhöht, was auf eine erhöhte Makrophagen-Infiltrierung hinweist.

Schlussfolgerung: Der Darmmikrobiom-abhängige Metabolit ImP stört die Insulinrezeptor-Signaltransduktion mit Deregulierung des PI3K/ AKT/ FOXO1 Signalwegs in Endothelzellen, wodurch deren funktionelle Zelleigenschaften wie Migration, Proliferation und angiogenetische Kapazität beeinträchtigt werden. Darüber hinaus fördert ImP die entzündliche Aktivierung von Endothelzellen, was zu einer erhöhten Adhäsion von Monozyten führt. Diese Effekte führen zu einer gestörten Gefäßheilung nach Verletzung und letztlich zu einer verstärkten Atherosklerose bei *Apoe*$^{-/-}$ Mäusen.

1. Introduction

1.1. Cardiovascular disease (CVD)

The cardiovascular system, consisting of the heart and blood vessels, is essential for the circulation of oxygen, nutrients, hormones, and cellular waste products across the body (Humphrey and McCulloch, 2003). The heart ensures a constant flow of oxygenated blood to organs and tissues while simultaneously receiving deoxygenated blood for reoxygenation in the lungs (Humphrey and McCulloch, 2003). Given these fundamental physiological roles, any disruptions of the cardiovascular system may cause cardiovascular diseases (CVDs) with potentially life-threatening risks. Atherosclerosis, characterized by endothelial dysfunction, chronic inflammation and plaque formation, is the most common CVD and can cause ischemia within different body districts, thus leading to peripheral artery disease, myocardial infarction and stroke (Roth et al., 2020; Ćurić et al., 2021).

1.1.1. Epidemiology and risk factors

The incidence of CVD still sparks concern worldwide as counts show unacceptably high mortality rates (Roth et al., 2020). Among these, atherosclerosis will continue to be the leading cause of most cardiovascular events by 2023 (Kong et al., 2022). In 2019, CVDs were responsible for approximately 17.9 million deaths, making up one-third (32%) of all global deaths (WHO). Global burden data on CVD prevalence shows that countries with low- and middle-income bear the greatest burden of heart attacks and strokes (~ 85%) compared to high-income countries (Roth et al., 2020; GBD 2019 Stroke Collaborator, 2021). The differences typically observed in CVD prevalence rates vary between ethnic or racial populations and progressively increase with age in both men and women. While men tend to have higher rates of CVD between the ages of 30 and 60, women over 80 years are at greater risk (Roth et al., 2020). Age, sex, and genetics are important un-modifiable risk factors for CVD (Caterina et al., 2006). Among modifiable risk factors are diabetes, hypertension, obesity, dyslipidemia, or lifestyle-associated factors such as diet, smoking, and physical inactivity, which raise the likelihood of developing atherosclerosis and contribute to the severity of the disease (Caterina et al., 2006; Roth et al., 2020; Ćurić et al., 2021). Of note, it has been reported that in individuals with a genetic predisposition for CVD, adopting a healthy lifestyle can lower their cardiovascular risk compared to those with a favorable

genetic background but with an unhealthy lifestyle (Khera et al., 2016). In addition, the economic burden of CVD significantly challenges public health globally and is substantially associated with steadily rising healthcare costs (Roth et al., 2020).

1.2. Pathogenesis of atherosclerosis

Atherosclerosis is a progressive disease causing vascular complications, characterized by endothelial dysfunction and chronic inflammation leading to the development of fatty deposits and plaque buildup in the inner lining of blood vessels (Harishkumar et al., 2022). Although it may occur in any arterial wall, it mainly affects large and medium-sized vessels such as coronary arteries. Additionally, atherosclerotic lesions often occur at branching sites or areas with strong turbulent blood flow (e.g., bifurcation) that are more prone to endothelial injury and chronic inflammation (Gimbrone, JR and García-Cardeña, 2016; Summerhill et al., 2019). Atherosclerotic plaques consist of lipids, cholesterol, or calcium deposits within the arterial walls, in which a variety of different cells, including foam cells, inflammatory cells, and smooth muscle cells, are highly present (Summerhill et al., 2019). As these diverse cell populations interact over time, they lead to arduous localized damage, causing arterial narrowing and vulnerability, thus restricting the blood flow, ultimately resulting in an increased risk of myocardial infarction, heart failure, or stroke (Harishkumar et al., 2022).

1.2.1. Stages of atherosclerosis

Atherosclerosis is a complex, multifactorial disease that proceeds in different dynamic stages. These steps include endothelial injury, lipid accumulation, leukocyte recruitment, foam cell formation, and plaque growth within the arterial walls (Summerhill et al., 2019; Zhang et al., 2022b). Additionally, the immune response plays a crucial role in promoting the progression of the disease, from triggering the innate inflammatory response via dendritic cells and macrophages to adaptive immune mechanisms of atheromatous plaques mediated by T-lymphocytes (Harishkumar et al., 2022; Zhang et al., 2022b).

1.2.2. Endothelial injury and immune response

Endothelial injury is a hallmark of many chronic inflammatory CVDs and an early factor of atherosclerosis development (Xu et al., 2021). The endothelium is a thin monolayer of endothelial cells (ECs) that line the circulating blood in the lumen and the vessel wall of arteries, veins, and capillaries (Krüger-Genge et al., 2019). It plays a critical role in maintaining cardiovascular health by regulating the transport of nutrients, gases, and other essential molecules across the semi-permeable vessel wall. In a normal physiological state, ECs regulate vascular tone, angiogenesis and cell hemostasis providing antioxidant, anti-inflammatory, and anti-thrombotic properties (Xu et al., 2021). Vascular tone regulation depends on balancing vasoconstrictor and vasodilator agents maintained by synthesizing and releasing various molecules, including nitric oxide (NO) (Krüger-Genge et al., 2019). In response to minimal physical stimuli like shear stress, acetylcholine, or cytokines, ECs secrete NO from L-arginine via endothelial nitric oxide synthase (eNOS) (Krüger-Genge et al., 2019). eNOS-derived NO diffuses to the adjacent smooth muscle cells inducing vasorelaxation and regulating blood flow and blood pressure (Gimbrone, JR and García-Cardeña, 2016). Moreover, the endothelium exerts anti-thrombotic functions by maintaining the balance between anti-coagulant and pro-coagulant factors, thereby preserving blood fluidity and preventing blot clotting (Rajendran et al., 2013; Krüger-Genge et al., 2019). In addition, the endothelium also regulates vascular integrity and vasculogenesis by secreting various angiogenic proteins (e.g., integrins, angiopoietins) or growth factors and cytokines, including vascular endothelial growth factor (VEGF) or fibroblast growth factor (FGF), which stimulate migration and proliferation during EC wound healing (Rajendran et al., 2013; Getzin et al., 2018). In angiogenesis, ECs promote the formation of new blood vessels obtained from pre-existing ones as the ECs proliferate to form a network (Eelen et al., 2020).

Endothelial dysfunction caused by hypertension or vascular intervention may lead to inflammatory responses that result in the activation of ECs promoting the expression of adhesion molecules (e.g., ICAM-1, VCAM-1, E-Selectin) and finally facilitate the infiltration of inflammatory cells (e.g., neutrophils, monocytes, and lymphocytes) into the injured arterial wall, which are crucial steps in the development of atherosclerosis (Xu et al., 2021). Selectin surface markers, including E-selectin, P-selectin, and L-selectin, are expressed on ECs and leukocytes (Ganesh et al., 2021; Xu et al., 2021).

They mediate leukocytes' initial rolling and tethering to the endothelium. Intercellular adhesion molecule-1 (ICAM-1) and vascular cell adhesion molecule-1 (VCAM-1) are expressed on the surface of activated ECs and play an essential role in the firm adhesion and transmigration of leukocytes into the arterial wall (Xu et al., 2021). ICAM-1 mediates the adhesion of leukocytes, including monocytes and T cells, to the endothelium, whereas VCAM-1 mediates the adhesion of leukocytes, including monocytes, to both the endothelium and smooth muscle cells (Cook-Mills et al., 2011). Activated ECs also produce pro-inflammatory cytokines, such as interleukin-1 beta (IL-1β), interleukin-6 (IL-6) and tumor necrosis factor-alpha (TNF-α), which further promote cell inflammation (Xu et al., 2021). The resulting accumulation of inflammatory cells at the injury site increases the inflammatory cascade signaling and cell damage, ultimately leading to atherosclerotic lesion initiation (Gimbrone, JR and García-Cardeña, 2016; Xu et al., 2021). Endothelial dysfunction is also characterized by the reduced production and bioavailability of NO, leading to oxidative stress through increased reactive oxygen species (ROS) production or a decrease in antioxidant defense molecules such as superoxide dismutase (SOD) (Gimbrone, JR and García-Cardeña, 2016; Xu et al., 2021).

1.2.3. Lipid accumulation

Following endothelial dysfunction and inflammatory response, lipids such as LDL-cholesterol and triglycerides accumulate in the arterial walls and promote atherosclerotic lesion formation (Summerhill et al., 2019). Hypercholesterolemia was identified as one of the most critical risk factors contributing to atherosclerosis and consequent coronary heart disease (Summerhill et al., 2019). Cholesterol and triglycerides are hydrophobic molecules that bind to lipoproteins necessary for their transportation in the blood (Feingold, 2000). These circulating lipoproteins include pro-atherogenic chylomicron remnants, very low-density lipoprotein (VLDL), intermediate-density lipoproteins (IDL), low-density lipoprotein (LDL), and anti-atherogenic high-density lipoprotein (HDL) (Feingold, 2000). VLDL, which are abundant in triglycerides, are synthesized by the liver and can be converted into IDL upon degradation of triglycerides from VLDL by adipose and muscle tissue. LDL is formed from VLDL or IDL and is the primary carrier of circulating cholesterol (Feingold, 2000). Furthermore, LDL can undergo diverse modifications that influence its structure and function. For example, oxidized LDL (oxLDL), glycated LDL (gLDL), acetylated LDL (acLDL), or

enzymatically modified LDL (eLDL) are known to promote the pro-atherogenic potential of LDL cholesterol leading to further increased inflammation (Liu et al., 2021b) and, consequently, infiltration of immune cells (e.g., monocytes/macrophages, T-cells, neutrophils) into the subendothelial space and eventually the formation of foam cells, fatty streaks and atherosclerotic lesions (Heinecke, 2006). However, oxLDL and acLDL are the major atherogenic lipoproteins recognized by macrophages and cause severe vascular damage through increased oxidative stress or enhanced senescence of endothelial progenitor cells that are crucial for endothelial regeneration (Heinecke, 2006). In contrast, atheroprotective HDL carries excess cholesterol from the peripheral tissues to the liver and intestine, where it is converted into bile acids and effluxed from tissues via reverse cholesterol transport (Feingold, 2000). Hence, elevated LDL and VLDL cholesterol levels and low HDL cholesterol levels are highly correlated with an increased risk for atherosclerotic cardiovascular events by inhibiting cholesterol efflux and promoting the formation of lipid-loaded macrophages and vascular smooth muscle cells (Liu et al., 2021b).

1.2.4. Foam cell formation

The conversion of LDL to oxLDL represents a solid inflammatory stimulus that triggers an innate immune response leading to increased recruitment of immune cells, such as monocytes, T-cells and neutrophils, to the injury site (Javadifar et al., 2021). These immune cells, along with other cells such as vascular smooth muscle cells, secret upregulated cell adhesion molecules and chemokines (e.g., monocyte chemoattractant protein-1/ MCP-1), and in response to endothelial cell activation the infiltrated monocytes differentiate into mature macrophages in the arterial intima and take up excess modified lipids, particularly oxLDL, leading to their transformation into foam cells (Javadifar et al., 2021; Gui et al., 2022). Macrophages are the central cells in the pathogenesis of atherosclerosis. In the presence of Th1 cytokines, macrophages further undergo differentiation into pro-inflammatory (M1) macrophages, whereas in the presence of Th2 cytokines, they differentiate into anti-inflammatory (M2) macrophages (Gui et al., 2022). However, some studies have found that the M2 phenotype does not always exert an atheroprotective function under certain stimuli and is probably more prone to foam cell formation (Gui et al., 2022). Internalization of oxLDL by macrophages is mediated by specific scavenger receptors on the surface of the macrophages, including CD36, SR-A1 and lectin-like oxLDL receptor-1 (LOX-1),

which recognize and bind to oxLDL (Liu et al., 2021b). In addition, macrophages also express several cholesterol transporters, such as ATP-binding cassette transporter ABCA1, ABCG1, and SR-BI, which regulate reverse cholesterol transport under normal conditions (Liu et al., 2021b; Gui et al., 2022). However, under pro-atherogenic conditions, these scavenger receptors are strongly upregulated, resulting in increased uptake of oxLDL cholesterol by macrophages. Once oxLDL is taken up by macrophages, it is hydrolyzed, forming free fatty acids, cholesterol, and other lipid metabolites (Javadifar et al., 2021). These lipids then accumulate within macrophages and lead to their conversion into foam cells in the arterial wall. Conversely, the expression of ABCA1 and ABCG1 is reduced in atherosclerosis, further increasing cholesterol accumulation in cells and promoting foam cell formation (Javadifar et al., 2021; Gui et al., 2022). As this process is unlimited, macrophages internalize too much cholesterol and eventually die (Javadifar et al., 2021; Gui et al., 2022). The subsequent release of mediators, the release of LDL from foam cells, and the constant influx of LDL from the vascular lumen lead to further infiltration of immune cells and, thus, to a vicious circle contributing to the formation of fatty streaks. These fatty streaks progress over time to form plaques containing increased vascular smooth muscle cells (Javadifar et al., 2021).

1.2.5. Vascular smooth muscle cell proliferation and fibrous tissue formation

Following inflammatory response and accumulation of foam cells, vascular smooth muscle cells (VSMCs) in the arterial media layer begin to proliferate and migrate into the intima of blood vessels, where they form a fibrous cap in and over the lipid-rich core of the atherosclerotic plaque (Liu et al., 2021b). VSMCs control vascular tone and blood pressure through their vasoregulatory ability and cell-cell interaction with neighboring ECs releasing NO to inhibit their proliferative and migratory activity (Perbellini et al., 2018). Under physiological conditions, a low proliferation rate is essential for proper wound healing and repair of new blood vessels (Liu et al., 2021a). However, under pathophysiological conditions, altered NO bioavailability or imbalance of other vasoactive mediators (e.g., endothelin-1 or serotonin) due to endothelial dysfunction can trigger excessive VSMC proliferation and migration (Perbellini et al., 2018). The proliferation of VSMCs can also be stimulated by various factors, including platelet-derived growth factor (PDGF), interleukin-1 (IL-1), or transforming growth

factor-beta (TGF-β), but also by mechanical forces such as shear stress (Perbellini et al., 2018; Sorokin et al., 2020). For example, overexpressed PDGF by activated platelets, macrophages, or ECs leads to the activation of fibroblasts and stimulates phenotypic modulation of VSMCs, which promotes vascular remodeling and leads to an increase in plaque size and fibrous cap formation (Perbellini et al., 2018; Sorokin et al., 2020). The fibrous cap is created by excessive accumulation of fibrous tissues from extracellular matrix deposits such as collagen, fibronectin, or elastin and by necrotic tissue accumulation in and around the lipid core, which contributes to plaque thickening and narrowing of the arterial lumen, indicative of a progression of advanced atherosclerotic lesions leading to plaque rupture (Sorokin et al., 2020; Javadifar et al., 2021).

1.2.6. Plaque rupture

Plaque rupture is a common event in the progression of atherosclerosis that can have severe consequences due to plaque instability (Bentzon et al., 2014; Javadifar et al., 2021). While stable plaques are characterized by the enrichment of SMCs, low-grade of inflammation, and reduced macrophage infiltration, plaque destabilization is characterized by a vulnerable plaque, thin fibrous cap, a large lipid core, high-grade of inflammation and less activated VSMCs, which promote plaque rupturing (Zhang et al., 2022b). Upon degradation of the fibrous cap and plaque rupture, the lipid-rich contents of the plaque are exposed to the bloodstream, triggering platelet activation and thrombus formation, which can completely occlude the affected artery, leading to acute coronary events such as myocardial infarction, stroke, or even death (Zhang et al., 2022b).

1.3. Diabetes mellitus

Vascular complications manifested in endothelial dysfunction, chronic inflammation, and oxidative stress are also the main features of diabetes mellitus leading to mortality and disability in diabetic patients (Sorrentino et al., 2007; Ye et al., 2022). Diabetes mellitus, classified into type 1 and type 2, describes a persistent metabolic disorder characterized by hyperglycemic conditions due to inadequate insulin secretion and/ or increased insulin resistance (Poznyak et al., 2020). Type 1 diabetes (T1D) can occur at an early age resulting from a destructive autoimmune reaction of the insulin-

producing pancreatic β-cells resulting in an insulin deficiency. Type 2 diabetes (T2D) is more prevalent in individuals over 30 years old and occurs due to increased insulin resistance, thus resulting in impaired glucose tolerance (Low Wang et al., 2016; Poznyak et al., 2020). ACVD is estimated to impact up to two-thirds of individuals with T2D throughout their lifetime (Low Wang et al., 2016). Individuals with insulin resistance experience higher rates of diabetes-related comorbid conditions, including hyperglycemia, arterial hypertension, dyslipidemia and obesity (Low Wang et al., 2016). These comorbidities can attenuate endothelial cell functions due to inflammation, oxidative stress leading to increased ROS levels, decreased NO bioavailability or enhanced leukocyte adhesion, thus contributing to the development and complexity of ACVD (Low Wang et al., 2016). Studies have reported that elevated glucose levels enhance endothelial cell permeability and upregulate the expression of adhesion molecules (Ye et al., 2022). Moreover, obese individuals with abnormal excessive body fat defined by high body mass index (BMI) are more prone to chronic inflammation and plaque formation in the arteries leading to the development of CVDs (Low Wang et al., 2016). Targeting common complications of diabetes mellitus by controlling blood glucose levels and blood pressure, lowering LDL-cholesterol levels and maintaining a balanced diet or regular exercise can prevent or reduce the burden of cardiovascular events (Low Wang et al., 2016).

1.4. The PI3K/ AKT/ FOXO1 signaling pathway

1.4.1. The phosphoinositide 3-kinase (PI3K) family

The Phosphatidylinositol-3-kinase (PI3K) is an intracellular lipid kinase enzyme that regulates various biological processes, such as cell survival, migration, metabolism, and proliferation (Ghigo et al., 2017). Mammals have eight different isoforms of PI3K, which can be categorized into three distinct classes according to their molecular structure and their catalytic and regulatory functions (Ghigo et al., 2017). The Class I PI3Ks are the most studied PI3K family that catalyzes the production of phosphatidylinositol-3,4,5-trisphosphate (PIP3) from phosphatidylinositol-4,5-bisphosphate (PIP2) through phosphorylation and thereby mediates cellular functions including cell growth, survival, proliferation and migration. Class I PI3K can be additionally divided into Classes IA and IB, comprising a catalytic and regulatory subunit. Class IA PI3Ks are activated by receptor tyrosine kinases (RTKs) and G-

protein-coupled receptors (GPCRs), while Class IB PI3Ks are usually activated by GPCRs (Ghigo et al., 2017). The catalytic p110 subunit is divided into p110α (encoded for the *PIK3CA* gene), p110β (for *PIK3CB*), and p110δ (for *PIK3CD*) defined as Class IA PI3K family, while Class IB PI3K comprises p110γ (for *PIK3CG*), respectively. Each catalytic subunits is related to a regulatory subunit, of which p85α, p55α, p50α (encoded for *PIK3R1* gene), p85β (for *PIK3R2*) and p55γ (for *PIK3R3*) are associated with Class IA PI3Ks, and p101 (for *PIK3R5*) or p84 (*PIK3R6*) with Class IB PI3K family (Ghigo et al., 2017). Class I PI3Ks, specifically p110α, are critical in regulating endothelial cell proliferation, migration, and morphogenesis, all essential for early embryonic angiogenesis (Yoshioka et al., 2012). Class II PI3K has three isoforms, PI3KC2α (encoding by *PIK3C2A* gene), PI3KC2β (*PIK3C2B*) and PI3KC2γ (*PIK3C2G*), which exert their catalytic functions without the presence of regulatory proteins and mainly generates phosphatidylinositol 3-phosphate (PI3P) or phosphatidylinositol-3,4-bisphosphate (PI(3,4)P2) in response to cellular signals (Yoshioka et al., 2012). They primarily regulate cellular processes such as endocytosis, intracellular membrane trafficking, and insulin signaling. In addition, they are also implicated in cell survival, proliferation, differentiation, and metabolism (Yoshioka et al., 2012). An essential component within the Class II PI3Ks is the phosphatidylinositol-4-phosphate 3-kinase C2 domain-containing subunit alpha (PI3KC2α) (Aki et al., 2015). In ECs, PI3KC2α exerts critical functions in regulating angiogenic processes and preserving the integrity of the endothelial barrier (Aki et al., 2015). Class III PI3Ks are responsible for producing only PI3P. However, they share a similar structure to Class I, consisting of heterodimers with a catalytic subunit (VPS34) encoded by the *PIK3C3* gene and a regulatory subunit (VPS15/p150) (Thillai et al., 2017). Their central role appears to be in transporting proteins and vesicles (Yoshioka et al., 2012). However, recent evidence indicates that Class III PI3Ks are also implicated in phagocytosis (He et al., 2021).

1.4.2. AKT/ PKB signaling

AKT is a well-known serine/ threonine protein kinase implicated in several cellular processes, such as cell survival, apoptosis, metabolism, migration and angiogenesis (Shiojima and Walsh, 2002). AKT comprises three homologs in mammalian: AKT1, AKT2, and AKT3, referred to as protein kinase B (PKB) α, -β, and -γ, correspondingly. AKT1 is widely expressed in tissues such as the brain, heart, or lung. AKT2 is

predominantly expressed in insulin-sensitive tissues like adipose tissue, liver, and skeletal muscle. AKT3 shows a high expression level in the brain (Shiojima and Walsh, 2002; Zheng and Cartee, 2016). The three homologs have similar activation mechanisms and share similar domain structures that include a pleckstrin homology (PH) domain at the amino-terminal region, a catalytic domain, which mediates its binding to other cellular proteins, and a carboxyl-terminal regulatory region known as the hydrophobic motif (HM) domain (Gallay et al., 2009; Zheng and Cartee, 2016). AKT is activated by various extracellular signals, such as growth factors and cytokines, and its activity is tightly regulated through phosphorylation and dephosphorylation events (Shiojima and Walsh, 2002). The activation of AKT relies on the phosphorylation at two primary sites: threonine 308 (Thr308) located at the catalytic region and serine 473 (Ser473) at the carboxy terminus (Gallay et al., 2009). Phosphoinositide-dependent kinase-1 (PDK1) mediates the phosphorylation of Thr308, while PDK2, which has been identified as the mammalian target of rapamycin complex-2 (mTORC2), is responsible for Ser473 phosphorylation (Gallay et al., 2009). Several studies have also shown that AKT is functionally full activated by undergoing double phosphorylation of Thr308 and Ser473 (Gallay et al., 2009). However, other phosphorylation sites have also been identified in AKT isoforms. For example, AKT1 can be phosphorylated at Ser477 and Thr479 by the kinases DNA-dependent protein kinase (DNA-PK) or cyclin-dependent kinase 2 (CDK2) (Gao et al., 2014; Long et al., 2021). Moreover, AKT2 undergoes phosphorylation at Thr309 and Ser474, while AKT3 can be phosphorylated at Thr305 and Ser472. These sites are analogous to Thr308 and Ser473 in AKT1 and AKT2, respectively (Long et al., 2021).

Initiation of the PI3K/AKT pathway occurs with the activation of PI3K by RTK (e.g., insulin receptor signaling) or GPCRs. Stimulation of these receptors by various extracellular ligands, such as growth factors or cytokines, triggers receptor dimerization and autophosphorylation of tyrosine residues within their intracellular regions (Long et al., 2021). Following receptor activation, the regulatory subunit p85 subsequently binds to the phosphorylated tyrosine residue, leading to the recruitment of the catalytic subunit p110 and full activation of PI3K. These phosphorylated tyrosine residues can also represent binding sites for insulin receptor substrate (IRS) proteins (Long et al., 2021). Activated PI3K enzyme then triggers the phosphorylation of specifically PIP2 on the 3-hydroxyl group of the inositol ring generating the second

messenger, PIP3. PDK1 and inactive AKT in the cytosol get recruited to the plasma membrane by PIP3, inducing Thr308 phosphorylation by PDK1 (Gallay et al., 2009; Long et al., 2021). Although phosphorylation at Ser473 is mainly mediated by mTORC2, PDK1, or other kinases like integrin-linked kinase (ILK) and DNA-PK, autophosphorylation of AKT can also result in phosphorylation at the Ser473 site, ultimately leading to cellular response for growth, proliferation, migration, and survival of the cells (Long et al., 2021). However, the PI3K/ AKT pathway can be negatively regulated through protein phosphatases such as the protein phosphatase 2A (PP2A), the PH domain and leucine-rich repeat protein phosphatase (PHLPP), or the tumor suppressor phosphatase and tensin homolog (PTEN) by dephosphorylating Thr308, Ser473, or PIP3, respectively (Long et al., 2021).

1.4.3. The FOXO family and FOXO1

The Forkhead Box O (FOXO) transcription factors have also been identified as potential downstream targets of AKT. They are highly conserved family members that regulate various biological processes, including cell proliferation, metabolism, longevity and apoptosis (Li et al., 2019; Jiramongkol and Lam, 2020). The forkhead (FOX) gene, classified as *dFOXO*, was first discovered in the fly *Drosophila melanogaster* due to a genetic mutation leading to an ectopic fork-like head structure (Carter and Brunet, 2007). Extensively genetic studies in the model organism of the nematode *Caenorhabditis elegans* have identified a single FOXO protein encoded by the *DAF-16* gene, which acts as a central regulator for aging, longevity and cell proliferation mediated by insulin/ insulin-like growth factor (IGF-1) signaling pathway (Jiramongkol and Lam, 2020). Both invertebrates possess only one FOXO gene (*dFOXO* and *DAF-16*), while in mammalian the FOXO family includes four members: FOXO1, FOXO3, FOXO4, and FOXO6 (Webb and Brunet, 2014). FOXO1, FOXO3, and FOXO4 are widely expressed in various tissues, including ECs, heart, adipose tissue, or liver, and exhibit significant similarities in their expression patterns and transcriptional functions compared to FOXO6, which is predominantly expressed in the brain (Dharaneeswaran et al., 2014). Numerous studies have demonstrated the pivotal role of both FOXO1 and FOXO3 in vascular development (vasculogenesis), with the major isoforms co-expressed in various tissues, particularly ECs (Oellerich and Potente, 2012). It has been reported that endothelial-specific deletion of FOXO1, but not FOXO3 *in vivo*, promoted endothelial angiogenic properties in a non-additive manner (Oellerich and

Potente, 2012; Dharaneeswaran et al., 2014). Thus, FOXO1 is suggested to be one of the major regulators of vasculogenesis (Dharaneeswaran et al., 2014).

1.4.3.1. The regulation of FOXO transcriptional activity

The FOXO protein family shares a conserved structure consisting of an N-terminal DNA-binding domain called the forkhead box (FOX), followed by a nuclear localization signal (NLS), a nuclear export sequence (NES) and a C-terminal transactivation domain (TAD) (Grossi et al., 2019). The FOX DNA-binding domain (FHD) is a highly conserved 100-amino acid sequence that forms a helix-turn-helix motif to allow the binding of FOXO proteins to specific promoter sequences (5'-TTGTTTAC-3´) of target genes and regulate their transcription functions implicated in cell cycle arrest, apoptosis, metabolism, and angiogenesis (Farhan et al., 2020). Upon binding to DNA, its C-terminal TAD interacts with several co-activator or -repressor proteins to regulate FOXO transactivation (Grossi et al., 2019; Farhan et al., 2020). The NLS and the NES are responsible for modulating the subcellular localization of FOXO (Wang et al., 2016a).

Moreover, the FOXO transcriptional activity can be regulated by multiple post-translational modifications (PTMs), which include phosphorylation, acetylation, ubiquitination, and methylation. These PTMs can modulate the subcellular localization, DNA-binding affinity and transcriptional activity of FOXO proteins (Wang et al., 2016b). Phosphorylation is a substantial PTM that represses the activity of FOXO transcription factors by various signaling pathways, particularly the insulin signaling pathway involving PI3K and AKT (Tsuchiya and Ogawa, 2017). Upon activation of the PI3K/ AKT signaling pathway induced by insulin or IGF-1 stimulation, activated AKT directly phosphorylates FOXO proteins at multiple conserved serine/ threonine residues such as Thr24, Ser256, Ser319 in FOXO1; Thr32, Ser253, Ser315 in FOXO3; Thr32, Ser184, Ser258 in FOXO4 (Psenakova et al., 2019). AKT-mediated phosphorylation of FOXO promotes the binding of FOXO to the 14-3-3 chaperone proteins, leading to its nuclear exclusion, followed by inhibition of DNA-binding and subsequent degradation of FOXO by cytoplasmic proteasomes, ultimately resulting in suppression of its transcriptional activity (Webb and Brunet, 2014; Farhan et al., 2020). This negative regulation of FOXO transcription factors by PI3K/ AKT reduces gene expression involved in apoptosis, stress response, and inflammation (Wang et al.,

2016a). Other kinases, which can block FOXO transcriptional activity via phosphorylation, involve for example serum- and glucocorticoid-inducing kinase (SGK), extracellular signal-regulated kinase (ERK), or I kappa B kinase (IKK) (Farhan et al., 2020). In contrast, increased oxidative or metabolic stress can mediate FOXO phosphorylation by different kinases such as mitogen-activated protein kinase (MAPK), AMP-activated protein kinase (AMPK), or c-Jun N-terminal kinase (JNK) promoting both nuclear accumulation and transcriptional activity of FOXOs (Farhan et al., 2020).

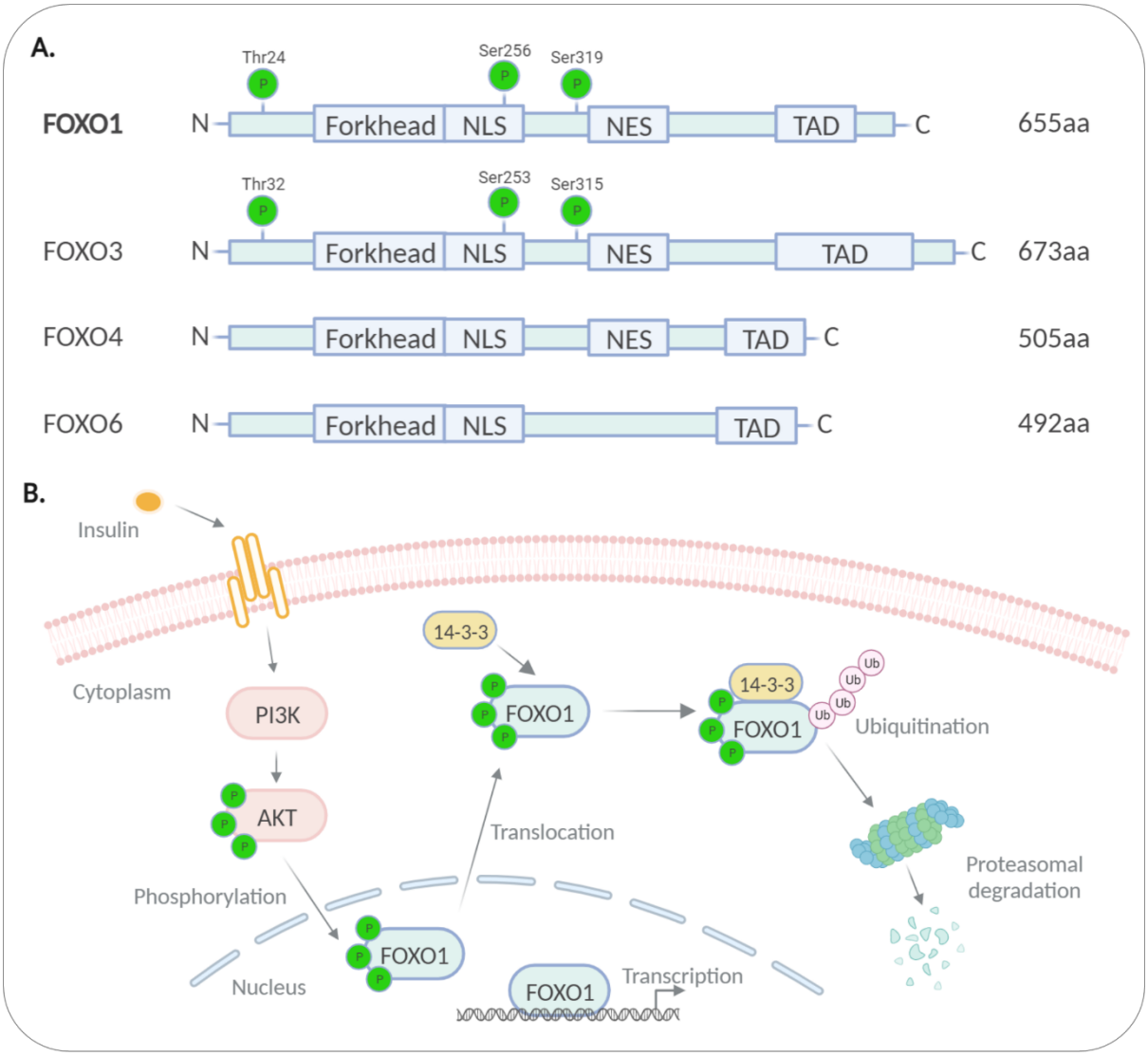

Figure 1: Domain structure of Forkhead Box O (FOXO) isoforms and PI3K/ AKT/ FOXO1 signaling pathway.

A. Schematic illustration of different FOXO isoforms (FOXO1, FOXO3, FOXO4, FOXO6) in mammals. FOXO proteins possess a highly conserved FOX DNA-binding domain (FHD) at the N-terminal domain that binds to specific promotor sequences in the target genes, a nuclear localization signal (NLS) as well as a nuclear export sequence (NES) that modulates FOXO nuclear-cytoplasmic localization, and a C-terminal transactivation domain (TAD) that regulates FOXO transactivation. AKT phosphorylation of FOXO1 and FOXO3 at threonine and serine

sites (Thr24/32, Ser256/253, and Ser319/315) are indicated, respectively. The FOXO proteins differ in their amino acid (aa) residue lengths. B. Regulation of FOXO1 via PI3K/ AKT signaling pathway. Upon insulin receptor stimulation and activation of the PI3K/ AKT signaling pathway, FOXO1 is phosphorylated at multiple conserved serine/ threonine residues through interaction with 14-3-3 chaperone proteins, leading to its nuclear exclusion and subsequent degradation of FOXO1 by cytoplasmic proteasomes and suppression of its transcriptional activity (adapted from (Tsuchiya and Ogawa, 2017); created with BioRender.com).

The transcriptional activity of FOXO proteins is also tightly regulated post-translationally by acetylation and deacetylation modifications. Acetylation of FOXO proteins is mediated by histone acetyltransferases (HATs) such as CREB-binding protein (CBP) and p300/ CBP, while deacetylation is controlled by histone deacetylases (HDACs) and NAD-dependent sirtuins (SIRTs) (Boccitto and Kalb, 2011). FOXO proteins undergo a negative feedback mechanism through acetylation and deacetylation processes (Tzivion et al., 2011). For example, studies have reported an inhibitory effect on FOXO1 transactivation by direct CBP/ p300-induced acetylation at lysine residues 242, 245, and 262 of FOXO1, resulting in attenuated DNA binding affinity to specific target genes (Boccitto and Kalb, 2011). Interestingly, it is also suggested that acetylated FOXO1 by CBP/ p300 may further support FOXO1 phosphorylation by AKT, allowing nuclear export and negative regulation of FOXO1 (Gross et al., 2009; Tzivion et al., 2011). Conversely, these HATs also have an activating effect on FOXO protein functions by acetylating nucleosomal histones to recruit CBP/ p300 to promotor regions, ultimately leading to enhanced transcriptional activity of FOXO-promoting pro-apoptotic gene expression (Tzivion et al., 2011). However, the deacetylation restores the transcriptional activity of FOXO and accelerates FOXO protein degradation (Wang et al., 2016b). Deacetylating function of SIRT1, which is located in the nucleus and activated in response to starvation or oxidative stress, directly binds to FOXO and deacetylates the acetylated lysine residues in an enzymatic activity-dependent manner, causing nuclear trapping and enhancing the transcriptional activity of FOXO (Hwang et al., 2013). Studies have shown that SIRT1-mediated deacetylation of FOXO1 and FOXO3 has increased autophagic and antioxidant functions via cross-talk with enhanced AKT phosphorylation (Yang and Dong, 2021). FOXO1-induced autophagic flux is essential in maintaining cardiac function under glucose deprivation or starvation conditions (Chong et al., 2012). In addition, deacetylation of FOXO3 has been linked to cell cycle arrest and resistance to oxidative stress while inhibiting its ability to induce apoptosis,

eventually resulting in cell survival, DNA repair, or antioxidant action (Grossi et al., 2019).

The ubiquitination proteasome system can also mediate the regulation of FOXO proteins. Since the degradation of FOXO proteins requires the ubiquitin-proteasome-dependent pathway, FOXO ubiquitination often operates with phosphorylation and acetylation (Rong et al., 2022). Ubiquitination can occur as mono- or poly-ubiquitination and is mediated by the E1 ubiquitin-activating enzyme, E2 ubiquitin-conjugating enzyme and E3 ubiquitin-ligase (Rong et al., 2022). E3 ubiquitin-ligases, including SKP2 and MDM2, play a key role in mediating the poly-ubiquitination of FOXOs. SKP2 mainly targets AKT-phosphorylated FOXO proteins, and MDM2 targets ERK-phosphorylated FOXOs, resulting in poly-ubiquitination and subsequent proteasomal degradation (Tzivion et al., 2011; Wang et al., 2016b). Although phosphorylation of FOXO proteins by AKT or ERK is essential to induce poly-ubiquitination, acetylation of FOXO1 is associated with a negative correlation to poly-ubiquitination due to increased nuclear entry and protein stability of FOXO1 (Wang et al., 2016b; Rong et al., 2022). In contrast, mono-ubiquitination mediates the nuclear translocation of FOXO, enhancing its transcriptional activity (Wang et al., 2016b). Moreover, under oxidative stress, MDM2-E3 ligase can also promote mono-ubiquitination for the transactivation of FOXO4 (Zhao et al., 2011).

Recent studies have demonstrated that methylation represents an additional mode of posttranslational regulation for FOXO transcription factors. FOXO methylation primarily occurs on arginine and lysine residues by the protein arginine methyltransferases (PRMTs) or lysine methyltransferases (KMTs) (Lee et al., 2023). PRMT1 is the major methyltransferase that methylates FOXO1 at arginine 248 and 250 residues on its consensus AKT phosphorylation site, which in turn prevents AKT-mediated phosphorylation of FOXO1 at serine 253, thus leading to increased nuclear FOXO1 localization and inhibition of subsequent protein degradation (Lee et al., 2023). Methylation of lysine 273 on FOXO1 by methyltransferase G9a or lysine 271 on FOXO3 by SETD7 negatively regulates FOXO proteins by reducing its stability and accelerating FOXO protein degradation (Lee et al., 2023). However, the regulation of FOXO activity highly depends on the organism, external stimuli, their upstream targets and tissue-specific expression (Grossi et al., 2019). Therefore, proper regulation of

these posttranscriptional modifications is crucial for the total functional capacity of FOXO proteins and can have significant implications in various cellular pathways, including inflammation and angiogenesis.

1.4.3.2. The role of FOXO1 in CVD

FOXO1 is the most extensively studied isoform implicated in the pathogenesis of CVD and diabetes (Yu et al., 2020). Studies have identified its critical role in modulating vascular and cardiac development (Kandula et al., 2016). Furthermore, based on various extracellular stimuli and tissues, FOXO1 regulates cellular processes, including angiogenesis, metabolism, oxidative stress, apoptosis, and inflammation (Puthanveetil et al., 2013; Kandula et al., 2016). Vascular development is a dynamic and tightly regulated process involving vasculogenesis, angiogenesis and vascular remodeling (Park et al., 2009). Angiogenic precursor cells play a key role in these processes and can differentiate into ECs to form embryonic blood vessels and new blood vessels from pre-existing cells through endothelial sprouting and vascular expansion (Park et al., 2009). FOXO1 has been recognized as a critical factor in regulating endothelial cell growth and coupling metabolic and proliferative activities (Wilhelm et al., 2016). This correlation indicates that ECs are susceptible to metabolic changes in FOXO1 activity. For example, endothelial-specific deletion of FOXO1 in mice resulted in vessel expansion caused by enhanced EC proliferation, while FOXO1 overexpression restricts EC sprouting and vascular growth leading to vessel thinning and hypo-branching (Wilhelm et al., 2016). However, a global deficiency of FOXO1 in mice has been shown to induce embryonic lethality due to impaired vasculogenesis, highlighting its importance in vascular development (Dharaneeswaran et al., 2014; Kandula et al., 2016). Controversially, myocardial-specific overexpression of FOXO1 in mice also leads to fatal consequences due to impaired cardiomyocyte proliferation, reduced cardiac size and thickness of myocardium, eventually ensuing cardiac cell death and heart failure (North and Sinclair, 2012; Boal et al., 2016). Notably, FOXO1 is considered a potential regulator of oxidative stress resistance that can be protective in ischemic heart disease (Kandula et al., 2016). It has been shown that under short-term oxidative stress conditions, FOXO1 increases the expression of antioxidant genes involved in DNA repair (e.g., superoxide dismutase, GADD45), promoting the activity of ROS-scavenging, thereby protecting cells from acute metabolic disturbances and DNA damage (Puthanveetil et al., 2013; Marchelek-Mysliwiec et al., 2022). Therefore,

a deficiency of FOXO1 in mouse cardiomyocytes has been associated with increased oxidative damage and decreased myocardial function after acute ischemia or myocardial infarction in response to metabolic stress (Boal et al., 2016). Interestingly, antioxidant protection by FOXO1 was not guaranteed in chronic hyperglycemia-induced oxidative stress (Kandula et al., 2016; Marchelek-Mysliwiec et al., 2022), a process that has been related to the pathogenesis of diabetic cardiomyopathy (DCM) (Kandula et al., 2016). Several studies have found a link between augmented FOXO1 activity and DCM mediating systemic insulin resistance and lipid accumulation of myocardial cells (Kandula et al., 2016). Under insulin resistance and diabetic states, FOXO1 phosphorylation is diminished due to PI3K/ AKT inactivation, causing FOXO1 to remain highly active in the nucleus and leading to metabolic disturbances, impaired angiogenesis, inflammation, increased cardiac cell death, and eventually to heart failure (Kandula et al., 2016; Xin et al., 2017). However, restoration of insulin sensitivity could be observed upon FOXO1 repression in mice (Xin et al., 2017). Furthermore, FOXO1 hyper-activation can also potentiate the development of atherosclerosis by positive regulation of adipocyte fatty acid binding protein (FABP4) gene transcription, leading to increased accumulation of myocardial lipids in the heart (Kandula et al., 2016; Yan et al., 2020). Remarkably, enhanced FOXO1 activity has also been shown to induce cardiac dysfunction and hypertrophy under high-fat diets due to metabolic disturbances, in particular glucose and lipid metabolism, provoked by upregulation of pyruvate dehydrogenase kinase 4 (PDK4) gene expression (Kandula et al., 2016). Additionally, HFD conditions and FOXO1 overexpression diminished insulin signaling by downregulating IRS1 activity followed by AKT inactivation, ultimately promoting insulin resistance (Battiprolu et al., 2012). Together, these data highlight the complexity of FOXO1 regulation in distinctive cell types upon different stimuli such as growth factors, oxidative stress, or nutrient deprivation, which are critical for developing CVDs, including myocardial ischemia, diabetic cardiomyopathy and atherosclerosis (Kandula et al., 2016).

1.5. Gut microbiome

Growing evidence indicates that the gut microbiome performs a variety of significant biochemical functions impacting numerous physiological processes in the human body (Kinross et al., 2011). The gut microbiome forms a remarkably dynamic ecosystem and constitutes the totality of diverse microorganisms residing within the gastrointestinal tract, including bacteria, viruses, and archaea (Gail A.M. Cresci and Kristin Izzo, 2019;

Deepjyoti Paul and Bhabatosh Das, 2022). The estimated microbial diversity within the human gut harbors more than 1000 bacterial species, which possess 100 times more genes than the human genome (Guinane and Cotter, 2013; Yang et al., 2021). Furthermore, these microbial communities of over 100 trillion microbes coexist in a symbiotic relationship with the host and are essential in maintaining human health (Deepjyoti Paul and Bhabatosh Das, 2022; Zhang et al., 2022a). A healthy gut microbiota community is typically characterized by high taxonomic diversity or microbial gene richness (Hou et al., 2022). Although the diversity of the gut microbiome varies widely among healthy individuals, the human microbiota is dominated by bacteria from four main phyla - *Bacteroidetes*, *Firmicutes*, *Actinobacteria* and *Proteobacteria* (Human Microbiome Project Consortium, 2012; Guinane and Cotter, 2013; Deepjyoti Paul and Bhabatosh Das, 2022). Variations in the gut compositions can also be observed across various anatomical regions of the gastrointestinal tract due to different environmental conditions (Hou et al., 2022). For example, *Proteobacteria* (such as *Enterobacteriaceae*) are commonly found in the small intestine, especially in environments with elevated bile concentrations. Conversely, anaerobic bacteria, like *Bacteroidetes*, are more abundant in the colon (Hou et al., 2022). Moreover, the diversity of the gut microbiome is also influenced by various other factors, including age, diet, lifestyle, host genetics and ethnicity (Jayaraman, 2019; Hou et al., 2022). Age and diet are determining factors in the variation of gut microbiota. Typically, there is an upward trend in microbiota diversity from childhood to adulthood, while a decline in diversity is observed in individuals over 70 years old (Hou et al., 2022). Numerous studies have consistently shown that diet plays a fundamental role in shaping gut microbiota composition, thereby influencing its functions (Singh et al., 2017; Zhang, 2022). For instance, maintaining a nutrition-balanced diet can preserve a “healthy gut”. In contrast, an unbalanced diet, such as a Western diet, profoundly impacts the gut microbiome diversity, e.g., leading to adverse effects on host immunity (Zheng et al., 2020; Zhang, 2022).

The gut microbiota performs a variety of functional aspects that impact the host's overall health through metabolic, trophic, and protective functions (Guarner and Malagelada, 2003). One of the key functions includes digestion and nutrient metabolism, where carbohydrates and other indigestible dietary components such as polysaccharides (e.g., resistant starches, cellulose, and gums) are enzymatically

fermented by intestinal organisms like *Bacteroides*, *Bifidobacterium*, *Fecalibacterium*, and *Enterobacteria* (Guarner and Malagelada, 2003; Jandhyala et al., 2015). As a result, short-chain fatty acids (SCFA) such as butyrate or propionate, amino acids and vitamins are microbially synthesized through fermentation serving as energy sources for the host (Jandhyala et al., 2015; Gadecka and Bielak-Zmijewska, 2019). The gut microbiota also has trophic effects, as it promotes the growth and differentiation of intestinal epithelial cells, thereby maintaining the barrier integrity of the intestinal mucosa that represents the primary interface between the external cell environment and the host immune system (Guarner and Malagelada, 2003). Moreover, the gut microbiota functions as an endocrine organ, producing inflammatory mediators and metabolites that modulate the host immunity (Yang et al., 2021). Studies conducted on germ-free animals revealed a strong correlation between the absence of beneficial microorganisms and significant disruptions in the structure of lymphoid tissues and immune functions compared to conventional colonized animals (Zheng et al., 2020). Apart from this, the gut microbiota plays a role in immune defense against invading pathogens through intestinal antimicrobial peptides (AMPs) as part of the innate immunity, whereas the secretion of IgG antibodies is part of the adaptive immunity (Zheng et al., 2020).

However, certain factors like medication intake (e.g., antibiotics), stress, or poor diet can disrupt the balance of the gut microbiome leading to a dysbiotic state that can contribute to the progression of cardiometabolic and cardiovascular diseases, including diabetes and atherosclerosis (Jörg et al., 2016; Gerhardt et al., 2021; Roessler et al., 2022). Although the exact mechanisms underlying these associations are not yet fully understood, the disease severity has shown a positive correlation with intestinal permeability (e.g., leaky gut), alterations in intestinal immunity, and shifts in the production of microbiome-derived metabolites with systemic effects (Papadopoulos et al., 2022). For example, elevated gut permeability is a hallmark feature observed in individuals with T2D, which results in microbial products entering the bloodstream and leading to metabolic endotoxemia (Gurung et al., 2020). In heart failure, the highly permeable intestinal mucosa and impaired intestinal barrier integrity also lead to the translocation of microbial components (e.g., mainly LPS) into the blood triggering the host immune response and vascular inflammation, thereby exacerbating the progression of heart failure (Yang et al., 2021). Several studies also found a link

between specific microbial-related metabolites and atherosclerotic vascular disease (Gerhardt et al., 2021).

1.5.1. Interaction of gut microbial metabolites and CVD

Shifts in the composition of gut microbes have been linked to altering levels of microbial metabolites, which are positively associated with multiple diseases, including CVD (Yang et al., 2021). Metabolomics approaches and 16S rRNA gene sequencing have provided unprecedented opportunities for profiling the gut microbial-metabolic axis in mammals, enabling quantitative measurements of alterations in microbiota-derived metabolites that are closely associated with a pathophysiological state (Yang et al., 2021). The metabolites generated in the gut are absorbed by intestinal epithelial cells and conveyed to the liver through the portal vein prior to entering the systemic circulation (Koh et al., 2018). While specific microbially-produced metabolites have been associated with the development of CVD, there are also beneficial metabolites produced by the gut microbiota. For instance, distinct bile acids (BAs) and short-chain fatty acids (SCFAs) are microbial metabolites and are considered as physiological modulators (Tang et al., 2019a). BAs (such as cholic acids) or secondary BAs (such as deoxycholate) are referred to as emulsifiers of fats and fat-soluble vitamins produced via the oxidation of cholesterol in the liver or from unrecycled BAs (Tang et al., 2019b). Decreased levels of BA in the gut have been linked to bacterial overgrowth and inflammation (Tang et al., 2019b). SCFAs are produced as a final byproduct through the fermentation of dietary fibers, sugar, or resistant starch by specific anaerobic gut bacteria and have been shown to modulate the host inflammation and blood pressure (Hou et al., 2022; Yan et al., 2022). SCFAs are a class of organic fatty acids, including acetic, butyric and propionic acids (Tang et al., 2019b; Haghikia et al., 2022). These SCFAs are highly abundant in the intestinal tract and serve as an important energy source. Moreover, they are systemically bioactive with essential physiological functions in the host (Tang et al., 2019b). SCFAs have been suggested to lower blood pressure by enhancing vascular compliance (Yan et al., 2022). In addition, preclinical studies have identified acetate-producing bacteria to exert potentially protective effects in preventing hypertension, cardiac hypertrophy, and the onset of fibrosis by indirectly enhancing intestinal barrier functions (Tang et al., 2019b). Also, the SCFA butyrate and propionate demonstrate a protective effect against hypertensive cardiovascular damage (Hou et al., 2022). Furthermore, individuals with

DM may have a reduced abundance of SCFA butyrate-producing bacteria, which are essential in reducing chronic inflammation, thus maintaining intestinal homeostasis (Hou et al., 2022). Notably, a recent study has demonstrated that propionate exerts both cholesterol-lowering and athero-protective effects in humans and mice (Haghikia et al., 2022). The research group showed that propionate decreases intestinal cholesterol absorbance by maintaining the immune balance and promoting regulatory T cells (Tregs) immunity in the gut. In addition, propionate was found to prevent the development of HFD-induced hypercholesterolemia and atherosclerosis in *Apoe*$^{-/-}$ mice (Haghikia et al., 2022).

However, other microbiota-related metabolites, such as trimethylamine N-oxide (TMAO) and trimethylamine (TMA), have been identified as predictors for CVD. TMAO is formed in the liver from circuiting TMA through the metabolism of dietary precursors, including phosphatidylcholine or choline (e.g., rich in eggs), L-carnitine (highly rich in red meat) or other TMA-containing high-fat foods (Tang et al., 2019a; Tang et al., 2019b). Numerous mechanistic animal models have demonstrated that TMAO promotes the progression of atherosclerosis and enhances vascular thrombogenicity (Tang et al., 2019b; Witkowski et al., 2022). Particularly, in stable patients undergoing elective cardiac evaluation, it has been observed that higher plasma levels of TMAO are associated with an elevated risk of CVD and that these individuals have a greater likelihood of experiencing adverse events of myocardial infarction, stroke, or death (Tang et al., 2019b). TMAO has also been shown to potentially contribute to inflammation and endothelial dysfunction, which are critical features of atherosclerosis (Brown and Hazen, 2018).

1.5.2. Imidazole Propionate (ImP)

Given the impact of the gut microbiome and diet on human health, there is growing evidence that microbiota-derived metabolites can potentially contribute to the onset and advancement of metabolic and cardiovascular diseases, such as atherosclerosis, hypertension, heart failure, obesity, and type 2 diabetes (Tang et al., 2017). Over the past few years, a novel microbial-produced metabolite known as imidazole propionate (ImP) has gained attention in the onset of cardiometabolic disorders, including type 2 diabetes and obesity (Koh et al., 2018; Molinaro et al., 2020). Indeed, a recent study has additionally identified a significant correlation between ImP and heart failure in humans (Molinaro et al., 2023).

ImP is generated from microbial processing of histidine, an essential aromatic amino acid found in dietary proteins such as meat, fish, eggs, dairy, or grains (Koh et al., 2018; Moro et al., 2020). The gut microbiome can metabolize dietary histidine to urocanate by the bacterial enzyme histidine ammonia lyase (encoded by the *hutH* gene). The urocanate intermediate is then enzymatically catalyzed by urocanate reductase (encoded by the *urdA* gene), ultimately resulting in ImP production (Figure 2) (Koh et al., 2018). Amino acid-derived ImP absorbed by the intestine reaches the liver through the portal vein and enters systemic blood circulation, eventually reaching host tissues and modulating host metabolism and inflammation (Koh et al., 2018).

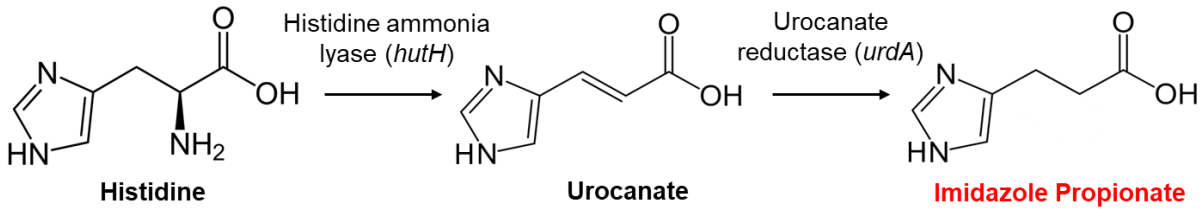

Figure 2: Schematic representation of imidazole propionate biosynthesis from histidine. Imidazole propionate (ImP) is microbially produced from dietary uptake of the aromatic amino acid histidine, which comprises an amino (-NH2) and carboxylic acid (-COOH) functional group and a heterocyclic imidazole side chain. Bacterial histidine ammonia-lyase (encoded by the *hutH* gene) metabolizes histidine to urocanate as the first step of histidine degradation. Urocanate is further catalyzed by the bacterial-producing enzyme urocanate reductase (encoded by the *urdA* gene), finally mediating ImP production in gut microbiota. Arrows in the illustration represent the corresponding enzymatic reactions and intermediates (modified from (Koh et al., 2018)).

Currently, studies on ImP and its contribution to disease development are limited. However, Koh et al. investigated the mechanistic role of ImP for the first time and demonstrated that ImP causes glucose intolerance and disrupts insulin signaling in both humans and mice (Koh et al., 2018). This valuable research has shed light on the underlying ImP-related mechanisms in T2D pathogenesis. Additionally, their study revealed that individuals with pre- and type 2 diabetes had higher ImP plasma levels compared to healthy individuals, suggesting that ImP may have a systemic impact on the human body. Remarkably, these outcomes were unrelated to the precursor compound, urocanate (Koh et al., 2018). Moreover, the research group could also demonstrate a rise in ImP production among T2D patients by challenging microbial communities with histidine using an *in vitro* gut simulator and fecal microbial culture experiments (Molinaro et al., 2020). Interestingly, elevated levels of ImP have been observed in individuals with low bacterial gene richness and the Bacteroides 2 enterotype, which is linked to a higher gene abundance related to the ImP biosynthesis

from dietary histidine. However, the elevated ImP levels are not solely due to high histidine intake but rather to the altered microbial metabolism of histidine (Molinaro et al., 2020).

Mechanistically, ImP has been shown to induce glucose intolerance and promote insulin resistance in mice by downregulating the expression of insulin receptor substrates (IRS) in the liver, muscle, and adipose tissue through sustained activation of p38γ/ p62/ mTORC1 signaling pathway (Koh et al., 2018). Additionally, Koh and colleagues have further analyzed the mechanism of ImP on the glucose-lowering effects of metformin, which is widely used as an oral drug for treating T2D (Koh et al., 2020). ImP elicits inhibitory functions on metformin action in T2D patients with high blood glucose levels. It contributes to insulin resistance by altering AMP-activated protein kinase (AMPK) activity in HEK293 cells and murine hepatocytes. This response was mediated by ImP-induced inhibitory AMPK serine phosphorylation via p38γ kinase activity, followed by basal AKT activation in the short term (Koh et al., 2020). In particular, the AKT(Thr308)/ AMPK axis is proposed as part of the mechanism for the ImP-induced inhibition on metformin action. However, insulin-stimulated hepatic-AKT(Ser473) phosphorylation was reduced upon long-term exposure to ImP due to the rapid turnover of IRS (Koh et al., 2020).

Little is known about the interaction between ImP and CVD; however, initial findings from a sub-analysis stratified according to CVD risk factors indicate increased circulating ImP concentrations in patients with overt CVD (Molinaro et al., 2020). Additionally, a recent study highlights that individuals with heart failure exhibited significantly higher plasma levels of ImP compared to control individuals, independently of the diabetic status. Increased ImP levels were associated with reduced left ventricular systolic heart functions (Molinaro et al., 2023). Moreover, there was a notable increase in the circulating levels of amino-terminal proANP and NT-proBNP, which are biomarkers of cardiomyocyte stress or strain. This increase was observed in parallel with rising levels of ImP in the highest quartile, where patients may have a significantly higher likelihood of experiencing heart failure with an increased risk for overall mortality (Molinaro et al., 2023). Our study on ImP in coronary artery disease further supports an association between ImP and atherosclerotic coronary artery disease (Nageswaran et al., 2023, *submitted*). Our study provides evidence that elevated plasma levels of ImP can effectively predict increased risks for prevalent

atherosclerotic coronary artery disease. These findings contribute to the understanding of the role of ImP and its underlying mechanisms in cardiometabolic and -vascular diseases, including atherosclerosis (Nageswaran et al., 2023, *submitted*).

1.6. Therapeutic intervention

Overall, atherosclerosis is a significant health concern and one of the major global causes of mortality (Kong et al., 2022). Early treatment and effective prevention strategies, including lifestyle modification (e.g., healthy diet, exercise, weight control, *etc*.) and pharmacological interventions, are crucial in reducing the risk of developing CVD and improving clinical outcomes (Libby and Everett, 2019; Kong et al., 2022). Current therapeutic strategies for atherosclerosis include management of lipid metabolism and hypertension or revascularization intervention for clinically manifested atherosclerosis, such as angioplasty or coronary artery bypass surgery (Hetherington and Totary-Jain, 2022). For example, statin or PCSK9-targeted therapy can mediate lipid-lowering effects by decreasing total and LDL-cholesterol levels in circulation. Thus, it has improved survival rates and reduced the implication of revascularization procedures in patients (Zimmermann et al., 2020; Hetherington and Totary-Jain, 2022). In addition, inhibition of PCSK9 has been shown to effectively reduce vascular and systemic inflammation and atherosclerotic progression (Kong et al., 2022).

Targeting the gut microbiome has emerged as a potential therapeutic strategy for treating CVDs in experimental settings. The microbiome-host axis includes multiple layers of interactions, such as dietary precursors, microbial communities, and their bioactive metabolites with potential therapeutic targets for modulating the host microbial community and phenotype (Witkowski et al., 2020). Therefore, different therapeutic approaches have been reported to directly modulate the gut microbiome promoting cardiovascular health (Tang et al., 2019a). Intake of antimicrobial agents, such as poorly absorbed antibiotics, may lead to suppression of microbial pathogens in the gut; however, these interventions may also have potential drawbacks as they can harm the gut microbiome in the long-term treatment by favoring the selection of bacterial communities, eventually resulting in antibiotic resistance (Witkowski et al., 2020). Furthermore, the use of probiotics and prebiotics has emerged as a more promising approach with potential therapeutic benefits. Probiotics (live microorganisms) and prebiotics (non-microbial compositions) have been shown to

have positive effects on gut microbial functions (Witkowski et al., 2020). For instance, in *Apoe*$^{-/-}$ mice, prebiotic supplementation of inulin-type fructans to the diet was observed to effectively reverse endothelial dysfunction in carotid arteries by activating the NO synthase/ NO pathway by NO-producing bacteria (Catry et al., 2018). In another mouse study, probiotic administration of *Akkermansia muciniphila* reduced aortic macrophage infiltration and atherosclerosis in *Apoe*$^{-/-}$ mice through gut barrier restoration (Li et al., 2016). Nevertheless, it remains uncertain whether most of the administered microbes can survive the acidic environment of the stomach during colonization in the colon and whether the observed beneficial effects are directly mediated by themselves or rather by secondary effects on host immune response and function or interindividual gut microbial diversity. Hence, predicting outcomes following probiotic or prebiotic administration has posed challenges (Witkowski et al., 2020).

Other potential therapeutic interventions include diet, novel host or bacterial enzyme inhibitors, and fecal microbial transplantation therapy, which may help to regulate gut microbiome-derived metabolite production. Recent data indicates that the microbiota significantly contributes to variations observed in metabolic responses to a specific diet (Koh et al., 2018). Dietary interventions have primarily focused on dietary fibers, which serve as substrates for bacterial fermentation producing beneficial metabolites, such as SCFCs, associated with improved host metabolism (Koh et al., 2018). A diet deficient in fiber and unsaturated fatty acids can lead to a dysbiotic microbiome, followed by increased microbial production of ImP (Molinaro et al., 2020). However, controlling food intake and nutrient precursors for defined metabolites generated by the gut microbiota can be more challenging (Witkowski et al., 2020). The Inhibition of *urdA*, the key enzyme responsible for ImP production from histidine, can be considered a novel therapeutic strategy to lower circulating ImP levels (Molinaro et al., 2020). Therefore, developing pharmacological interventions for drugging the microbiome using nonlethal microbiota-targeting inhibitors may present a novel, effective therapeutic approach to treat and prevent CVDs (Witkowski et al., 2020).

2. Objective of the study

In recent years, there has been growing interest in the relationship between cardiovascular disease and the gut microbiome. Dysregulation of the gut microbiome influences host tissue-specific metabolism through small bioactive metabolites derived

by intestinal microorganisms that may contribute to the pathogenesis of several cardiometabolic and -vascular disorders. Imidazole propionate (ImP) is a microbially derived metabolite from bacterial histidine metabolism, which is increased in patients with pre- and type 2 diabetes, both correlated with a higher risk of developing cardiometabolic and -vascular events. The increase in ImP production is related to altered gut microbiome observed in diabetic patients. High ImP plasma concentrations also contributed to the pathogenesis of heart failure. In line with this, our research group identified elevated ImP plasma levels in patients with atherosclerotic coronary artery disease compared to the healthy group. However, the underlying molecular mechanisms of ImP in cardiovascular diseases, including atherosclerosis, remain unknown. Based on these findings and the fact that endothelial dysfunction represents a fundamental step in the progression of atherosclerosis, the study focused on the effects of ImP on endothelial cell function and inflammatory activation, as well as on endothelial regeneration after injury *in vivo* and the development of atherosclerosis in atheroprone *Apoe*$^{-/-}$ mice.

3. Methods and Materials

3.1. *In vitro* experiments

3.1.1. Cell culture of HAECs

Primary human aortic endothelial cells (HAECs) (Cell Applications) were used between passages 7 and 9 for *in vitro* experiments. HAECs were cultured in Endothelial Growth Medium-2 (EGM-2) supplemented with 10% fetal calf serum (FCS), 100 units/ml penicillin and 100 µg/ml streptomycin at 37 °C in 18.6% O2 and 5% CO2 atmosphere in a humidified incubator. At 80-90% confluence, the cells were washed with 10 ml of 1x PBS to remove the remaining media and dead cells. Afterward, cells were detached from the flask surface with 2.5 ml of Trypsin-EDTA for 5 minutes at 37°C, and the trypsin solution was neutralized with 7.5 ml of fresh EGM-2 containing 10% FCS. The cell suspension was transferred into a 15 ml falcon tube and centrifuged for 5 min at 300 x g at RT. The supernatant was carefully aspirated, and the cell pellet was resuspended in the appropriate volume of fresh EGM-2 media for cell counting using a hemocytometer (Neubauer cell chamber). Different cell densities were used for different experimental approaches. All treatments were performed in a serum-low culture medium to synchronize the cell cycle and reduce serum protein interference.

3.1.2. Cell culture of THP-1

Human THP-1 monocytes were cultured in RPMI 1640 medium supplemented with 2 mM L-glutamine, 10% FCS, 100 U/mL penicillin and 100 µg/mL streptomycin. THP-1 cells were grown at 37°C under 5% CO_2 humid atmosphere prior to experiments.

3.1.3. Wound healing assay

Endothelial wound healing was assessed by cell scratch assay *in vitro*. First, 24-well culture plates were coated with 10 µg/ml fibronectin in 1x of PBS (PromoCell) for 7 min at 37°C. Then 6 x 10^4 HAECs per well were seeded on a fibronectin-coated 24-well plate and cultured overnight. Before treatment, cells were serum-starved (0.5% FCS) for 5 h at 37°C in a cell culture incubator. Following starvation, the endothelial cell monolayer was scraped with a sterile p200 pipette tip generating a straight scratch. Cell debris was watched off using 300 µl of pre-warmed culture medium and HAECs were treated with 10 nM ImP, 100 nM ImP, 10 ng/ml recombinant tumor necrosis factor-alpha (TNF-α) or control for 16 h. Pictures of the wound area were taken before treatment (time point zero) and 16 h post migration using a phase-contrast microscope (EVOS). The width of the scratch was measured by NIH ImageJ image analysis software.

3.1.4. Tube formation assay

Angiogenesis was analyzed in HAECs on Matrigel using growth factor-reduced basement membrane extract (BME, Gibco) in a 96-well flat bottom plate. In brief, 60 µl of ice-cold BME was placed in each well and incubated at 37°C for 30 min. After coating, HAECs were seeded on top of the Matrigel at a cell density of 1.5 x 10^4/well. Then, cells were stimulated in 100 µl of conditioned medium with control, 50 ng/ml insulin-like growth factor 1 (IGF-1), 100 nM ImP or 10 ng/ml recombinant TNF-α for 16 h. After HAECs formed tubular networks, cells were stained with 6 µM of Calcein AM solution (R&D System, USA) for 15 min at 37°C. Representative images were then taken using a fluorescent inverted microscope (BZ-X; Keyence Corporation, Ōsaka Japan), and endothelial tube formation was quantified with the *Angiogenesis Analyzer* tool in ImageJ software.

3.1.5. Flow cytometry

Cellular adhesion molecule expressions of ICAM-1, VCAM-1 and E-selectin were analyzed by fluorescence-activated flow cytometry (FACS). HAECs (6 x 10^4 /well) were seeded on 24-well plates and stimulated with a control medium, 10 nM ImP or 100 nM ImP for 24 h. Following stimulation, supernatant was collected into FACS tubes and attached cells were washed with 1x of PBS, trypsinized, and collected for FACS analysis. Cells were incubated using the following antibodies: ICAM-1/ CD54 (AF700, clone: HA58, 1:100), VCAM-1/ CD106 (APC, clone: STA, 1:100) and E-selectin/ CD62E (PE/ Cy7, clone: HAE-1f, 1:100) for 15 min at RT. All antibodies were purchased from BioLegend (San Diego, USA). Fluorescence-minus controls (FMOs) and unstained HAECs were included in the measurements. Samples were acquired using an Attune Nxt Flow Cytometer (Thermo Fisher Scientific, Waltham, MA, USA), and gating of the cell-specific population was analyzed with Kaluza software (version 5.0; Beckman & Coulter, Brea, CA). Changes in the expression of cellular adhesion molecules were expressed as percentages.

3.1.6. Flow adhesion assay

Monocyte-endothelial cell interaction was assessed by a flow-based adhesion assay. Briefly, 200 µl of 0.2 x 10^4 HAECs were seeded at confluence in Ibidi y-shaped chamber slides (ibidi GmbH, Germany) for 5 h. Once cell attachment was achieved, flow chambers were connected to the ibidi pump system using yellow/green perfusion sets and incubated overnight under unidirectional flow conditions using a shear stress of 20 dyn/cm^2. After acclimatization, cells were stimulated with control, 10 nM ImP, 100 nM ImP and 10 ng/ml recombinant TNF-α for 24 h, respectively. Next, cultured THP-1 monocytes (1 × 10^6 cells/ml per condition) were labeled with 1,1'-dioctadecyl-3,3,3',3'-tetramethylindocarbocyanine cell stain (DiI; Invitrogen, Carlsbad, USA) for 15 min at 37°C, and subsequently after one time washing the cells with PBS, the monocytes were perfused through the chambers for 30 min. After flow termination, non-adherent monocytes were removed with PBS and cells were fixed with 4% PFA. The number of adherent monocytes to HAECs was captured from different fields using a fluorescence phase-contrast microscope (BZ-X; Keyence Corporation) and was quantified by ImageJ software.

3.1.7. RNA extraction for RNA sequencing

Total RNA was extracted from ECs after stimulation with ImP (100 nM) or control for 12 h using the RNeasy Mini Kit (Qiagen, Hilden, Germany) according to the manufacturer´s instructions. The RNA purity and yield were measured with NanoVue (GE Healthcare), and ribosomal RNA integrity was confirmed by native agarose gel electrophoresis stained with ethidium bromide (EtBr). In brief, RNA samples (500 ng) were loaded on a 1% agarose gel with 0.5 µg/ml EtBr in 1x of TAE buffer and run at 100 V for 1 h. An intact RNA as a positive control and the DNA ladder (Nippon Genetics Europe GmbH) were included in the analysis. Total RNA was visualized under an ultraviolet (UV) light to assess RNA integrity. High-quality RNA samples of three replicates from three independent experiments were carried out for next-generation sequencing (NGS). RNA library preparation, sequencing and alignment of the reads were outsourced to GENEWIZ from Azenta Life Sciences (Leipzig, Germany). Library preparation was performed using the NEBNext Ultra II Directional RNA Library Prep Kit following the manufacturer's instructions (oligodT enrichment method). The samples were sequenced on an Illumina Novoseq 6000 platform with 150bp paired-end reads. Sequences were trimmed to remove adapter sequences and nucleotides with poor quality using Trimmomatic (v0.36). The trimmed reads were mapped to the human genome reference ENSEMBL version 86 using the STAR aligner (v2.5.2b). Gene counts were calculated with the featureCounts program in the Subread package (v1.5.2), only counting unique gene hits. The mean number of total reads per sample was 29.2±3.5 million, of which 99.6% were mapped, resulting in an average of 25±3.8 million counts per sample. Differential gene expression (DGE) was tested using the DESeq2 package (v1.36.0) in RStudio (v2022.07.2+576) with R (v4.2.1). Genes with an adjusted P-value <0.1 were considered as differentially expressed between control and ImP.

3.1.8. Western blotting

Whole-cell lysates from ECs were obtained using RIPA buffer (50 mM Tris, 150 mM NaCl, 1 mM EDTA, 1 mM NaF, 1 mM DTT, 10 mg/mL aprotinin, 10 mg/mL leupeptin, 0.1 mM Na3VO4, 1 mM PMSF, and 0.5% NP-40, pH 7.5). Briefly, cells were washed with ice-cold PBS prior to cell lysis with RIPA buffer for 10 min on ice. Adherent cells were scraped off the dish and cell lysates were centrifuged at 14.000 rpm for 10 min

at 4°C. The pellet was discarded, and the protein concentration was determined using Pierce™ BCA Protein Assay Kit (Thermo Scientific) according to the manufacturer´s description. A total protein of 20 µg of each sample was mixed with 1x Laemmli buffer and incubated at 95°C for 5 min. Extracted cell lysates and a molecular weight marker were separated on 8-10% SDS-PAGE under reducing conditions before being transblotted onto PVDF membranes (Merck). The membranes were blocked in 5% bovine serum albumin (BSA) or 5% skim milk in TBST for 1 h at RT and probed with primary antibodies against PI3 Kinase Class II α (Cell Signaling, 1:2000), Phospho-AKT(Ser473) (Cell Signaling, 1:1000), AKT (Cell Signaling, 1:1000), Phospho-FOXO1(Thr24) (Cell Signaling, 1:2000), FOXO1 (Cell Signaling, 1:2000) and GAPDH (Merck, 1:10´000) overnight at 4°C. Membranes were then washed three times in TBST for 10 min prior to incubation with horseradish-peroxidase-conjugated anti-rabbit or anti-mouse secondary antibody (Southern Biotechnology) for 1 hour at RT. Proteins were detected with SuperSignal® West Dura Extended Duration Substrate (Thermo Scientific) and the intensity of chemiluminescence was measured using a UVP ChemStudio PLUS imaging system (Analytik Jena). The expression of PI3KC2α, total AKT and total FOXO1 were normalized against GAPDH protein while phosphorylated AKT(Ser473) and phosphorylated FOXO1(Thr24) were normalized to the total protein content of AKT or FOXO1.

3.1.9. Immunocytochemistry

HAECs were cultivated on fibronectin-coated glass coverslips (round, 12 mm; Carl Roth), placed in a 12-well plate and treated with or without ImP (100 nM) for 24 h. After stimulation, cells were washed and fixed with 4% PFA for 15 min, permeabilized with 0.5% Triton X-100 in PBS for 15 min, and then blocked with 5% horse serum for 1 h, all at RT. Coverslips were rinsed with 0.1%BSA in PBS between each step. HAECs were stained overnight for anti-FOXO1 (Cell Signaling, 1:100) followed by DyLight 594-conjugated goat anti-rabbit secondary antibody (Invitrogen, 1:100) for 1h. Cell nuclei were counterstained with 4′,6-diamidino-2-phenylindole (DAPI; 0.1 µg/ml; Roche Diagnostics, Rotkreuz, Switzerland), respectively. Coverslips were washed three times and mounted in Kaiser's glycerol gelatin (Merck). The fluorescence intensity of nuclear FOXO1 staining was analyzed with a Keyence fluorescence microscope.

3.1.10. siRNA transfection

HAECs were plated at a density of 3 x 10^5 cells/well in the 6-well format before being transfected with *FOXO1* small interfering RNA (siRNA) or scramble siRNA (Santa Cruz) for 4 h in serum-free Opti-MEM medium (Gibco) using Lipofectamine RNAiMAX transfection Kit (Invitrogen) according to the manufacturer's protocol. After transfection, the medium was replaced with EGM-2 full medium overnight. Transfected cells were isolated for protein analysis as described previously and *FOXO1* gene silencing efficacy was confirmed on protein levels by Western blot. In addition, a rescue experiment of *FOXO1* siRNA transfection in HAECs treated with or without ImP (100 nM) for 24 h was designed to observe the rescue of the knockdown phenotype.

3.2. Mouse experiments

All mice used for these experiments were purchased from Charles River Laboratories, Germany. Adult male apolipoprotein E knockout (*Apoe*$^{-/-}$) mice (19-20 weeks of age) and wild type C57BL/6J mice (10 weeks of age) were housed in a specific pathogen-free facility ("Forschungseinrichtungen für Experimentelle Medizin" = FEM, Charité University Medicine Berlin, Germany) on a 12 h of day/night cycle with food and water *ad libitum*. All animal care and experimental procedures were conformed to the German/ European law for animal protection and were approved by the local ethics committee ("Das Landesamt für Gesundheit und Soziales" = LaGeSo, Berlin, Germany; *G0116/20* and *G0026/22*). The experimental animals were acclimatized to the environment for one week before the start of the treatment.

3.2.1. *In vivo*: Carotid Injury model

To investigate the effect of ImP on vascular regeneration *in vivo* carotid artery injury was performed in C57BL/6J mice that were assigned randomly to either the vehicle group (n=6) or the ImP group (n=6) for a total of 25 days (Figure 3). Normal water or ImP (400 µg/day, Santa Cruz) was administered via the drinking water. Carotid artery injury in mice was induced as described in (Sorrentino et al., 2007). In brief, animals were anesthetized with the inhalation of a gas mixture of oxygen and isoflurane using an anesthesia machine (Aestiva 3000, Datex Ohmeda). During anesthesia and surgery, the body temperature was monitored using a rectal thermometer and maintained at 37°C by a controlled heating pad to prevent hypothermia in mice. After

shaving and disinfecting the left neck area of the mouse, a small straight incision was made at the lower neck part. The skin was gently separated and underlying tissues (glands, muscular layer) around the incision wound were blunt dissected apart. The left carotid artery (LCA) was isolated and freed of overlying connective tissues and adjacent nerves. Subsequently, carotid injury was induced to LCA by an electric impulse of 2 Watt for 2 seconds over a length of 4 mm (scaled against millimeter paper) using a bipolar microforceps (VIO 50 C, Erbe Elektromedizin GmbH, Germany). After the arterial injury, underlying tissues and skin were carefully conjoined and the wound was closed with tissue adhesive (Histoacryl®, B. Braun, Germany). Mice were sacrificed 3 days after carotid injury and Evans blue staining of the vessels under deep isoflurane inhalation anesthesia followed by terminal blood collection by cardiac puncture.

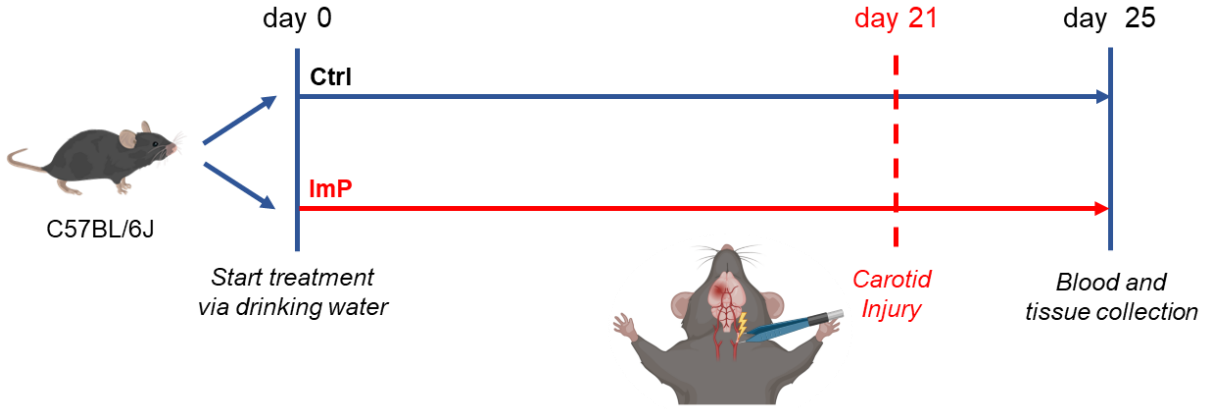

Figure 3: Experimental design of the murine carotid injury model.
For the assessment of the re-endothelialization after arterial injury, C57BL/6J mice were administered to control (Ctrl) or ImP (400µg/day) via drinking water for a total of 25 days (n=6). At day 21, carotid injury (CI) was induced to the left carotid artery (LCA) by an electric impulse of 2 Watt for 2 seconds over a length of 4 mm using a bipolar microforceps. After 3 days of CI and recovery animals were sacrificed for blood and tissue collection (CI model was created with BioRender.com).

3.2.2. Evans blue staining

Vascular re-endothelialization was assessed 3 days after carotid injury by Evans blue perfusion. Mice were injected with 50 µl of 5% Evans blue dye (Sigma) via the left heart ventricle. After two min of circulation, common carotid arteries (uninjured right carotid artery and injured left carotid artery) were isolated, rinsed in PBS and opened longitudinally before being fixed on microscope slides. Images of the denuded area visualized by Evans blue staining were obtained using a brightfield microscope (Axioskop 40, Zeiss). The re-endothelialization area was measured longitudinally as

the ratio of the remaining blue stained area (de-endothelialization area) to the total injured artery area (4mm) using imaging analyzer software (ImageJ, NIH, MD, USA).

3.2.3. *In vivo*: Atherosclerosis model

Apoe$^{-/-}$ mice were used to study the effect of ImP on the development of atherosclerosis. Male mice were randomly divided into a control group (n=8) or ImP group (n=8) and were fed a standard chow diet (SCD, crude fat 4.2%, cholesterol 14 mg/kg; ssniff, Germany, E15000) or a high-fat diet (HFD, crude fat 34.6%, cholesterol 290 mg/kg; ssniff, Germany, E15741) for 6 weeks (early stage of atherosclerosis) or 12 weeks (late stage of atherosclerosis). Simultaneously, ImP (800 µg/day) or vehicle were orally administered via drinking water. All mice were euthanized at the end of experiments following intraperitoneal injection of ketamine (200 mg/kg; CP-Pharma), deep isoflurane anesthesia and terminal blood sampling by cardiac puncture. Organs were collected and stored at -80°C for further examination (Figure 4).

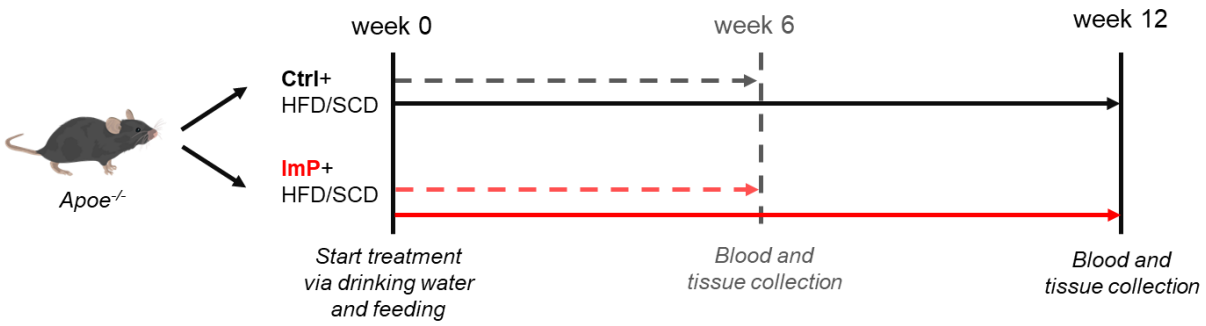

Figure 4: Experimental design of the mouse model of atherosclerosis.
For atherosclerotic plaque progression analysis Apoe-/- mice were fed a standard chow diet (SCD) or a high-fat diet (HFD) for 6 weeks (early atherosclerosis) or 12 weeks (late atherosclerosis) and additionally treated without (Ctrl) or with 800 µg ImP via drinking water for the same experimental duration (n=8). At termination of the experiment mice, were sacrificed for blood and tissue collection.

3.2.4. ImP plasma measurement

To assess the efficacy of the ImP drinking protocol in mice, blood was collected by cardiac puncture using a 1 ml syringe coated with ethylene-diamine-tetraacetic acid (EDTA, 0.5 M, pH 8) to prevent clotting. Whole blood was transferred into a 1.7 ml tube containing 50 µl of EDTA and gently mixed before being processed for plasma collection. Blood tubes were centrifuged at 1500 x g for 10 min at 4°C. Plasma samples were stored at −80°C for further analyses or shipped to the collaboration laboratory at the University of Gothenburg (Bäckhed group, Department of Molecular and Clinical

Medicine, Wallenberg Laboratory, Sweden) for plasma ImP measurement using an ultra-high-performance liquid chromatography (UHP-LC) coupled to tandem mass spectrometry (Metabolon, Durham, NC, USA) (Koh et al., 2018). Data quantification was performed in our laboratory.

3.2.5. Lipoprotein profile analysis

Murine EDTA-plasma samples from the control and ImP group fed an HFD for 6 or 12 weeks were sent to the collaboration laboratory at the Institute for Cardiovascular Prevention (IPEK) (AG Döring, Ludwig-Maximilians University (LMU), Munich, Germany) for quantification of lipoprotein fractions and cholesterol measurement. Briefly, fractions of different lipoproteins (VLDL, LDL, HDL) were separated and purified based on the flow-through time using a fast-performance liquid chromatography (FPLC) and gel filtration on Superose 6 columns (GE Healthcare) (Paulin et al., 2017). Total cholesterol levels were also measured in plasma samples using a commercial enzymatic-based assay (c.f.a.s., Cobas, Roche Diagnostics, #03039773190). Data quantification was performed in our laboratory.

3.2.6. *En face* of aorta

Atherosclerotic plaques in the aorta were assessed by *en face* method. After sacrifice and *in situ* perfusion of the vasculature with 5 ml 1x of phosphate-buffered saline (PBS), the aorta, including the distributing branches, were isolated from the mouse and adventitial adipose and connective tissues around the aorta were carefully dissected using a stereomicroscope (SMZ745T, Nikon). The aorta and the aortic arch branches were longitudinally cut open and placed in small tubes. Following overnight fixation with 1 ml of 4% PFA in 1 x of PBS at 4°C, aortas were washed twice in 1ml of PBS for 5 min at room temperature (RT) and incubated two times in 1 ml of 60% of isopropanol for 5 min. Next, aortic samples were stained with 0.5% Oil Red O (ORO) in 60% isopropanol for 30 min at RT under gentle shaking using a tube rotator. Following the staining process, the aortas were subjected to two washes using 60% isopropanol until the supernatant became clear. Subsequently, the aortas were placed on a black background for further analysis. *En face* preparation of the aortic arch region was photographed, and the plaque area was calculated as the percentage of ORO-stained area to the total aortic arch area.

3.2.7. Histological analysis

For histological evaluation of atherosclerosis progression in *Apoe*$^{-/-}$ mice, aortic roots were obtained from the base of the heart, known as the basis cordis. The heart tissues were embedded in Tissue-Tek OCT compound (Sakura) and frozen at −80°C until the cutting procedure. For sectioning the aortic roots, tissues were cut into 6 µm thick cryo-sections of the aortic root using a cryostat microtome (Microm HM 560, Thermo Fisher Scientific) and were fixed on glass slides (Super Frost Plus, Thermo Scientific). Before ORO-staining, sections were fixed in 4% PFA for 10 min and washed twice in PBS for 5 min. Tissue sections were then incubated in 78% methanol (diluted in double-distilled water/ ddH_2O) for 5 min and stained for 10 min in fresh ORO working solution (= filtered stock solution of 0.5% ORO in methanol was further diluted by 40% using 1 M NaOH in ddH_2O). Following ORO-staining, samples were cleaned in water to remove any excess stain and subsequently, the nuclei were lightly stained in hematoxylin. Finally, the slides were mounted in Kaiser's glycerol gelatin for preservation. The atherosclerotic plaque area was quantified by ImageJ software as a percentage of the total aortic root area.

3.2.8. Immunohistochemistry

Immunohistochemistry of frozen sections of the aortic roots was performed using the Avidin-Biotin Complex (ABC) Kits (Vector Laboratories). Briefly, acetone-fixed sections were washed in PBS before treatment with 0,075% H2O2 for 10 min to block endogenous peroxidase activity. The slides were then blocked with 10% rabbit serum (Dako) in an Avidin-Biotin blocking solution (Vector Laboratories) for 30 min each. Sections were incubated with primary antibody against CD68 (Abcam, 1:100) for 1 h and washed in PBS before being incubated with anti-rat biotinylated secondary antibody (Dako, 1:100) for 1 h. The slides were then treated with an ABC-HRP Kit for Peroxidase (Vector Laboratories) for 30 min, followed by AEC (3-amino-9-ethyl-carbazole, Sigma) staining for 12 min. Aortic roots were counter-stained in hematoxylin solution (Carl Roth) for 15 s and washed in ddH2O before mounting with gelatin medium. Macrophage accumulation was determined in lesions by calculating the percentage of CD68-positive staining to the total aortic root area.

3.3. Statistical analysis

Statistical analyses for the in vitro and in vivo analyses were performed by GraphPad Prism 9 (GraphPad Software, Inc) and presented as mean ± SEM. Normal distribution of data was calculated using the Shapiro-Wilk test and was analyzed by unpaired two-tailed Student t-test (for two groups) or one-way ANOVA followed by Bonferroni post hoc test (for ≥3 groups). Nonparametric statistical analyses were performed using the Mann-Whitney U test for two groups or the Kruskal-Wallis test, followed by the Dunn post hoc test for multiple comparisons (for ≥3 groups).

4. Materials

Table 1: Chemicals, buffer, solution

Chemicals, buffer, solution	Cat. No.	Composition/ company
primary human aortic endothelial cells (HAECs)	304-05a, Lot:2139	Cell Applications
Endothelial Cell Growth Medium-2 (EGM-2)	C-22111	PromoCell GmbH
Endothelial Cell Growth Basal Medium-2 (EBM-2)	C-22111	PromoCell GmbH
Imidazole Propionate (ImP)	sc294276 (CAS1074-59-5)	Santa Cruz
recombinant TNF-α	210-TA-005	R&D System
recombinant IGF-1	100-11-100UG	Peprotech, Inc.
RPMI 1640 medium	A1049101	Gibco®, Thermo Fisher Scientific
Opti-MEM medium	31985070	Gibco®, Thermo Fisher Scientific
fetal calf serum	S-10-M	cc-pro GmbH
Penicillin-Streptomycin (10.000 U/ml)	15140-122	Gibco®, Thermo Fisher Scientific
1x Phosphate-buffered saline	D8537-500ML	Sigma-Aldrich
ammonium persulfate	BP179-100	Fisher Scientific
TEMED	A1148,0025	PanReac AppliChem

Chemicals, buffer, solution	**Cat. No.**	**Composition/ company**
Trypsin-EDTA (0.05 %)	25300-054	Gibco®, Thermo Fisher Scientific
human fibronectin protein	C-43060	PromoCell GmbH
acrylamide/ bis solution	10681.01	Serva Electrophoresis GmbH
agarose gel	A9539-100G	Sigma-Aldrich
FastGene 1 kb DNA Ladder Plus	MWD1P	Nippon Genetics Europe GmbH
5x TAE Buffer:		
242 g Tris-base	188.4	Carl Roth
57.1 ml of 1 M acetate	A6283-500ML	Sigma-Aldrich
100 ml of 0.5 M EDTA	8043.2	Carl Roth
ethidium bromide	E1510-10ML	Sigma-Aldrich
RIPA Buffer (1 ml):		
1 M Tris-base, pH 7.5	188.4	Carl Roth
5M NaCl	HN00.3	Carl Roth
0.5 M EDTA, pH 8.0	8043.2	Carl Roth
10% NP-40	74385-1L	Sigma-Aldrich
0.5 M NaF	201154-5G	Sigma-Aldrich
1 M dithiothreitol (DTT)	R0861	Thermo Scientific™
2 mg/ml Aprotinin	13718.01	Serva Electrophoresis GmbH
2 mg/ml Leupeptin	51867.02	Serva Electrophoresis GmbH
10 mM Na3VO4	P0758S	New England BioLabs
0.1 M PMSF	6367.1	Carl Roth
PierceTM BCA Protein Assay Kit	23225	Thermo Scientific™
Lämmli Buffer (6X):		
0.75 M Tris-HCl, pH 6.8	9090.3	Carl Roth
6% sodium dodecyl sulfate (SDS)	L5750-500G	Sigma-Aldrich
30% glycerol	3783.3	Carl Roth
60 mM DTT	R0861	Thermo Scientific™

Chemicals, buffer, solution	Cat. No.	Composition/ company
0.03% bromophenol blue	B5525-5G	Sigma-Aldrich
PageRuler™ Plus Prestained Protein Ladder	26616	Thermo Scientific™
PageRuler™ Plus Prestained Protein Ladder	26619	Thermo Scientific™
glycine	1.04201.100	Merck Millipore
Tween®20	663684B	VWR
Immobilon-PSQ PVDF membrane	ISEQ00010	Merck Millipore
skim milk powder	42590	Serva Electrophoresis GmbH
bovine serum albumin (BSA) Fraktion V	8076.5	Carl Roth
SuperSignal™ West Dura Extended Duration Substrate	34075	Thermo Scientific
Geltrex™ LDEV-Free, Reduced Growth Factor Basement Membrane Matrix	A14133-02	Gibco
Calcein AM	4892-010-01	R&D System
Ibidi µ-Slide y-shaped slides	80126	ibidi GmbH
Ibidi Perfusion Set (yellow-green)	10964	ibidi GmbH
Vybrant™ DiI Cell-Labeling Solution	V22885	Invitrogen
RNeasy Mini Kit	74104	Qiagen
glass coverslips	01-2460/S	R. Langenbrinck GmbH
normal horse serum	31874	Invitrogen
Lipofectamine RNAiMAX transfection Kit	13778150	Invitrogen
histoacryl tissue adhesive	1050052	B. Braun
Evans blue dye	E2129-10G	Sigma-Aldrich

Chemicals, buffer, solution	Cat. No.	Composition/ company
Super Frost Plus microscope glass slides	03-0060	R. Langenbrinck GmbH
standard chow diet (SCD, crude fat 4.2%, cholesterol 14 mg/kg)	E15000-04	ssniff, Germany
high fat diet (HFD, crude fat 34.6%, cholesterol 290 mg/kg)	E15741-34 D12492 (II)	ssniff, Germany
Image-iT™ fixative solutions (4% PFA)	FB002	Invitrogen
ROTI®Histofix	P087.5	Carl Roth
acetone	20065.293	VWR
isopropanol	CP41.2	Carl Roth
ethanol	5054.1	Carl Roth
Tissue-Tek OCT compound	4583	Sakura
Oil Red O (ORO) dye	A12989.22	Alfa Aesar
hematoxylin solution	T865.2	Carl Roth
hydrogen peroxide	8070.2	Carl Roth
normal rabbit serum	X0902	Agilent Dako
avidin-biotin blocking solution	SP-2001	Vector Laboratories
ABC-HRP Kit for peroxidase	PK-4000	Vector Laboratories
3-amino-9-ethyl-carbazole (AEC)	A5754	Sigma-Aldrich
kaiser′s glycerol gelatine	1.09242.0100	Merck
4′,6-diamidino-2-phenylindole (DAPI)	10236276001	Roche Diagnostics

Table 2: Antibodies

Antibody	Cat. No	Company
PI3 Kinase Class II α (D3Q5B)	12402S	Cell Signaling Technology
anti-phospho AKT(Ser473)	4060S	Cell Signaling Technology
anti-AKT	9272S	Cell Signaling Technology

Antibody	Cat. No	Company
anti-phospho FoxO1 (Thr24)/ FoxO3a (Thr32)	9464S	Cell Signaling Technology
anti-FOXO1 (C29H4)	2880S	Cell Signaling Technology
anti-GAPDH (clone 6C5)	MAB374	Merck Millipore
HRP-conjugated goat anti-mouse IgG (H+L)	1031-05	SouthernBiotech
HRP-conjugated goat anti-rabbit IgG(H+L)	4050-05	SouthernBiotech
DyLight 594-conjugated goat anti-rabbit	35560	Invitrogen
Alexa Fluor® 700 anti-human CD54 (ICAM-1)	353126	BioLegend
APC anti-human CD106 (VCAM-1)	305810	BioLegend
PE/ Cyanine7 anti-human CD62E (E-selectin)	336016	BioLegend
recombinant anti-CD68 (rat monoclonal [FA-11])	ab5344	Abcam
anti-rat biotinylated secondary antibody	E0468	Dako

Table 3: RNAi duplex

RNAi duplex	Cat. No	Company
FKHR/ FOXO1 siRNA (human)	sc-35382	Santa Cruz
scrambled siRNA (control)	sc-37007	Santa Cruz

Table 4: Electrical devices

Electrical device	Company
Ultrapure water system (Purantity PU 20+ UV/UF) (ddH_2O)	VWR European Cat. No. 171-1230
anesthesia machine	Aestiva 3000, Datex Ohmeda

rectal thermometer	PhysioSuite, Kent Scientific
heating pad	PhysioSuite, Kent Scientific
bipolar microforceps	VIO 50 C, Erbe Elektromedizin GmbH
brightfield microscope	Axioskop 40, Zeiss
Centrifuge 5427R	Eppendorf
stereomicroscope	SMZ745T, Nikon
Microm HM 560 cryostat microtome	Thermo Fisher Scientific
cell culture incubator (Binder CB220)	Franz Binder GmbH & Co
cell culture hood (Herasafe 2023)	Thermo Scientific
phase-contrast microscope	EVOS
fluorescent inverted microscope	BZ-X; Keyence Corporation
Attune Nxt Flow Cytometer	Thermo Fisher Scientific
ibidi Pump	ibidi GmbH
NanoVue	GE Healthcare
UVP ChemStudio PLUS imaging system	Analytik Jena GmbH
Tecan Infinite® 200 PRO reader	Tecan Group
Mini-PROTEAN Tetra Cell	Bio-Rad Laboratories, Inc.

5. Results

5.1. ImP impairs endothelial cell migration

To investigate the potential impact of ImP on endothelial migratory property, a conventional scratch wound assay was conducted using human aortic endothelial cells (ECs). The migration of ECs was significantly attenuated after 16 hours in response to both 10 nM and 100 nM concentrations of ImP compared to the control cells (Figure 5A, B). As a positive control, the stimulation of HAECs with TNF-α (10 ng/ml) resulted in decreased migration, demonstrating the inhibitory effect on the migratory ability of the cells. The results are presented as the mean difference with a 95% confidence interval (CI) between the control and treatment groups. The wound closure rate was assessed by calculating the percentage of the gap area between the initial time point (0 h) and the 16 h time point of treatment.

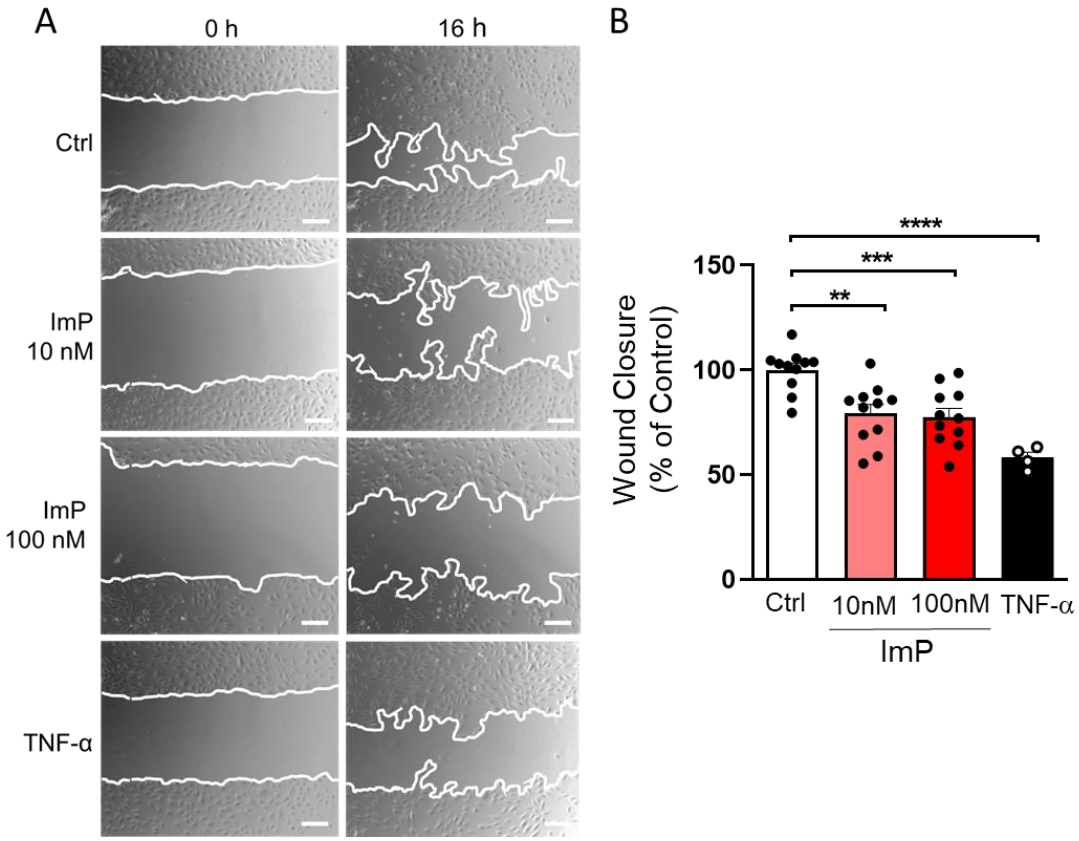

Figure 5: Imidazole propionate impairs migratory ability of endothelial cells.
(A) Representative images of HAECS migration treated with and without ImP, or TNF-α as a positive control, are plotted at time 0 h (baseline) and 16 h (after treatment). The leading edges of migrating cells are highlighted in white. The images were captured at a 10X magnification, and the scale bars represent 250 µm. (B) Quantification of EC migration ability (n=11/4). The wound healing area was compared between the control group (Ctrl) and those groups treated with 10 nM ImP, 100 nM ImP, or 10 ng/ml TNF-α. The data are presented as mean ± SEM

(95% CI) and were analyzed with one-way ANOVA followed by the Bonferroni post hoc test for multiple comparisons (**=*P*<0.01, ***=*P*<0.001, ****= *P*<0.0001).

5.2. ImP disturbs tube formation of endothelial cells

To examine the impact of ImP on the tube formation capability of HAECs indicative of their angiogenic potential, the cells were seeded onto a Matrigel matrix and subsequently stimulated with 100 nM ImP, recombinant TNF-α (10 ng/ml) or IGF-1 (50 ng/ml). Following staining with Calcein AM, the ability of HAECs to form tube-like structures was captured at time point 16 h and determined by counting the total number of segments (Figure 6A). Quantitative data were expressed as percentages to untreated controls and mean difference scores with 95% CI. The results indicate that treatment with 100 nM ImP resulted in a significant decrease in tube formation of HAECs. The finding was evidenced by the presence of disrupted cellular segments, which differed noticeably from the untreated control group (Figure 6A, B). In addition to the treatment with 100 nM ImP, a decrease in tube formation was also observed in the positive control cells treated with TNF-α. Interestingly, unstimulated control and IGF-1, known as a pro-angiogenic factor, showed similar tube-forming ability. These findings indicate that both the control and IGF-1-treated cells displayed clear tube morphogenesis.

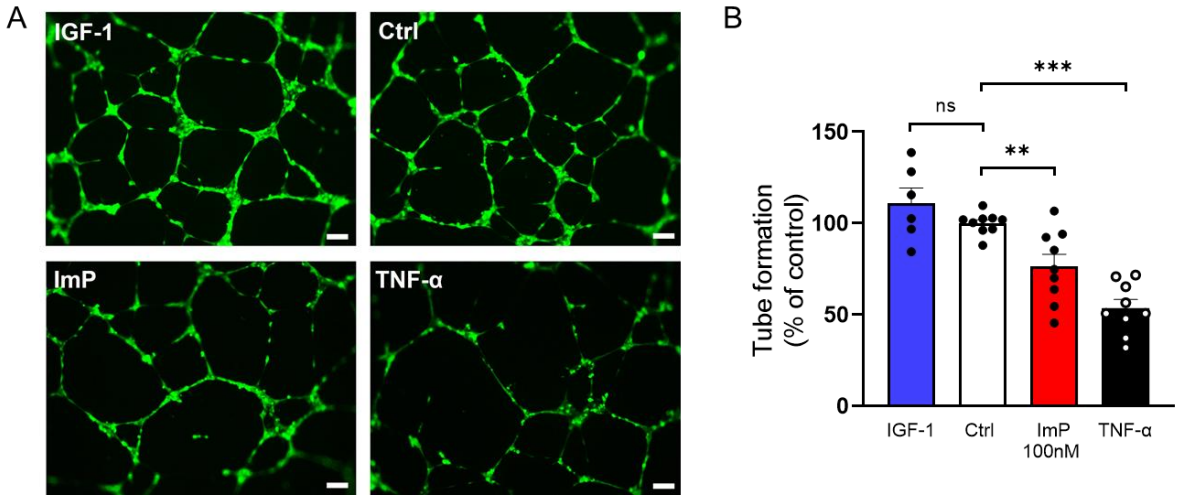

Figure 6: Imidazole propionate diminishes angiogenic properties of endothelial cells. (A) The representative images illustrate the tube formation of HAECs following treatment with IGF-1 (50 ng/ml), control (Ctrl), ImP (100 nM), or TNF-α (10 ng/ml). The endothelial cell tube structures on the Matrigel were stained with Calcein-AM, resulting in green fluorescence. The images were captured at a 10X magnification, and the scale bar represents 100 µm. (B) The graph displays the percent change in tube formation capacity quantified by measuring the total number of segments (n=9). Data are mean ± SEM (95% CI) and were tested with one-way

ANOVA followed by the Bonferroni post hoc test for multiple comparisons (ns=no significance, **=P<0.01, ***= P<0.001).

5.3. ImP increases expression of adhesion molecules ICAM-1, VCAM-1 and E-selectin

Flow cytometry analysis of HAECs was conducted to assess the impact of ImP on endothelial inflammatory activation. For this, the cells were treated with ImP (10 nM and 100 nM) and, subsequently, the expression levels of cellular adhesion molecules, including ICAM-1, VCAM-1, and E-selectin, were quantified. Interestingly, treatment of ECs with 10 nM ImP for 24 h resulted in an upregulation of ICAM-1 expression (Figure 7A). Moreover, there was a tendency towards upregulation of E-selectin and VCAM-1 level without a significant difference compared to the control group (Figure 7B, C). Treatment with 100 nM ImP significantly induced inflammatory activation of HAECs, enhancing the expression of all three adhesion molecules when compared to the control group.

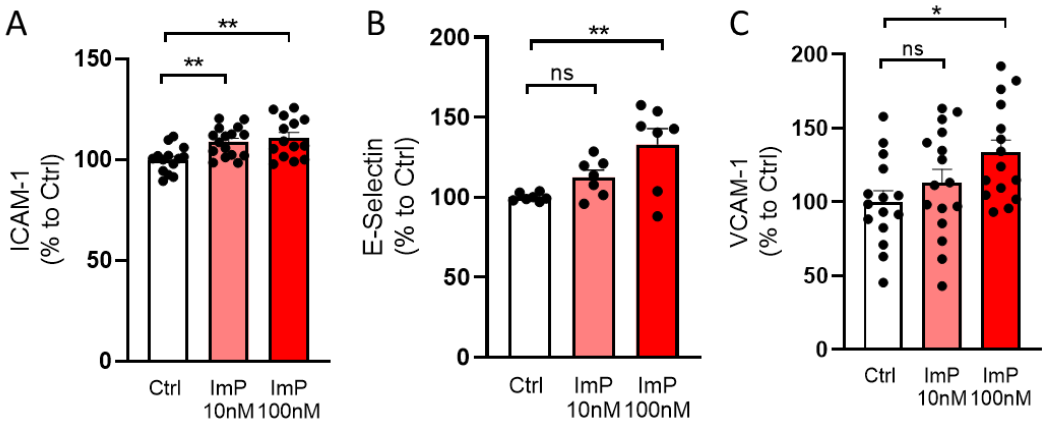

Figure 7: Imidazole propionate promotes endothelial inflammation by inducing the expression of cellular adhesion molecules.
The activation of endothelial cells was assessed after 24 hours of stimulation with ImP at concentrations of 10 nM and 100 nM. The expression levels of pro-inflammatory adhesion molecules, including (A) ICAM-1, (B) E-Selectin and (C) VCAM-1 were measured using flow cytometry. The results were expressed as the percentage of mean fluorescence intensity (MFI) relative to the control cells (n=7/14). The data are presented mean ± SEM (95% CI) between control and 10 nM or 100 nM ImP and were analyzed by one-way ANOVA followed by the Bonferroni post hoc test for multiple comparisons (*ns*=no significance, *=*P*<0.05, **=*P*<0.01).

5.4. ImP increases adhesion of monocytes to endothelial cell monolayer

The adhesion of monocytes to ImP-activated ECs under constant shear flow conditions was evaluated using a flow-based adhesion assay (Ibidi). In this experiment, HAECs

were subjected to stimulation with two different concentrations of ImP, 10 nM or 100 nM, for a duration of 24 h under a shear stress of 20 dyn/cm^2. Following the stimulation, THP-1 monocytes were allowed to roll on the HAEC monolayer, and the number of adhered THP-1 monocytes was quantified from multiple fields of view. The results demonstrated no significant increase in monocyte adhesion to HAECs following stimulation with 10 nM ImP. However, the higher concentration of ImP (100 nM) exhibited a tendency to enhance the adhesion of THP-1 monocytes to ECs after 24 h when compared to control cells (Figure 8A, B).

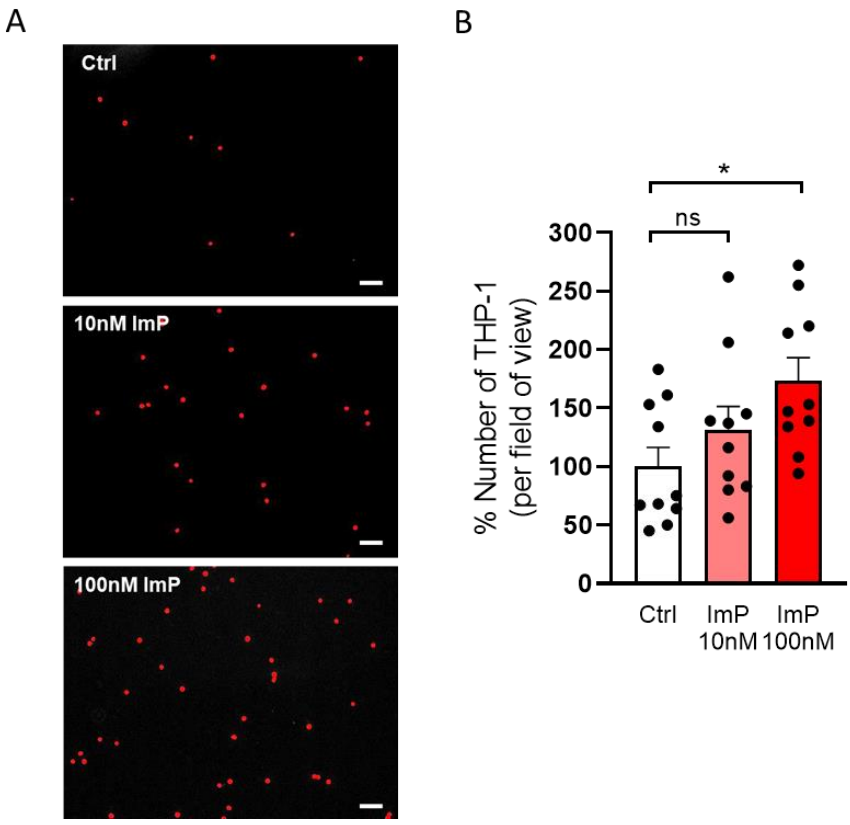

Figure 8: Imidazole propionate increases adhesion molecules.
(A) Illustrative images displaying DiI-labeled THP-1 monocytes (red dots) adhered to endothelial cells upon 24 h stimulation in the absence or presence of ImP (10 nM or 100 nM). The images were captured at a magnification of 10X, and the scale bars indicate a length of 100 µm. (B) Quantification of THP-1 adhesion to HAECs was determined as a percentage per field of view (n=10). The data are analyzed by the Kruskal-Wallis test followed by the Dunn post hoc test for multiple comparisons (*ns*=no significance, *=*P*<0.05).

5.5. RNA integrity control

Total RNA from ImP-treated ECs and control cells were extracted and subjected to RNA sequencing. Before the samples were outsourced for NGS analysis, RNA integrity control was confirmed by agarose gel electrophoresis stained with EtBr. The gel images depict two bands representing the 28S and 18S ribosomal RNA (rRNA)

species. High-quality RNA is considered as the ratio of 28S:18S bands, which results in 2.0 or higher (Schroeder et al., 2006). After calculating the band intensities of 28S and 18S of each probe by ImageJ, the results showed a value of about 2.1, which is indicative of intact and high-quality RNA similarly observed to the positive control (Figure 9).

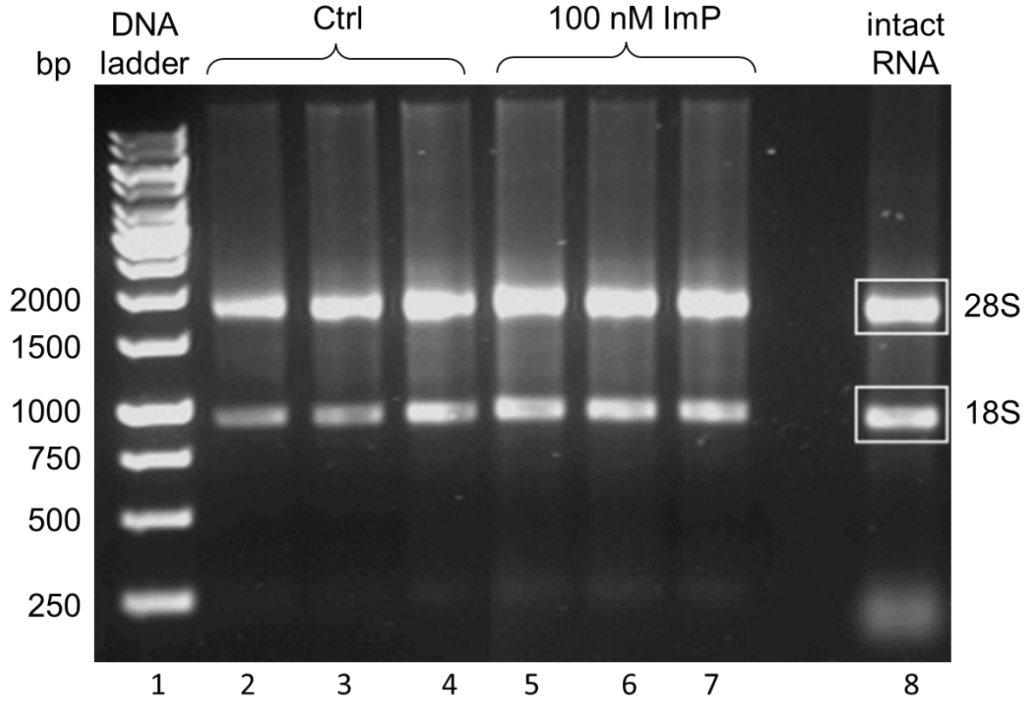

Figure 9: RNA integrity of human endothelial cells assessed by agarose gel electrophoresis.
High-quality RNA of HAECs was prepared for RNA sequencing. Intact RNA was evaluated by 1% agarose/ EtBr gel representing 28S and 18S rRNA bands in a proportion of 2:1. Lane 1 represents the DNA ladder (100-10.000 base pairs (bp)), lane 2-4 the control group, lane 5-7 the ImP group, and lane 8 the positive control showing an intact RNA with a 28S:18S rRNA ratio. RNA samples were from three different experiments.

5.6. ImP deregulates PI3K and other angiogenesis-related genes

To gain better insights into the molecular mechanism underlying the effects of ImP on endothelial cell functions, RNA sequencing was conducted on ECs treated with ImP and untreated ECs. The observed changes in gene expression between control and ImP (100 nM) were visualized using a heat map, a volcano plot and a box plot, highlighting the specific genes that are affected by ImP treatment. The Z-score method and hierarchical cluster analysis (Ward's method) in the heat map were employed to identify variations in values between the samples and to normalize genes based on their standard deviations from the mean (white=zero mean) (Figure 10A). The volcano

plot depicted the negative log(10) adjusted P-value (y-axis) plotted against the log2-fold change (x-axis) in gene expression between the control and ImP-treated group (Figure 10B). Red dots represent genes with lower expression in ImP-treated HAECs compared to control, while blue dots represent genes with higher expression. As a result, 52 genes were differentially expressed between the control and ImP conditions. Among these genes, 18 genes were upregulated (red-colored clusters) and 34 genes were downregulated (blue-colored clusters) in the ImP-treated group compared to the control group. Notably, reduced expression of the *PIK3C2A* gene, which encodes phosphatidylinositol-4-phosphate 3-kinase C2 domain-containing alpha polypeptide (PI3KC2α), was found in ImP-treated ECs compared to controls. Moreover, transcript counts of different isoforms from the PI3K family, including *PIK3C3, PIK3CA*, and *PIK3CB,* were also downregulated upon ImP stimulation (Figure 10C).

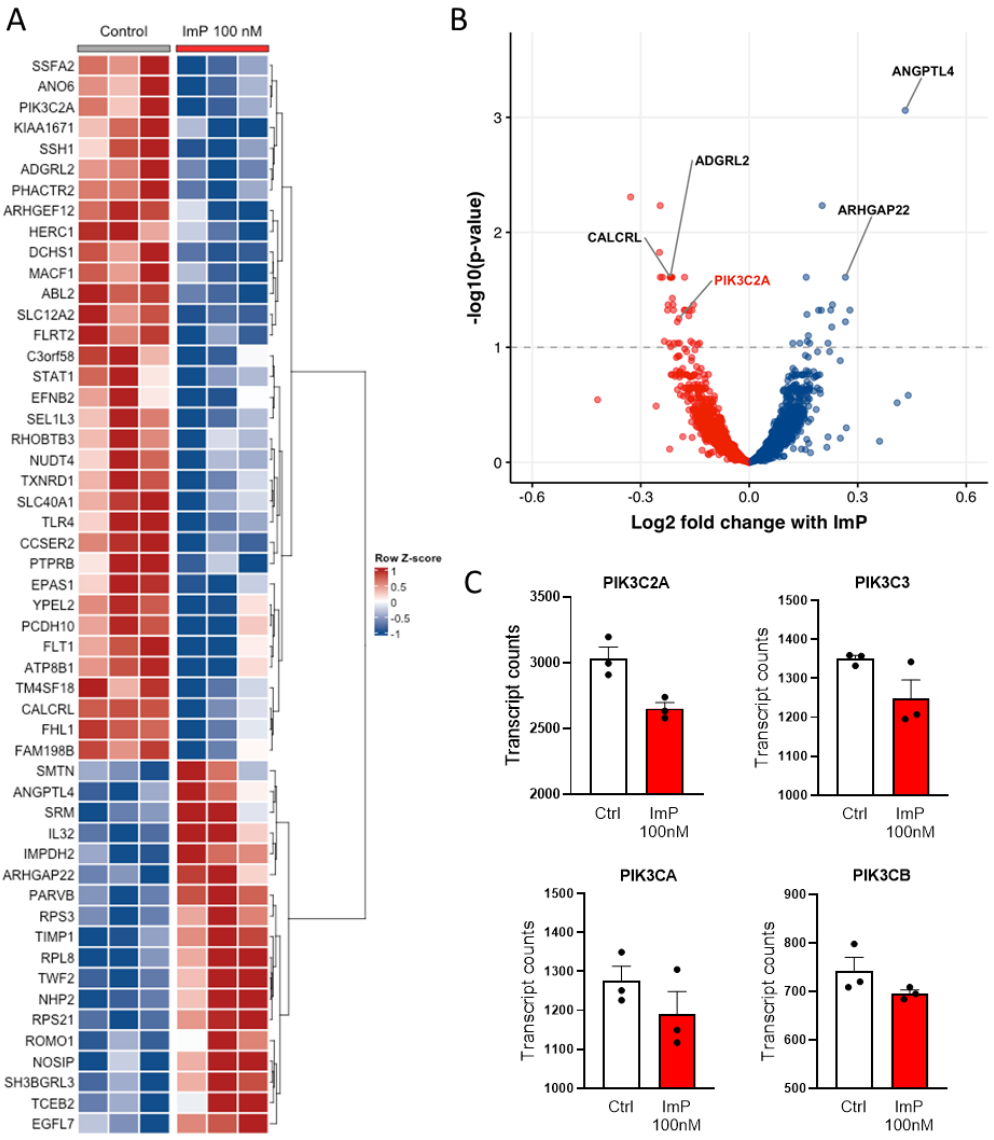

Figure 10: Transcriptomic profiling of HAECs revealed that ImP treatment led to the deregulation of angiogenic-related genes, including PI3K isoforms.
RNA sequencing analysis of HAECs and differentially expressed genes are illustrated here: (A) Heatmap with 52 differentially expressed genes between ImP (100 nM) and control group (adjusted p-value < 0.1). Gene counts were transformed to Z-scores (zero mean, unit variance scaling). The dendrogram on the right was drawn using hierarchical clustering (Ward's method). Upregulated genes are clustered in red and downregulated genes are clustered in blue. Color-intensive ranges were defined as standard deviations away from the mean (zero mean=white range) with a similar trend in gene expression. (B) Volcano plot demonstrates differentially expressed genes in endothelial cells of the control or ImP group. Red dots indicate genes with lower expression in ImP-treated HAECs compared to control, while blue dots indicate genes with higher expression. The x-axis denotes the log2 fold change values analyzed and the y-axis represents the –log10 adjusted P-values. Genes of interest, including *CALCRL*, *ADGRL2*, *ARHGAP22*, *ANGPTL4* and *PIK3C2A*, were highlighted in the plot. (C) Box plots of transcript count from genes of different isoforms from the PI3K family: *PIK3C2A*, *PIK3C3*, *PIK3CA* and *PIK3CB*. Quantitative data were from three independent experiments (n=3) and differential gene expression was analyzed using DESeq2 and R-software.

In addition, several genes involved in angiogenesis and inflammation were differentially expressed after ImP treatment: adhesion G protein-coupled receptor L2 (*ADGRL2*), calcitonin receptor-like receptor (*CALCRL*), VEGF receptor-1/fms related receptor tyrosine kinase 1 (*FLT1*), transmembrane 4 L six family member 18 (*TM4SF18*), dachsous cadherin-related 1 (*DCHS1*), fibronectin leucine rich transmembrane protein 2 (*FLRT2*), angiopoietin-like 4 (*ANGPTL4*), Rho GTPase activating protein 22 (*ARHGAP22*) and interleukin 32 (*IL32*) (Figure 11).

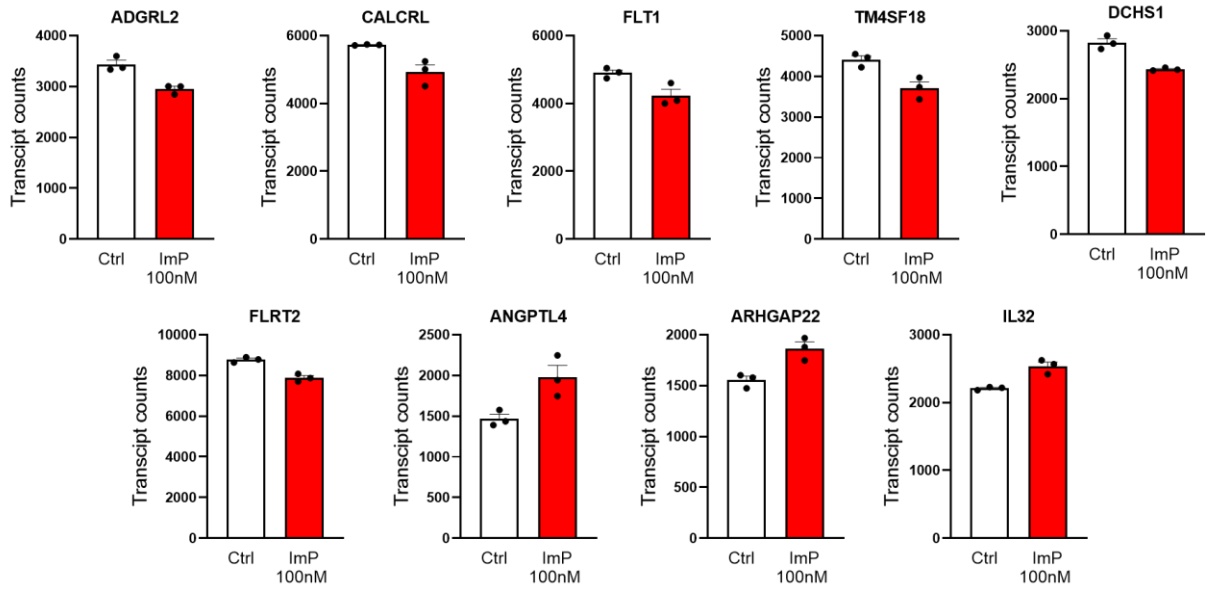

Figure 11: Imidazole Propionate downregulates several genes involved in angiogenesis and inflammation.
Box plot charts illustrating key down- or upregulated genes involved in angiogenesis/inflammation pathways, including *ADGRL2*, *CALCRL*, *FLT1*, *TM4SF18*, *DCHS1*, *FLRT2*, *ANGPTL4*, *ARGHGAP22*, and *IL32*. Represented data are transcript counts differentially expressed in endothelial cells after treatment with and without ImP (100 nM) and from three independent experiments.

5.7. ImP suppresses PI3K expression on protein level

To determine the impact of ImP on the protein expression of PI3KC2α, encoded by the *PIK3C2A* gene, human ECs were untreated and treated with different concentrations of ImP (10 nM, 100 nM and 500 nM), or TNF-α (10 ng/ml) for 24h. The protein level of PI3KC2α was quantified and normalized to the GAPDH expression (Figure 12). The findings demonstrated that ImP treatment exerted an inhibitory effect on the activation of PI3KC2α in a concentration-dependent manner. The expression of PI3KC2α was partially suppressed by 10 nM ImP compared to untreated cells (Ctrl). Furthermore, 100 nM and 500 nM ImP significantly decreased the protein level of PI3KC2α after 24 h of treatment. Like ImP, stimulation with TNF-α also resulted in a more pronounced reduction in the expression of PI3KC2α and was used as a positive control for suppressing PI3K signaling in HAECs.

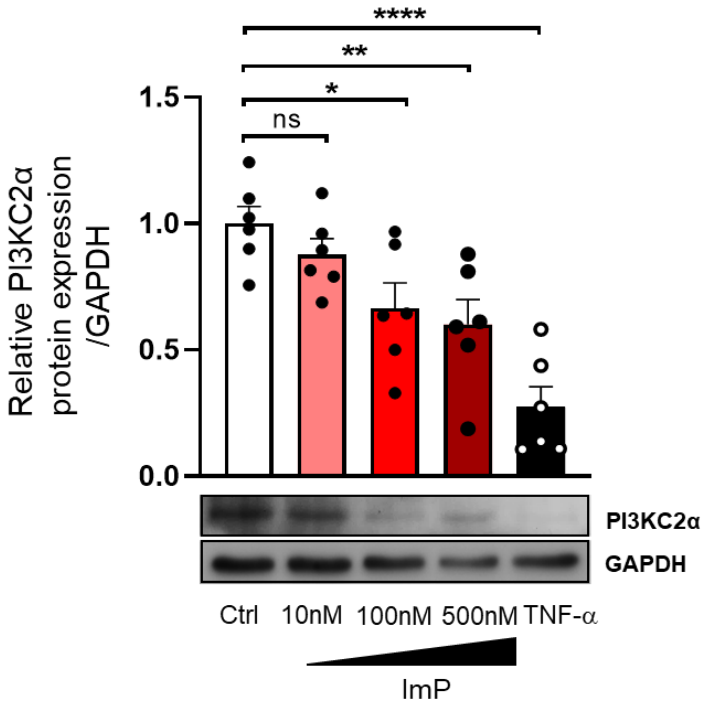

Figure 12: Imidazole propionate decreases PI3K signaling in endothelial cells.
Quantitative analysis of PI3KC2α protein activation was performed using western blotting in human endothelial cells. The cells were unstimulated or stimulated with 10 nM ImP, 100 nM ImP, 500 nM ImP or 10 ng/ml TNF-α (n=6) for 24h. The quantitative data demonstrates a dose-dependent inhibitory effect of ImP on PI3KC2α protein activation. Below are representative western blot images of PI3KC2α expression normalized to GAPDH expression. The data are presented as mean ± SEM and were analyzed by one-way ANOVA followed by the Bonferroni post hoc test for multiple comparisons test (*ns*=no significance, *=*P*<0.05, **=*P*<0.01, ****=*P*<0.0001).

5.8. ImP reduces IGF-1 induced phosphorylation of AKT

To further examine whether ImP impairs AKT activation, a major downstream target of PI3K signaling, ECs were pre-treated with and without 100 nM ImP for 24 h. Subsequently, the cells were stimulated with 50 ng/ml IGF-1 for different short time points (0, 5 and 15 min). Normalization to total AKT expression revealed that pre-treatment with 100 nM ImP significantly inhibited the IGF-1-induced phosphorylation of AKT at Serine 473-activating phosphorylation site, as observed at both the 5 min and 15 min time points compared to the control group. Of note, relative AKT phosphorylation response upon 15 min of IGF-1 stimulation was slightly decreased in both the groups compared to the 5 min time point (Figure 13A). Quantification of total AKT normalized to GAPDH expression showed no significant change in ImP-treated HAECs versus control (Figure 13B). In Figure 13C, the representative western blot demonstrates the pronounced repression of AKT(Ser473) phosphorylation induced by ImP.

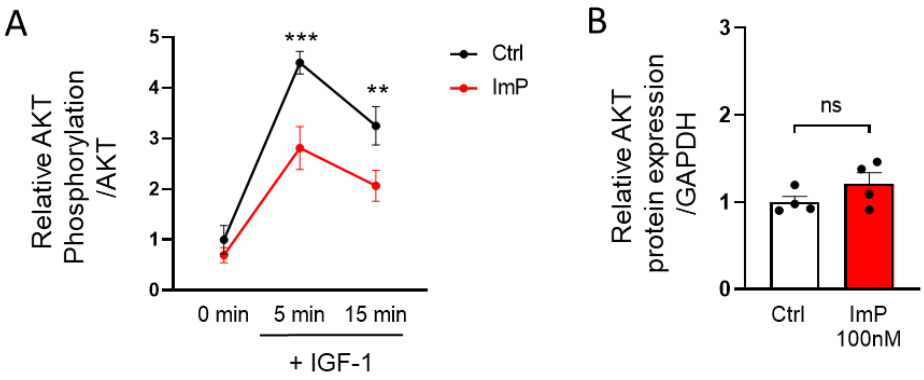

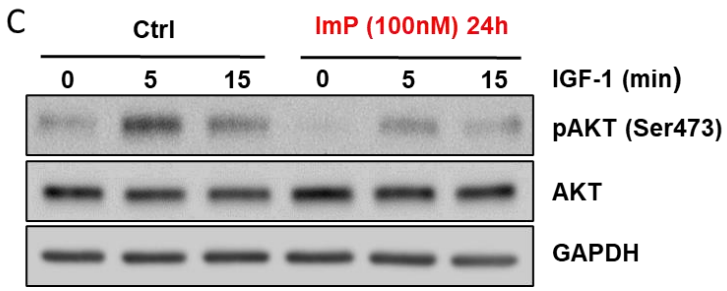

Figure 13: Imidazole propionate represses IGF-1 induced AKT phosphorylation in endothelial cells.
HAECs were treated with 100 nM ImP for 24 h, followed by IGF-1 stimulation for 0, 5 and 15 min. (A) Quantification of AKT(Ser473) phosphorylation normalized to total AKT protein expression. The data were analyzed by two-way ANOVA followed by the Bonferroni post hoc test for multiple comparisons. (B) Quantitative data of total AKT protein levels, normalized to GAPDH expression, were analyzed using an unpaired two-tailed Student's *t*-test. All data are presented as mean ± SEM (*ns*=no significance, **=*P*<0.01, ***=*P*<0.001, n=4). (C) Representative western blot images display the protein levels of phospho-AKT(Ser473), AKT and GAPDH.

5.9. ImP decreases phosphorylation of endothelial FOXO1 and raises total FOXO1 expression

To further analyze the role of PI3K/AKT signaling in ImP-mediated actions, a downstream target of AKT, the Forkhead box protein O1 (FOXO1), was examined. The protein levels of phosphorylated FOXO1 and total FOXO1 were evaluated in untreated cells and cells pre-treated with ImP, followed by stimulation with 50 ng/ml IGF-1 for 0, 5, and 15 minutes.

This study revealed two notable findings. Firstly, pre-treatment with ImP resulted in a significant reduction in IGF-1-induced FOXO1 phosphorylation at the Threonine-24 site after 5 min and 15 min of stimulation compared to control cells. Notably, even without insulin receptor stimulation by IGF-1 (0 min), ImP treatment led to a substantial decrease in FOXO1(Thr24) phosphorylation (Figure 14A). Secondly, treatment with 100 nM ImP significantly increased the overall abundance of cytosolic FOXO1 in ECs after 24 h compared to untreated controls (Figure 14B). These changes in protein expression were clear in the representative western blots shown in Figure 14C.

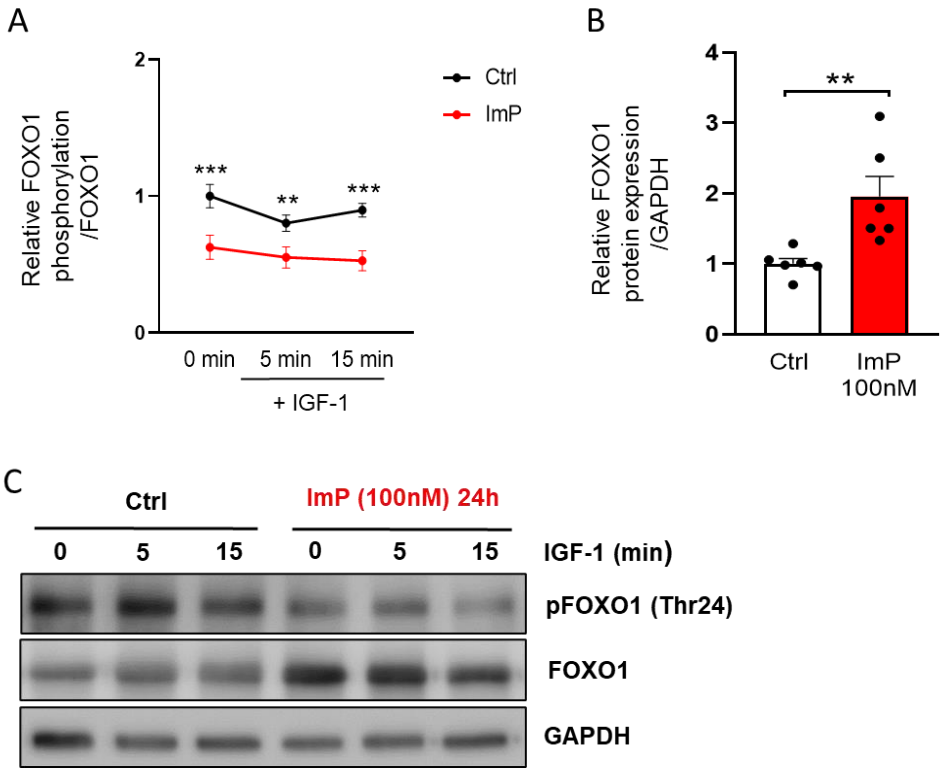

Figure 14: Imidazole Propionate attenuates FOXO1 phosphorylation and increases basal FOXO1 level in HAECs.
Endothelial cells were stimulated with or without 100 nM ImP for 24 h, followed by 50 ng/ml IGF-1 stimulation for 0, 5 and 15 min. The effects of ImP on FOXO1(Thr24) phosphorylation and total FOXO1 protein expression were assessed. (A) Quantification of FOXO1(Thr24) phosphorylation normalized to total FOXO1 protein expression. Data are analyzed by two-way ANOVA followed by the Bonferroni post hoc test for multiple comparisons. (B) Quantitative results of total FOXO1 protein level normalized to GAPDH expression, analyzed using an unpaired two-tailed Student's *t*-test. All data are presented as mean ± SEM (**=*P*<0.01, ***=*P*<0.001, n=6). (C) Representative western blots illustrating the expression levels of phospho-FOXO1(Thr24), FOXO1 and GAPDH.

5.10. ImP elevates nuclear FOXO1 in endothelial cells

To investigate the effect of ImP on the transcriptional activity of FOXO1, the nuclear translocation of FOXO1 was examined through immunofluorescent imaging in both control and ImP-treated ECs. The nuclear and cytoplasmic expression of FOXO1 was assessed by counting DAPI-stained nuclei (blue) and measuring the red fluorescence intensity per field of view. The results revealed that stimulation with 100 nM ImP for 24 h significantly increased the nuclear localization of FOXO1 in HAECs, while in untreated control cells the majority of FOXO1 remained in the cytoplasm (Figure 15A, B). Moreover, FOXO1 was less abundant in the cytoplasm upon ImP treatment as compared to the control (Figure 15 C). These findings provide further evidence for the

ImP-mediated deregulation of angiogenesis and pro-inflammatory action in ECs through transactivation and localization of FOXO1.

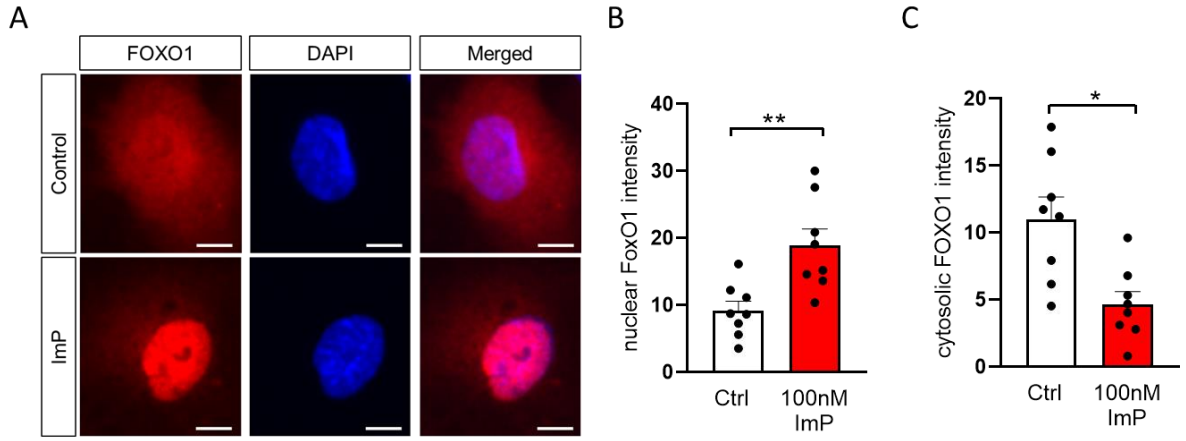

Figure 15: Imidazole Propionate positively mediates FOXO1 nuclear-cytoplasmic distribution in ECs.
Endothelial cells were treated with and without 100 nM ImP for 24 h before detecting the nuclear-cytoplasmic distribution of FOXO1 using immunocytochemistry. (A) Immunofluorescence staining was performed to visualize the nuclear and cytoplasmic accumulation of FOXO1 (red) with DAPI-stained nuclei (blue) in HAECs. Representative images were captured at 40X magnification and scale bars represent 10 µm. (B) Quantification of nuclear FOXO1 intensity. (C) Quantification of cytoplasmic FOXO1 intensity. Data were analyzed using an unpaired two-tailed Student's *t*-test, and the results are presented as mean ± SEM (*=*P*<0.05, **=*P*<0.01, n=8).

5.11. Silencing of *FOXO1* rescues pro-inflammatory phenotype of ImP

To study the role of FOXO1 in ImP-induced inflammation, RNAi-mediated silencing of *FOXO1* was performed in ECs. The cells were transfected with FOXO1-specific siRNA for 4 h and stimulated with ImP for 24 h. Control experiments were also conducted to optimize transfection conditions. These included untreated control cells, transfection with lipofectamine reagent alone, and transfection with scramble siRNA/non-targeting control. Initially, the efficiency of FOXO1 silencing was assessed through protein expression analysis. Representative data in Figure 16A demonstrated a significant reduction in FOXO1 protein expression after 4 h of siRNA transfection compared to untreated control, lipofectamine reagent alone or scramble siRNA. This finding confirms the successful knockdown of FOXO1 in HAECs, validating the effectiveness of the RNAi-mediated silencing approach.

Following siRNA transfection, ECs were stimulated with 100 nM ImP for 24 h. The expressions of pro-inflammatory adhesion molecules, including ICAM-1 and VCAM-1 were assessed using FACS analysis. The results demonstrated that silencing of *FOXO1* remarkably attenuated the rise of both cellular adhesion surface markers in ImP-treated cells compared to cells treated with ImP alone without *FOXO1* silencing (Figure 16B, C). Interestingly, the percentage change in expression of these adhesion molecules showed a similar trend among cells transfected with scramble siRNA, *FOXO1* siRNA and *FOXO1* siRNA in combination with ImP treatment. Indeed, these findings are consistent with the earlier observations in this study regarding the increased expression of ICAM-1 and VCAM-1 upon ImP treatment.

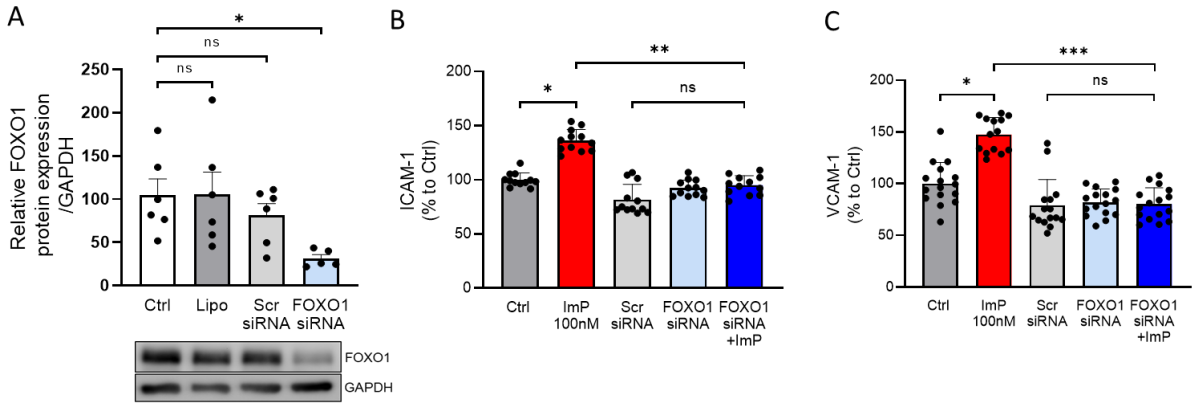

Figure 16: FOXO1 silencing in HAECs prevent Imidazole propionate induced inflammatory phenotype.
(A) Endothelial cells were subjected to FOXO1 silencing, and knockdown efficacy was evaluated at the protein level using western blot analysis. HAECs were untreated or stimulated with lipofectamine alone, scrambled (Scr) siRNA and *FOXO1* siRNA for 4 h, followed by 100 nM ImP for 24 h, respectively. Quantitative data confirmed a significant reduction in total FOXO1 expression compared to control conditions (n=5/6). Below are the representative western blots illustrating FOXO1 protein levels normalized to GAPDH expression. (B, C) Expression of adhesion markers ICAM-1 and VCAM-1 were determined by flow cytometry after FOXO1 silencing. All data are presented as mean ± SEM and were analyzed by two-way ANOVA followed by the Bonferroni post hoc test for multiple comparisons (ns=no significance, *=P<0.05, **=P<0.01, ***=P<0.001; n=12/16).

5.12. ImP impairs vascular regeneration after carotid injury *in vivo*

A mouse carotid injury model was employed to further investigate the systemic risk of ImP and its impact on endothelial cell functions. Adult C57BL/6J mice were divided into control and ImP (400 µg/day) groups. The mice were exposed to their respective treatments via drinking water for a duration of three weeks. Following the treatment, carotid injury (CI) was induced specifically to the left carotid artery of the mice. *En face*

staining with Evans blue dye was performed three days after the carotid injury to assess arterial regeneration. Thereby, areas of the injured carotid arteries were stained blue, indicating the binding of Evans blue dye. In contrast, areas with regenerated functional endothelium did not bind to the dye. The results revealed that treatment with ImP significantly impaired the wound healing process compared to control mice. This was evidenced by more intense blue staining in the injured areas of the carotid arteries in ImP-treated mice (Figure 17A, B). In contrast, the uninjured carotid artery, which served as a control for the non-specific binding of Evan's blue dye, remained clear (Figure 17A).

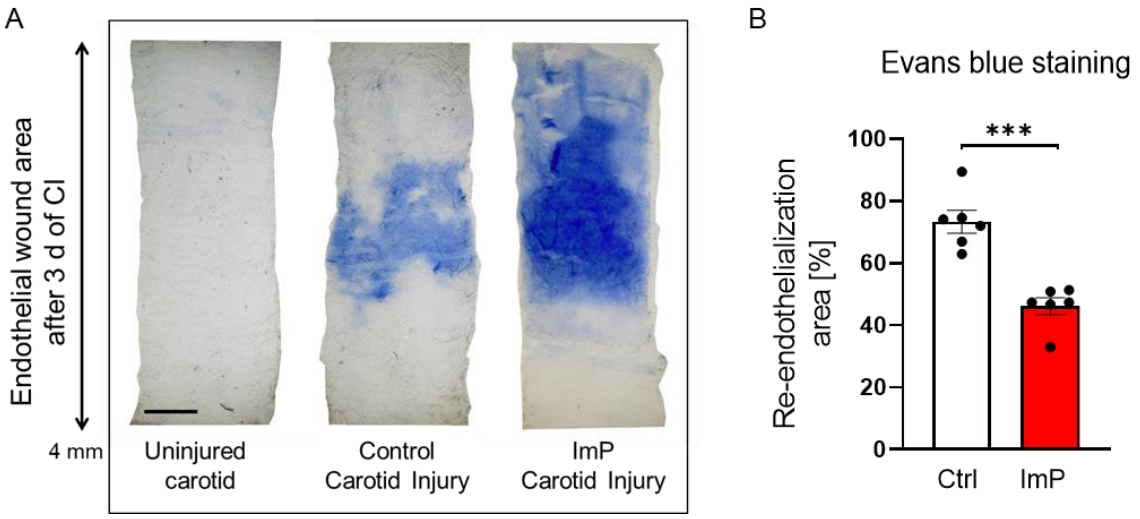

Figure 17: ImP impairs arterial regeneration after carotid injury *in vivo*.
Male C57BL/6 mice were administered either vehicle or ImP (400 µg/day) for three weeks before carotid injury (CI). After 3 days of CI, vascular regeneration was assessed by Evans blue staining. (A) Representative *en face* photographs of Evans blue-stained carotid arteries were taken, including the uninjured carotid as a negative control for non-specific dye binding, the carotid of the control group after CI, and the carotid of the ImP-treated group after CI. The blue-stained area corresponds to the area of de-endothelialization (injury). The scale bar, shown in the image at a 5X magnification, represents 500 µm. (B) Quantification of re-endothelialization as the ratio of blue-stained area to total injured area in percentage (n=6). The data, represented as mean ± SEM, were analyzed using an unpaired two-tailed Student's *t*-test (***=*P*<0.001).

5.13. ImP promotes atherosclerotic plaque formation in *Apoe*$^{-/-}$ mice

Considering that ImP worsens endothelial cell physiology in both *in vitro* and *in vivo* models, the effect of ImP on the development of symptomatic atherosclerosis was investigated using atherogenic *Apoe*$^{-/-}$ mice. The mice were divided into four groups and subjected to different dietary and treatment conditions. Specifically, they were fed either an SCD or an HFD for a duration of 6 or 12 weeks. In addition to the dietary

conditions, the mice were simultaneously treated with either control or ImP (800µg/day) via drinking water. After the designated treatment period, atherosclerotic plaque formation was evaluated in both the total aortic arch and the aortic roots of the mice at the early stage (6 weeks) and late (12 weeks) stages of atherosclerosis. This evaluation was performed using Oil Red O staining, which allows for the visualization and quantification of lipid-rich atherosclerotic plaques.

The results demonstrated that mice fed an HFD and additionally treated with ImP developed early signs of plaque formation at branches of the aortic arch after 6 weeks compared to the control (Figure 18A, C). The effects of ImP on atherosclerosis progression were further observed at the late phase of atherosclerosis (12 weeks), indicating a progressive impact of ImP on aortic arch lesions of *Apoe*$^{-/-}$ mice (Figure 18B, D). In contrast, SCD-fed mice showed only mild lesions in the aortic arch area, with no significant differences observed between the control and ImP-treated groups at both the 6-week and 12-week time points.

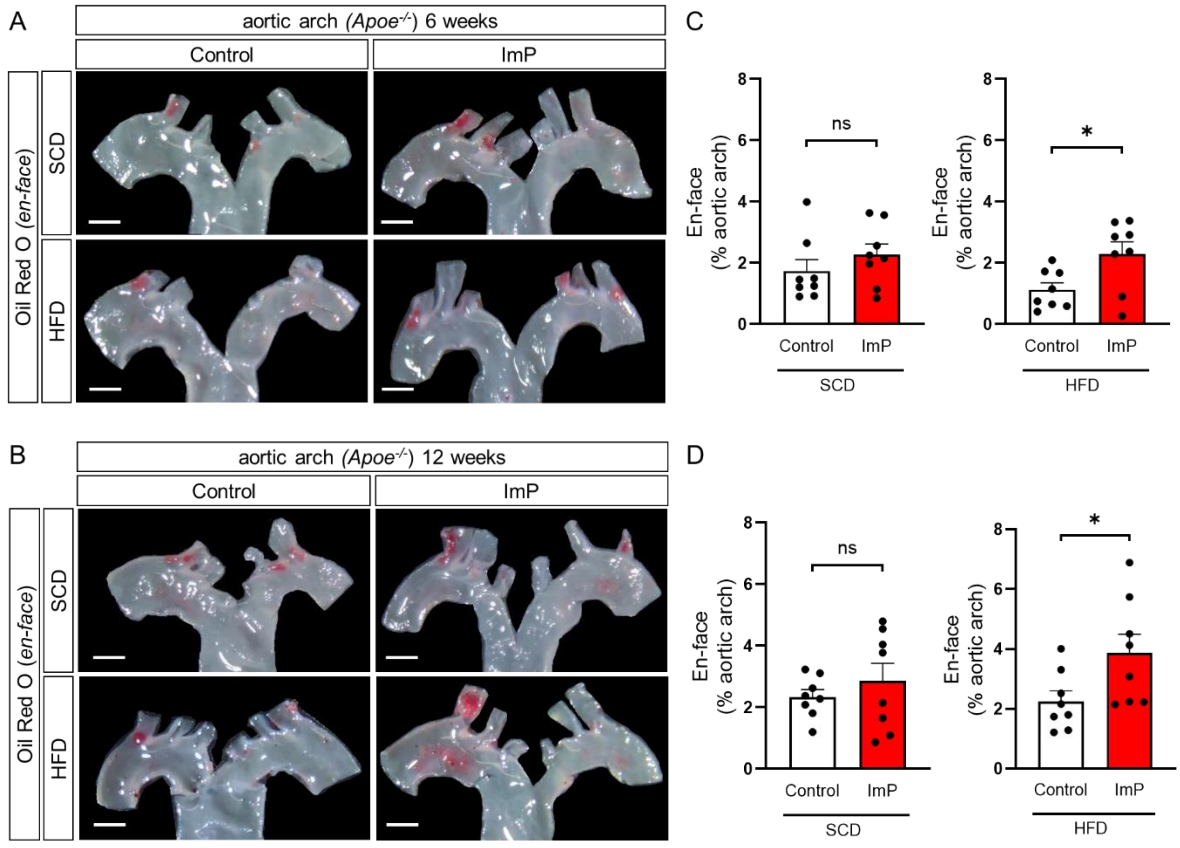

Figure 18 : ImP promotes atherosclerotic plaque formation in aortic arch of *Apoe*$^{-/-}$ mice. (A, B) Representative en *face* images of Oil Red O (ORO) stained plaque areas in the aortic arch of mice treated with either control or ImP (800 µg/day) while being fed a high-fat diet (HFD) or a standard chow diet (SCD) for 6 and 12 weeks (scale bar=1mm). (C, D) Quantitative data of atherosclerotic plaque formation at 6 and 12 weeks. The plaque area is expressed as

a percentage of the total aortic arch area. The data are presented as mean ± SEM and were analyzed by an unpaired two-tailed Student's *t*-test (*ns=no significance, *=P<0.05*, n=8).

In order to investigate the potential impact of ImP on the development of advanced atherosclerotic plaques in the aortic root regions of *Apoe*$^{-/-}$ mice, cryosections of heart base tissues were prepared and subjected to ORO staining. Atherosclerotic plaque development was quantified from SCD- and HFD-fed mice exposed to control and ImP in drinking water for 6 or 12 weeks. The results showed a tendency towards increased plaque formation in mice treated with ImP and receiving the SCD diet for both 6 and 12 weeks. Similar observations were made for mice on the HFD diet for 6 weeks, with no notable changes compared to the control group (Figure 19A, C). Interestingly, a significant increase in plaque formation was observed in mice treated with ImP and exposed to the HFD diet for 12 weeks compared to the control group (Figure 19B, D).

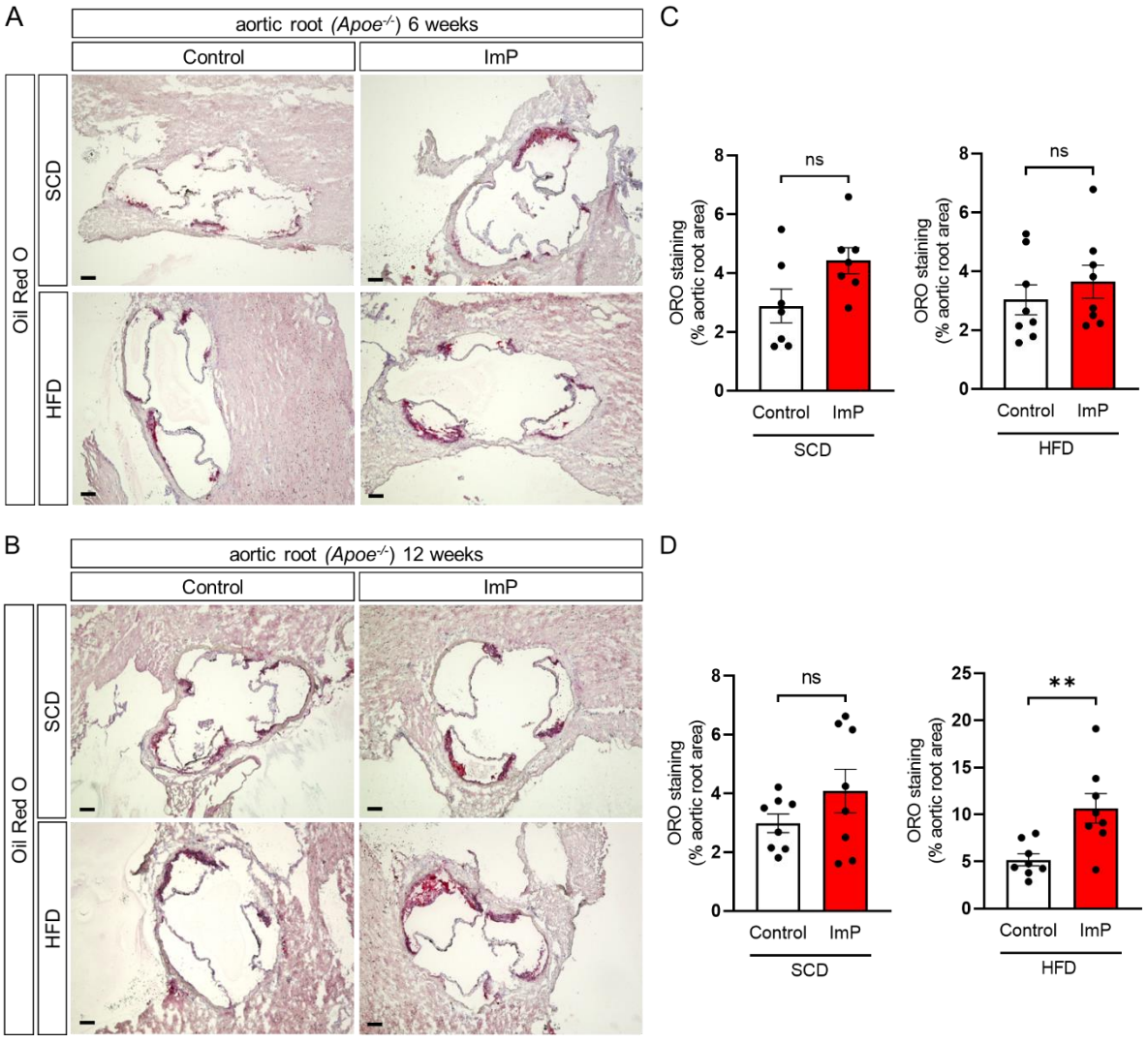

Figure 19: ImP enhances atherosclerotic plaque formation in aortic roots of *Apoe*$^{-/-}$ mice. (A, B) Representative images of Oil Red O (ORO) staining in cryosections in aortic roots in the hearts of *Apoe*$^{-/-}$ mice treated with control or ImP (800 µg/day) and additionally fed a high-fat diet (HFD) or a standard chow diet (SCD) for 6 and 12 weeks. Scale bars represent 100 µm. (C, D) Quantitative data of atherosclerotic lesion formation after 6 and 12 weeks of treatment. The plaque area is expressed as a percentage of the total aortic root. The data are presented as mean ± SEM and were analyzed by an unpaired two-tailed Student's *t*-test (*ns=no significance, **=P*<0.01, n=8).

5.14. Imidazole Propionate increases CD68+ macrophages infiltration in atherosclerotic plaques

To assess whether ImP is positively associated with inflammatory response activity and macrophage infiltration, CD68 macrophage expression was quantified in the atherosclerotic plaques of *Apoe*$^{-/-}$ mice. Aortic root sections from mice treated with ImP for 12 weeks were stained for CD68 and the obtained results were compared with those from the control mice in the SCD and HFD diet groups. The results demonstrated no significant changes between ImP-treated mice and control mice from the SCD group. However, in *Apoe*$^{-/-}$ mice treated with ImP and subjected to a 12-week HFD feeding, there was a noticeable increase in CD68+ macrophages within the plaque lesion compared to the control animals (Figure 20 A, B).

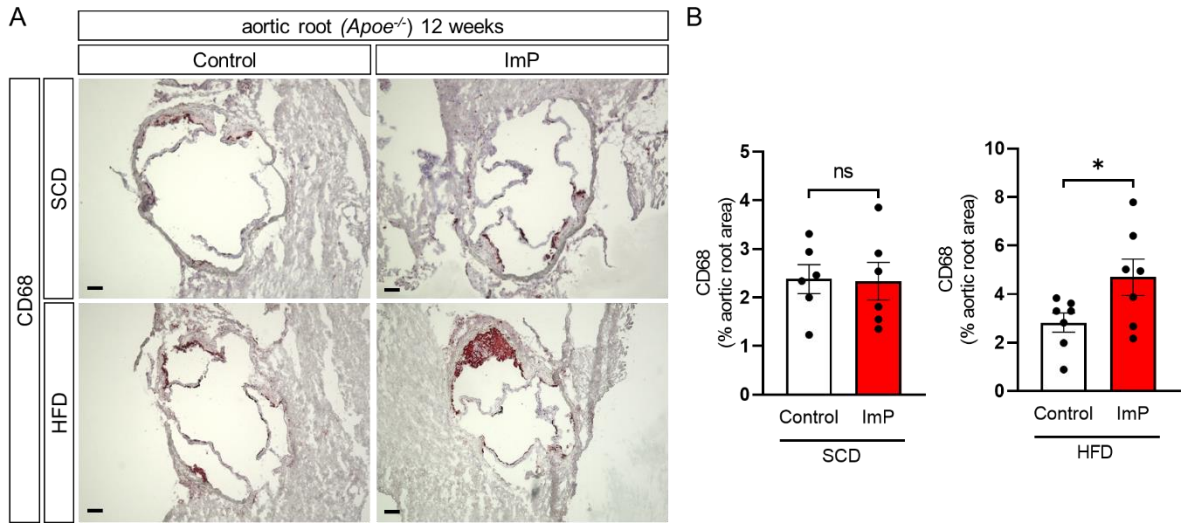

Figure 20: ImP augments CD68+ macrophage in murine atherosclerotic plaques. (A) Representative CD68 macrophage staining in aortic roots of *Apoe*$^{-/-}$ mice treated with control or ImP (800 µg/day) and additionally fed a high-fat diet (HFD) for 12 weeks. The scale bars represent 100 µm. (B) Quantitative data of CD68+ macrophages in atherosclerotic plaque area calculated from total aortic root area as a percentage. Data are mean ± SEM and were analyzed by an unpaired two-tailed Student's *t*-test (*ns=no significance, *=P<0.05*, n=8).

5.15. ImP does not affect lipid metabolism in *Apoe*$^{-/-}$ mice

The study aimed to examine the impact of ImP on lipid metabolism, in particular the levels of triglycerides, VLDL (very low-density lipoprotein), LDL (low-density lipoprotein), and HDL (high-density lipoprotein). For this purpose, plasma samples from ImP-treated and control mice fed an HFD for 6 and 12 weeks were analyzed by a collaborating research group in Munich using FPLC and gel filtration on Superose 6 columns. The obtained results of the lipid profile analysis revealed no significant differences between the control group and the group treated with ImP in terms of the measured lipid markers, which include total cholesterol, VLDL, LDL and HDL (Figure 21A, B).

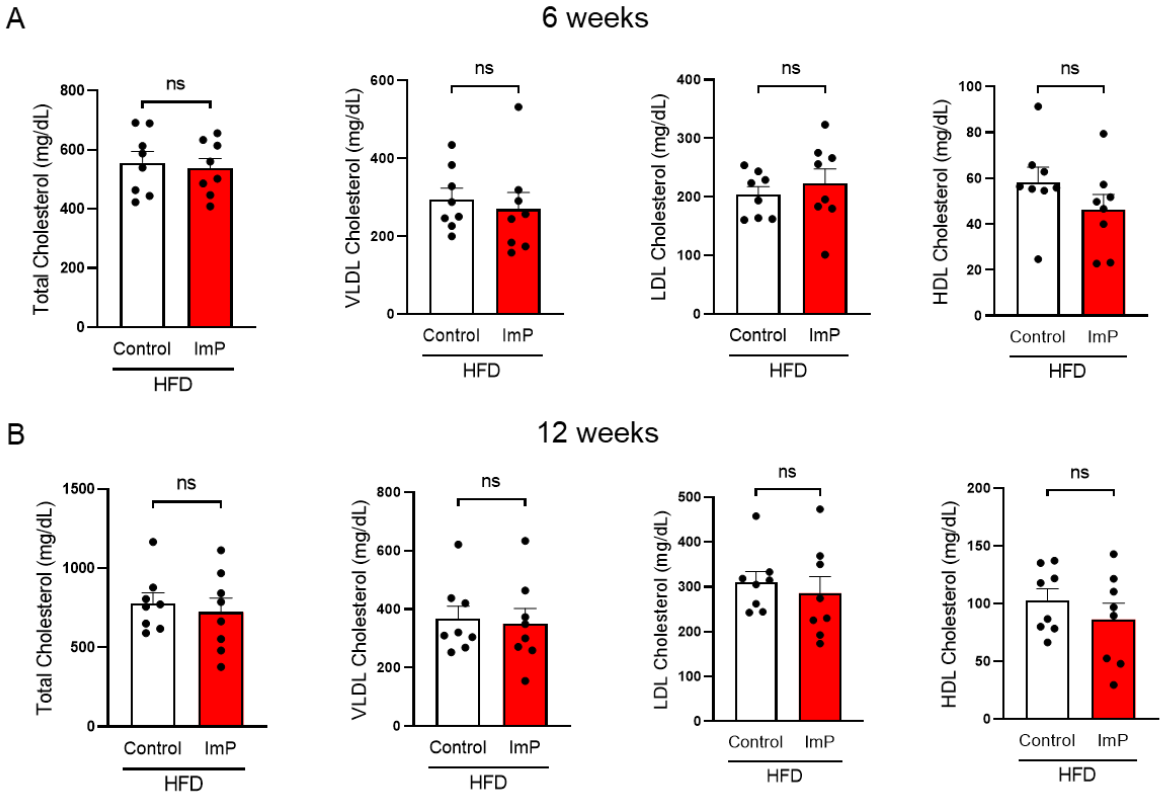

Figure 21: Lipid profiling analysis in plasma of *Apoe*$^{-/-}$ mice.
Plasma levels of lipid fractions (mg/dL) of total cholesterol, very low-density lipoprotein (VLDL), low-density lipoprotein (LDL) and high-density lipoprotein (HDL) from *Apoe*$^{-/-}$ mice receiving vehicle or ImP (800 µg) in drinking water and additionally fed an HFD for (A) 6 and (B) 12 weeks. Data are mean ± SEM and were analyzed by an unpaired two-tailed Student's *t*-test (*ns=no significance*, n=8).

5.16. Efficacy of ImP drinking protocol in *Apoe*$^{-/-}$ mice

To evaluate the effectiveness of the ImP treatment, plasma samples were obtained from *Apoe*$^{-/-}$ mice that were subjected to the ImP or received a vehicle control via

drinking water. ImP measurements were performed by the collaboration group in Sweden using a liquid chromatography-mass spectrometry (LS/ MS). The LC/ MS measurements demonstrated elevated levels of the metabolite ImP in the animals that received a daily treatment of 800 µg of ImP for both 6 and 12 weeks, in comparison to the control group of animals. ImP-treated mice exhibited ImP concentrations ranging from 300 nM to 1000 nM, whereas the control group had ImP levels below 50 nM. These findings emphasize the effectiveness of the experimental protocol and procedure in achieving the desired effect (Figure 22A, B).

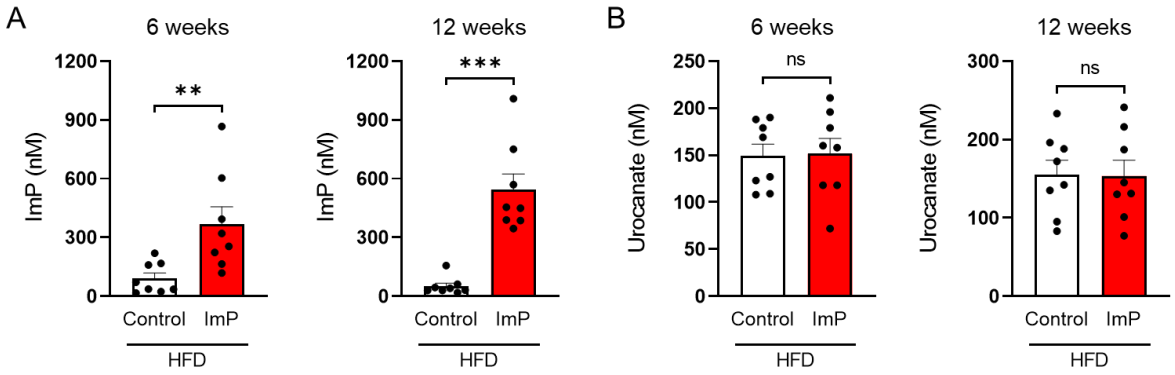

Figure 22: ImP plasma levels in *Apoe*$^{-/-}$ mice indicative for an efficient drinking protocol. Plasma metabolite concentration of ImP (nM) in *Apoe*$^{-/-}$ mice after 6- and 12-weeks of treatment with vehicle or ImP (800 µg/day). (B) Levels of precursor urocanate (nM) in murine plasma. The data are presented as mean ± SEM and were analyzed by an unpaired two-tailed Student's *t*-test (*ns=no significance,* **=*P*<0.01, ***=*P*<0.001, n=8).

6. Discussion

Atherosclerotic cardiovascular disease (ACVD) is a prevalent global health concern, leading to a high risk of mortality and disability among individuals with type 2 diabetes (T2D) (Low Wang et al., 2016). T2D and insulin resistance are independently associated with increased cardiovascular risk, primarily attributed to the early onset and progression of advanced vascular complications. Endothelial injury is considered an early and critical marker of ACVD pathophysiology (Gimbrone, JR and García-Cardeña, 2016; Chen et al., 2021).

Upon vascular injury, endothelial denudation triggers a cascade of cellular and molecular responses leading to vascular wall remodeling and ultimately to an aggravated pro-atherogenic phenotype. These involve the activation of endothelial cells (ECs), leukocytes, and vascular smooth muscle cells (VSMCs). Activation of ECs results in increased expression of pro-inflammatory adhesion molecules (ICAM-1, VCAM-1, Selectins), initiating leukocyte rolling and adhesion (Xu et al., 2021). By

attracting circulating leukocytes to the site of injury, activated monocytes engulf lipoproteins, which have accumulated within the arterial wall, into lipid-loaded macrophages (Low Wang et al., 2016). Additionally, these cells secrete cytokines and inflammatory mediators, such as TNF-α and interleukins, which contribute to the inflammatory response within the vessel wall resulting in a phenotypic switch in both macrophages and VSMCs. This switch involves their proliferation, migration, and dedifferentiation. Following arterial injury, secretion of collagen by modulated VSMCs leads to the formation of fibrous cap and contributes to extracellular matrix deposition (Low Wang et al., 2016; Döring et al., 2017). Depending on the extent of the injury and the endogenous repair ability of the cells, adjacent ECs can rapidly repair the lost and damaged cells within the endothelium, maintaining their vascular integrity. However, impairment of the regenerative capacity of ECs, such as migration or angiogenic ability, contributes to adverse vascular wall remodeling, thereby promoting the development of atherosclerosis (Schober et al., 2014; Döring et al., 2017). Moreover, chronic hyperglycemia and hyperinsulinemia (e.g., impaired insulin signaling) can exacerbate endothelial dysfunction and the pathological progression of ACVD, leading to increased plaque vulnerability and ultimately worsening clinical outcomes (Chen et al., 2021).

Recent findings have demonstrated that altered gut microbiota and its metabolites shape the host vascular phenotype associated with cardio-metabolic diseases (Witkowski et al., 2022). The gastrointestinal tract represents a vast and diverse ecosystem that generates a substantial quantity of microbial metabolites, which get absorbed into the portal circulation and mediate directly or indirectly the host physiology (Witkowski et al., 2022). For example, TMAO, a bioactive metabolite synthesized from trimethylamine-containing nutrients such as choline and carnitine, has been indicated to promote the progression of atherosclerosis and enhance vascular thrombogenicity (Tang et al., 2019b; Witkowski et al., 2022). Importantly, clinical studies regarding the prognostic significance of TMAO indicate that higher levels of circulating TMAO are linked to the presence of vulnerable coronary plaques, directly contributing to an increased risk of adverse cardiovascular outcomes (Xu et al., 2020; Witkowski et al., 2022). Initial animal experiments confirmed that feeding mice with a choline- or carnitine-rich diet exhibited augmented levels of TMAO, increased formation of cholesterol-laden macrophage foam cells and more

pronounced development of atherosclerotic plaques in the aorta. These pro-atherogenic effects were abolished in germ-free mice lacking gut microbes (Tang et al., 2019a). Remarkably, mice treated with an inhibitor of TMA-lyase (e.g., 3,3-dimethyl-1-butanol) also resulted in inhibition of TMA production and, thus, in reduced conversion to TMAO and decreased atherosclerotic burden (Tang et al., 2019a).

Gut metagenomic analyses have linked the dysbiotic state of the gut microbiome with metabolic syndromes involved in the pathophysiology of T2D and obesity, both of which can accelerate the progression of ACVD (Poznyak et al., 2020; Qin et al., 2021). Numerous studies have revealed that in patients with both CAD and T2D, there was a notable reduction in the levels of beneficial bacteria (e.g., *Bacteroidetes*), along with a concurrent increase in the abundance of opportunistic pathogens (e.g., *Firmicutes* and *Proteobacteria*) (Sanchez-Alcoholado et al., 2017). The elevated ratio of *Firmicutes* to *Bacteroidetes* also correlates with a higher prevalence of obesity in mice fed an HFD diet (Qin et al., 2021). Above all, butyrate-producing bacteria, which exert anti-inflammatory properties due to increased SCFA production, were found to be lower in obese and diabetic patients as compared to healthy subjects (Qin et al., 2021). Studies have discovered that treatment with metformin, an antidiabetic drug, may have beneficial effects on the microbiota imbalance and functions by promoting the growth of SCFA-producing bacteria, thereby partially restoring T2D-associated gut dysbiosis and lowering cardiovascular outcome (La Cuesta-Zuluaga et al., 2017).

In the past few years, there has been growing interest in a novel identified microbial-produced metabolite, imidazole propionate (ImP), which is generated through histidine metabolism by T2D-associated gut microbiome (Koh et al., 2018; Molinaro et al., 2020). The amino acid-derived ImP, which enters the systemic blood circulation through the portal vein, was present at higher concentrations in patients with pre- and type 2 diabetes compared to the healthy control group. This key finding was in line with increased ImP production in T2D patients after challenging their microbial communities with histidine using an *in vitro* gut simulator and fecal microbiota, suggesting a causal relationship with an altered gut microbiome commonly observed in diabetic populations (Molinaro et al., 2020). Collectively, the presence of a low microbial gene richness and the Bacteroides 2 enterotype, which are associated with obesity, have been linked to elevated levels of circulating ImP that can modulate low-grade inflammation, potentially

contributing to inflammatory processes and the development of T2D (Molinaro et al., 2020). In addition, gut bacterial strains with pro-inflammatory properties, such as *Streptococcus mutans*, *Eggerthella lenta*, *Clostridium symbiosum*, or *Ruminococcus gnavus*, which were more prevalent in patients with T2D and inflammatory bowel disease, have also been identified as potential producers of ImP (Molinaro et al., 2020). Contrarily, bacteria possessing anti-inflammatory functions, such as butyrate-producing bacteria *Faecalibacterium prausnitzii*, were less abundant in those subjects, implying the involvement of ImP in gut inflammation (Molinaro et al., 2020).

Although histidine is a precursor of ImP synthesis, the Swedish group has found that dietary histidine intake may not directly influence the ImP levels between healthy control and T2D patients (Molinaro et al., 2020). Instead, unhealthy dietary patterns (e.g., high intake of cheese or low intake of vegetables and nuts) and/ or altered immune system are linked to higher ImP levels resulting from enriched ImP-producing bacteria through an alternative metabolic pathway of histidine (Koh et al., 2018; Molinaro et al., 2020). Hence, enhanced levels of ImP are more likely attributed to factors such as host inflammation, gut dysbiosis, and dietary habits rather than histidine intake alone (Molinaro et al., 2020).

Furthermore, when administered to mice, ImP resulted in the activation of p38γ and subsequent activation of two distinct downstream signaling pathways associated with pathological conditions: (*i*) p62-mTORC1-S6K1, leading to impaired glucose tolerance and insulin signaling at insulin receptor substrate (IRS) levels; (*ii*) AKT-AMPK, leading to reduced glucose-lowering effects of metformin and contribution to insulin resistance (Koh et al., 2018; Molinaro et al., 2020). Of note, hyperactivation of p38γ/ mTORC1 signaling is not only associated with diabetic complications such as retinopathy or nephropathy but also with the onset of CVDs and heart failure, especially in cardiac remodeling in mouse models (Koh et al., 2018; Molinaro et al., 2023). A recent study revealed that individuals with heart failure displayed significantly elevated plasma levels of ImP with reduced left ventricular systolic heart functions compared to those without heart failure. These findings were independent of diabetes or other traditional risk factors and related to increased circulatory levels of amino-terminal proANP and NT-proBNP, biomarkers of cardiomyocyte stress or strain. Furthermore, this increase in ImP plasma levels was associated with an augmented risk for overall mortality, suggesting that ImP directly impacts the prognosis and outcomes of patients (Molinaro et al., 2023).

Ongoing research and preliminary results from a sub-analysis of a cohort indicate a potential association between CVD risk factors and elevated circulating ImP concentrations in overt CVD (Molinaro et al., 2020). However, the specific role of ImP in coronary heart disease has not been examined so far. Within our group, yet unpublished data has shown a direct correlation between elevated ImP plasma levels and atherosclerotic coronary artery disease in patients, further strengthening putative detrimental effects on cardiovascular health (Nageswaran et al., 2023, *submitted*). Consequently, given that T2D predisposes to endothelial dysfunction and the onset of atherosclerotic cardiovascular disease (Sorrentino et al., 2007; Ye et al., 2022), and given the key findings that patients with T2D and/ or coronary heart disease (ACVD) have higher plasma levels of the microbial-derived metabolite ImP, our research group hypothesized that ImP may impact endothelial cell physiology to an extent that leads to vascular complications of atherosclerosis. Hence, the study investigated whether ImP has the potential to disrupt normal endothelial cell functions *in vitro* and *in vivo* after carotid injury and whether ImP contributes to the progression and development of atherosclerotic lesions in atheroprone *Apoe*$^{-/-}$ mice. By addressing these questions, the study aims to shed light on the underlying mechanism of ImP in ECs and its potential role in the pathogenesis of ACVD.

Findings from this work showed that the gut microbially produced metabolite ImP significantly impaired insulin receptor signaling through dysregulation of PI3K/ AKT/ FOXO1 signaling pathway in ECs, thereby affecting their functional properties such as migration, proliferation and angiogenic capacity. Moreover, ImP promoted inflammatory activation of ECs, leading to upregulation of cellular adhesion molecules, including ICAM-1, VCAM-1, and E-selectin, increasing the adhesion of monocytes and, thus, contributing to the inflammatory response. Silencing of *FOXO1* rescued ImP-induced pro-inflammatory phenotype in ECs. In addition, ImP treatment in mice resulted in impaired vascular regeneration after carotid injury and, consequently, increased atherosclerosis in atheroprone *Apoe*$^{-/-}$ mice. These findings suggest that ImP plays a significant role in the pathology of vascular complications and highlight ImP as a potential therapeutic target for managing atherosclerosis-related disorders.

6.1. Effect of Imidazole propionate on endothelial cell physiology

Endothelial dysregulation is a characteristic hallmark of the early stages of atherosclerosis due to a systemic pathological state of the blood vessels (Xu et al., 2021). In a normal physiological state, ECs play a crucial role in regulating vascular tone, promoting angiogenesis, maintaining hemostasis, and serving as an interface with various beneficial properties, including antioxidant, anti-inflammatory, and anti-thrombotic functions (Xu et al., 2021). During angiogenesis, ECs perform a wide range of functions, including degradation of the extracellular matrix, migration, proliferation, lumen formation, and vessel stabilization (Kaur et al., 2011). Harmful circulating stimuli can overwhelm the protective mechanisms of the vascular endothelium, compromising migration and angiogenic capacities of ECs and ultimately initiating vascular injury (Getzin et al., 2018; Xu et al., 2021). Following vascular injury, the denudation of ECs triggers a series of cellular and molecular reactions, as mentioned above, leading to pathogenic remodeling of the vascular wall and, ultimately, to an aggravated pro-atherogenic phenotype (Low Wang et al., 2016).

This study used primary human aortic endothelial cells (HAECs) as an *in vitro* model to investigate endothelial cell functions and their response to ImP stimuli. Endothelial cell types like HUVECs (Human Umbilical Vein Endothelial Cells) and HAECs (Human Aortic Endothelial Cells) have been broadly used as *in vitro* models to study functional and molecular biological aspects related to cardiovascular health. Moreover, these human cell lines allow to investigate specific cellular responses and mechanisms in a controlled laboratory environment. Despite the similar cellular features and morphogenesis of HAECs and HUVECs in a 2D cell culture system, HAECs present a greater angiogenic potential, including endothelial migration and vascular sprouting, in a 3D microfluidic angiogenesis system compared to HUVECs (Seo et al., 2016). Additionally, HUVECs are characteristically venous, transporting blood from the placenta to the fetus under low pressure, whereas HAECs as an arterial cell line are more suitable for studying the molecular dynamics and functional properties of ECs in the arterial system (Maurya et al., 2021).

Initial findings demonstrated that 10 nM and 100 nM of ImP significantly reduced gap closure in an *in-vitro* scratch injury assay, suggesting an impaired EC migratory capacity. Additionally, stimulation with TNF-α (10 ng/ml) resulted in reduced migration

of HAECs, serving as a positive control to illustrate the inhibitory effect of ImP on EC migratory. EC tube formation on basement membranes involves all essential stages of angiogenesis, including endothelial cell adhesion, migration, alignment, and the ultimate formation of tube-like structures (Arnaoutova and Kleinman, 2010). The results showed that stimulation with 100 nM ImP resulted in a significant reduction in tube formation. Similar effects were also observed in the negative control using TNF-α treatment impairing the capability of HAECs to form functional capillary-like structures. This was evidenced by disrupted cellular segments in ImP-pretreated ECs (or TNF-α). The control and IGF-1-treated cells displayed clear tube morphogenesis, indicating a potential pro-angiogenic effect of IGF-1 on HAECs (Lin et al., 2017). These results suggest that ImP adversely impaired the migratory and angiogenic properties of ECs, which are essential for the wound healing process in the vessel wall (Eelen et al., 2020).

Moreover, in response to extensive injury and impaired regenerative capacity, ECs switch to an inflammatory state mediated by pro-inflammatory molecules that contribute to the progression of vascular complications, with chronic inflammation leading to leukocyte recruitment and accumulation to the injury site as foam cells (Low Wang et al., 2016). The results revealed that ImP significantly led to the upregulating expression of cellular adhesion-molecules ICAM-1, VCAM-1 and E-selectin, consequently facilitating increased adhesion of THP-1 monocytes to HAECs surface under 20 dyn/ cm^2 shear flow conditions. These cellular and molecular changes promote interactions between leukocytes and ECs under a shear flow environment, contributing to the inflammatory response associated with ImP. Indeed, hemodynamic forces, mainly perturbed shear stress, have been reported to impact ECs morphology and phenotype, thus contributing to the development of vascular diseases (Chiu and Chien, 2011; Mendez et al., 2022). The potential involvement of hemodynamic forces in endothelial dysfunction was initially proposed based on the observation that the earliest atherosclerotic lesions tend to develop preferentially at arterial branches and curvatures, where the blood flow is disturbed accompanied by low and oscillatory shear stress (< 4 dyn/cm^2) (Mendez et al., 2022). In addition, low shear stress levels can lead to persistent activation of several atherogenic genes in ECs, e.g., the monocyte chemotactic protein-1 (MCP-1) and adhesion molecules, which promotes the infiltration of monocytes into the arterial wall or platelet-derived growth factors (PDGFs)

that advocates EC turnover and stimulates SMC migration into the subintimal space (Chiu and Chien, 2011). By contrast, in straight regions of the arterial vessels, the blood flow is laminar with high shear stress (> 15-20 dyn/ cm^2), resulting in an atheroprotective EC phenotype and downregulation of these genes. However, in this study, the impact of ImP on HAECs was assessed under controlled high-flow shear stress conditions (20 dyn/ cm^2) to determine whether ImP may impair endothelial biology through pro-inflammatory actions independent of pathophysiological hemodynamic setups. Overall, these results suggest that ImP mediates leukocyte rolling and their firm adhesion and potentially induces transmigration across the endothelial barrier by upregulating the expression of vascular adhesion molecules E-selectin, ICAM-1, and VCAM-1.

Although the concentration of 10 nM ImP has shown notable mediated effects on ECs compared to the control cells, previous studies on ImP in patients with T2D have indicated that low levels of ImP are considered physiological values, commonly found in the blood of individuals without T2D (Koh et al., 2018; Koh et al., 2020; Molinaro et al., 2020). This implies higher levels of ImP may be associated with the pathological state of T2D. Based on these clinical studies, high ImP concentrations, peaking at about 1000 nM, have been observed in individuals with pre- and type 2 diabetes (Molinaro et al., 2020). Similar values of ImP were also found in patients with CVD and heart failure (Molinaro et al., 2023). Specifically, elevated circulating ImP levels reaching about 100 nM, have been noted in the upper quartile of ImP analysis, indicating an increased risk for prevalent CVD, including heart failure. Considering these findings, the study focused on a concentration in the lower close pathological range while also falling within a range found in non-diseased subjects, allowing to explore the effects of ImP within a biologically relevant context.

To assess the physiological response of ImP to vascular regeneration, a murine carotid injury (CI) model was adapted as a translational approach. Microscopic analysis revealed that mice treated with ImP exhibited a larger denuded vessel area at the site of injury than the healthy control group 3 days after CI. This suggests an impaired endothelial wound healing process *in vivo* induced by ImP, which strongly supports the previous findings *in vitro*. Endothelial injury is considered a critical stage in the early development and progression of ACVD and is closely associated with endothelial

dysfunction commonly observed in diabetic patients with cardiovascular events (Sorrentino et al., 2007). The recruitment of specific monocyte subsets (Ly6C^{low}/ Ly6C^{high}) also plays a crucial role in endothelial regeneration after arterial injury (Getzin et al., 2018). Getzin et al., reported that an increase in Ly6C^{low} monocytes and a decrease in inflammatory Ly6C^{high} monocytes may protect the endothelium and promote endothelial wound healing through CX_3CL1-CX_3CR1 interaction inducing clearance of injured ECs (Getzin et al., 2018). However, reduced levels of EPCs or Ly6C^{low} monocytes have been linked to impaired EC regeneration contributing to endothelial dysfunction and, thus, an increased risk of atherosclerotic lesion formation (Werner et al., 2003; Getzin et al., 2018).

6.1.1. Molecular mechanism underlying the pathogenic effects of ImP

Initial findings provide evidence that ImP has detrimental effects on endothelial cell physiology, triggering EC inflammation, both representing pivotal hallmarks of early atherosclerosis. The RNA sequencing analysis provided insights into the underlying molecular mechanism through which ImP exerts its anti-angiogenic and pro-inflammatory functions in ECs.

Transcriptomic profiling of HAECs identified several genes that were differentially expressed between the ImP and control conditions. These genes were associated with angiogenesis and inflammation, such as *ADGRL2*, *CALCRL*, *FLT1*, *TM4SF18*, *DCHS1*, *FLRT2*, *ANGPTL4*, *ARGHGAP22* and *IL32*. The gene *ADGRL2* (adhesion G protein-coupled receptor L2), which was formerly known as *LPHN2*, encodes the latrophilin 2 protein, an adhesion GPCR (Vezain et al., 2018) and was found to be downregulated in response to ImP treatment. This gene is associated with promoting angiogenic and neurotrophic processes in ECs and mouse tissue explants through its interaction with de-glycosylated leucine-rich -2-glycoprotein 1 (LRG1)/ LPHN2 complex (Yin et al., 2022). ImP treatment also led to the downregulation of other pro-angiogenic genes, including Calcitonin receptor-like (*CALCRL*), vascular endothelial growth factor receptor 1 (*FLT1*), and transmembrane 4 L six family 18 (*TM4SF18*). *CALCRL* is a G protein-coupled receptor expressed on ECs for adrenomedullin, which is a peptide vasodilator that participates in cardiovascular development with angiogenic and vasoprotective functions (Nicoli et al., 2008; Menon et al., 2017). Lack of *CALCRL* exhibits significant modifications in vascular development and angiogenesis characterized by abnormalities in the arterial formation and impaired sprouting and

organization of intersomitic vessels (Nicoli et al., 2008). *FLT1*, also known as VEGFR1), encodes a receptor for vascular endothelial growth factor (VEGF) that can bind to VEGFA/ B and placenta growth factor (PGF) and thereby conferring angiogenic activity (Autiero et al., 2003). *TM4SF18* functions as a positive feedback modulator of VEGF signaling and regulates angiogenic activity *in vivo* by controlling endothelial speed and robustness (Page et al., 2019). Furthermore, *DCHS1*, a member of the cadherin superfamily, and *FLRT2*, a member of the fibronectin leucine-rich transmembrane family, were also decreased upon ImP treatment. Both genes are involved in heart development and morphogenesis, regulating endothelial cell migration in valve formation or in the placental labyrinth in mice (Durst et al., 2015; Tai-Nagara et al., 2017). In contrast, angiopoietin-like 4 (*ANGPTL4*), a Rac-specific GTPase isoform of ARHGAP22 (p68RacGAP) and interleukin 32 (*IL32*) were upregulated by ImP. These genes are involved in the negative regulation of cell migration and angiogenesis but also map inflammatory processes (Aitsebaomo et al., 2004; Nold-Petry et al., 2009; Meyer and Akdis, 2013). These findings highlight the potential role of ImP in modulating angiogenic and inflammatory signaling in ECs.

Notably, decreased expression of the *PIK3C2A* gene (Phosphatidylinositol-4-Phosphate 3-Kinase Catalytic Subunit Type 2 Alpha), which encodes PI3K family proteins, was found in ImP-treated HAECs. The gene encodes the lipid kinase PI3KC2α (phosphatidylinositol-4-phosphate 3-kinase C2 domain-containing subunit alpha), a member of the Class II PI3Ks, which plays a pivotal role in the regulation of angiogenesis and the maintenance of the endothelial barrier integrity (Yoshioka et al., 2012; Aki et al., 2015). Deficiency of PI3KC2α, specifically the C2α domain, leads to reduced angiogenesis and abnormal vascular hyperpermeability accompanied by vascular damage. At the cellular level, PI3KC2α plays a critical role in various endothelial cell functions, including migration, proliferation, and survival. It is also essential for the assembly of VE-cadherin at intercellular junctions, which is crucial for preserving endothelial integrity and vascular barrier function (Yoshioka et al., 2012). Yoshioka et al., also specified that complete knockout of PI3KC2α in mice leads to early and fully pervasive embryonic lethality due to impaired vasculogenesis (Yoshioka et al., 2012; Mountford et al., 2015). Unlike Class I and III PI3Ks, which consist of both catalytic and regulatory subunits essential for their localization and activation, Class II has three isoforms (PI3KC2α, PI3KC2β, and PI3KC2γ) and exerts their catalytic

functions without the presence of regulatory subunits. They possess a lipid kinase catalytic domain and a C-terminal C2 domain, which primarily generates lipid messengers, phosphatidylinositol 3-phosphate (PI3P) and phosphatidylinositol-3,4-bisphosphate (PIP2), in response to cellular signals (Yoshioka et al., 2012). Of note, the PI3KC2α-mediated activity of PIP2 is elementally linked to the stimulation of AKT in response to insulin (Jean and Kiger, 2014; Margaria et al., 2019).

Furthermore, the gene expression profiling has also revealed a notable downregulation in other PI3K isoforms upon ImP treatment, including *PIK3CB* and *PIK3C3*. In general, the Class I and III PI3K enzymes have been extensively explored, with numerous studies elucidating their regulatory mechanisms and functions in oncogenic and ECs (Boukhalfa et al., 2020; Koch et al., 2021). Several studies have shown that Class I PI3Ks, comprising PI3Kα (encoded by *PIK3CA*), PI3Kβ (encoded by *PIK3CB*), PI3Kδ (encoded by *PIK3CD*), and PI3Kγ (encoded by *PIK3CG*), transduce extracellular signals downstream from activated plasma membrane receptors and produce the phosphatidylinositol-3,4,5-trisphosphate (PIP3) from PIP2 that primary triggers a cascade of intracellular events upon insulin receptor activation, and thus promote cell growth, proliferation, migration and metabolism through lipid-activated enzymes such as AKT (Boukhalfa et al., 2020). Class III PI3Ks (or VPS34 encoded by *PI3KC3*) mainly generate PI3P and are linked to both autophagy (complex I) and endocytic trafficking (complex II) in various tissues (Koch et al., 2021). Autophagy plays a crucial role in vascular injury, and a recent study has demonstrated that downregulation of PI3KC3 expression impaired the proliferative, migratory and autophagic ability of HUVECs, thus contributing to the aggregation of vascular endothelial injuries observed in patients with diabetes and hypertension (De Meyer, Guido R Y et al., 2015; Zhang et al., 2019). The primary roles of PI3Ks can be categorized based on their predominant functions, with Class I and II primarily involved in cell signaling processes (e.g., insulin signaling), while Class II and III are primarily involved in membrane trafficking processes (endosomal) (Jean and Kiger, 2014). The various classes of PI3Ks play diverse cellular roles by modulating specific phosphoinositide pools. While Class I PI3Ks primarily produce PIP3 and PIP2, and Class III PI3Ks generate PI3P *in vivo*, Class II PI3Ks are also capable of producing both PI3P and PIP2 *in vivo* (Margaria et al., 2019). All classes of PI3Ks have the capability to produce PI3P *in vitro*. Furthermore, both Class I and Class II PI3Ks can generate PIP2. Moreover, conflicting

data shows that the C2 domain of PI3KC2α also binds to PIP3, a unique signaling lipid generated at the plasma membrane upon insulin receptor stimulation and first revealed for AKT/ PKB (Koch et al., 2021). However, further investigations are required to analyze the fundamental alterations in the enzymatic functions of PI3K induced by ImP. Overall, these data suggest that ImP has a broad impact on various isoforms of PI3K, resulting in impaired vascular cell physiology and regenerative processes in ECs.

Notably, compared to other isoforms, the gene expression of *PIK3C2A* was most prominently regulated by ImP. Thus, the study focused on further investigating PI3KC2α expression at protein levels. The findings indicated a dose-dependent decrease in the protein expression of PI3KC2α in ECs upon stimulation with ImP, suggesting that the ImP-induced suppression of *PIK3C2A* gene expression reduced PI3KC2α protein synthesis. The detailed regulatory mechanisms of how ImP regulates *PIK3C2A* gene expression remain to be explored.

Next, the study focused on the downstream target of PI3K, AKT/ PKB, due to its critical involvement in various endothelial cell functions. The PI3K/ AKT pathway is pivotal in regulating cellular processes such as angiogenesis, vascular tone, control of adhesion, and recruitment of leukocytes to the vessel wall (Morello et al., 2009). As described above, activated PI3K upon insulin of IGF-1 stimulation triggers the phosphorylation of PIP2 on the 3-hydroxyl group of the inositol ring to generate PIP3 lipid messenger, which in turn leads to translocation of AKT to the plasma membrane, thus resulting in AKT phosphorylation and activation through upstream kinases such as PDK-1 or -2 (Shiojima and Walsh, 2002; Gallay et al., 2009). Among the three AKT isoforms, AKT1, which is primarily expressed by ECs, is mainly associated with cardiovascular functions (Lee et al., 2018). For example, severe impairment in the repair of ischemic limbs was observed in global AKT1 knockout mice, underscoring the essential role of AKT1 in vascular remodeling compared to other isoforms (Lee et al., 2018). Activation of AKT1 is a critical event within the insulin signaling pathway, involving phosphorylation at two major sites, Thr308 and Ser473 (Gallay et al., 2009). However, insulin receptor activation usually requires a transient stimulation period for AKT activation due to the negative feedback mechanisms of the insulin signaling. Consequently, this feedback loop leads to the dephosphorylation of AKT, serving to dampen its signaling activity (e.g., via inhibition of IRS-1/ PI3K association) (Tian,

2005). Hence, in this study, ECs were subjected to stimulation with the insulin analog, IGF-1, for 0, 5 and 15 min after 24h of exposure to ImP. As a result, ImP significantly reduced IGF-1-induced AKT phosphorylation at the active site of Ser473 at both short-time points of 5 and 15 min compared to control cells, further supporting the deleterious effects of ImP on vascular endothelial cells, as pre-treatment with ImP inhibited AKT activity by suppressing PI3K signaling.

The dysregulation of the PI3K/ AKT signaling pathway has been implicated in distinct human diseases, including cancer, diabetes, and cardiovascular diseases. AKT regulates a wide range of downstream targets, including GLUT4, eNOS, caspases and transcription factors (Manning and Cantley, 2007). In insulin-responsive tissues (e.g., muscle and adipose tissue), insulin stimulates AKT activation leading downstream to the translocation of glucose transporter 4 (GLUT4) to the plasma membrane, facilitating the uptake of glucose into cells (Huang et al., 2009). However, impaired AKT/ GLU4 signaling was associated with insulin resistance and hyperglycemia (Huang et al., 2009). In cardiovascular diseases, PI3K/ AKT signaling is involved in many aspects of vascular regulation, including endothelial cell function, vascular smooth muscle cell proliferation, inflammation, and apoptosis. For example, activation of AKT in ECs increases in NO production through AKT-mediated activation of eNOS by direct phosphorylation of Ser1177, which promotes vasodilation, vascular remodeling, and angiogenesis (Manning and Cantley, 2007). Furthermore, eNOS-derived NO has been linked to potential atheroprotective effects, such as inhibiting apoptosis, suppressing SMC proliferation, preventing platelet aggregation and adhesion, and attenuating leukocyte activation and adhesion. Collectively, these actions of eNOS-derived NO contribute to its role in maintaining vascular health and protecting against atherosclerosis-related processes (Fernández-Hernando et al., 2007).

In addition to variations in substrate expression under different conditions, AKT probably exhibits stimulus-specific variations in substrate use (Manning and Cantley, 2007). Multiple studies have consistently reported that phosphorylation of Ser473 or Thr308 can result in only partial activation of AKT, while phosphorylation of both residues is required for maximal AKT activity (Gallay et al., 2009). The dependency of full AKT activation on Thr308 and/ or Ser473 phosphorylation is still controversial. It has been established for quite some time that phosphorylation of Ser473 is not indispensable for the activation of AKT by growth factors. However, it substantially

increases AKT activity, ranging from 5- to 10-fold (Manning and Cantley, 2007). Moreover, it has been suggested that dual phosphorylation of both Thr308 and Ser473 may not be essentially required for all AKT functions. For example, Thr308 phosphorylation alone is sufficient for the regulation of downstream effectors such as GSK3, TSC1/ 2, and mTORC1, while Ser473 phosphorylation has a strong target substrate specificity to FOXO1/ 3a (Gallay et al., 2009).

Among the FOXO isoforms, FOXO1 is one of the major isoforms implicated in vascular complications linked to the pathogenesis of diabetes and CVD (Yu et al., 2020). FOXO1 regulates cellular processes, including angiogenesis, metabolism, apoptosis, and inflammation, based on diverse extracellular stimuli and tissues (Puthanveetil et al., 2013; Kandula et al., 2016). In ECs, upon activation of the PI3K/ AKT signaling pathway, e.g., by insulin receptor stimulation, the FOXO1 transcription factor is functionally blocked through AKT-dependent phosphorylation leading to the inhibition of DNA binding, exclusion of FOXO1 from the nucleus, and its sequestration in the cytoplasm (Potente et al., 2005). The nuclear exclusion of FOXO1 promotes the activation of various genes regulating endothelial cell proliferation and angiogenic activity (Wilhelm et al., 2016). Here, ImP treatment led to reduced phosphorylation of FOXO1 at the Thr24 residue and increased endogenous levels of FOXO1, suggesting that ImP treatment diminishes the ability of AKT to proteasomally degrade FOXO1. To further confirm FOXO1 nuclear-cytoplasmic distribution, immunocytochemistry was performed in HAECs. The results revealed that ImP significantly increased nuclear FOXO1 expression, accompanied by a corresponding decrease in cytoplasmic FOXO1 levels compared to control cells. The pronounced accumulation of FOXO1 in the nucleus highlights ImP-mediated disinhibition of FOXO1 due to suppression of intracellular PI3K/ AKT signaling. Considering that AKT has been demonstrated to phosphorylate FOXO1 at three conserved residues, including Thr24, Ser256 and Ser319, promoting its association with 14-3-3 proteins and, consequently, its inactivation(Webb and Brunet, 2014; Farhan et al., 2020), it would be intriguing to explore the ImP-mediated effects on dephosphorylation of FOXO1 at additional potential sites. Several studies have also discussed the cross-talk between various signaling pathways involved in the phosphorylation of serine/threonine residues. For example, PKA and SGK have been denoted as additional kinases to regulate FOXO1 transcriptional activity through phosphorylation at AKT phosphorylation sites Thr24 and

Ser319, highlighting the complexity of FOXO1 regulation (Lee et al., 2011). As mentioned above, AKT/ FOXO1 regulatory mechanisms can also be modulated by other post-translational modifications such as acetylation, methylation and ubiquitination (Tzivion et al., 2011). It has been suggested that acetylated FOXO1 by CBP/ p300 may further support FOXO1 phosphorylation by AKT, allowing nuclear export and negative regulation of FOXO proteins (Gross et al., 2009; Tzivion et al., 2011).

Overall, the experiments provide valuable mechanistic insights into the adverse effects of ImP on the regenerative capacity of ECs manifested by reduced migratory and angiogenic potential. These findings are consistent with previous reports revealing that overexpression of FOXO1 in HUVECs results in decreased endothelial cell sprouting and migration. Contrariwise, FOXO1 silencing promoted the angiogenic ability of HUVECs (Potente et al., 2005; Ronnebaum and Patterson, 2010). However, a global deficiency of FOXO1 in mice has been shown to induce embryonic lethality due to impaired vasculogenesis, highlighting its importance in vascular development (Dharaneeswaran et al., 2014; Kandula et al., 2016). Other studies also linked augmented FOXO1 activity with insulin resistance and lipid accumulation of myocardial cells (Kandula et al., 2016). Under insulin resistance and diabetes states, FOXO1 phosphorylation is diminished due to AKT inactivation, causing FOXO1 to remain highly active in the nucleus, leading to metabolic disturbances, impaired angiogenesis, inflammation and increased cardiac cell death, and eventually to heart failure (Kandula et al., 2016; Xin et al., 2017). However, restoration of insulin sensitivity could be observed upon FOXO1 repression in mice (Xin et al., 2017). Furthermore, FOXO1 hyper-activation can potentiate the development of atherosclerosis by positive regulation of adipocyte fatty acid binding protein (FABP4) gene transcription, leading to increased accumulation of myocardial lipids in the heart (Kandula et al., 2016; Yan et al., 2020). In addition, HFD conditions and FOXO1 overexpression diminished insulin signaling by downregulating IRS1 activity followed by AKT inactivation, ultimately promoting insulin resistance (Battiprolu et al., 2012).

Indeed, FOXO1 overexpression in HUVECs also promoted oxidative stress and inflammation due to reduced NO bioavailability (Menghini et al., 2015). Additionally, FOXO1 mediates pro-inflammatory response by increasing the expression of its targets ICAM-1 and VCAM-1, both *in vitro* and *in vivo* (Jian et al., 2020; Liu et al., 2020; Dudek et al., 2022). Here, silencing of *FOXO1* abolished ImP-induced increase in

ICAM-1 and VCAM-1 levels in HAECs compared to control siRNA groups, including scramble siRNA (Scr siRNA) and *FOXO1* siRNA. These findings further support the contribution of a FOXO1-dependent pathway in ImP-mediated endothelial inflammation and vascular remodeling.

6.2. Effect of Imidazole propionate in the development of atherosclerosis

Given the initial finding that ImP impairs endothelial cell functions by eliciting a pro-inflammatory response, it was investigated whether ImP ultimately contributes to the development of atherosclerotic plaque formation *in vivo* at early and late stages. During the early stage of atherosclerotic development, LDL fractions accumulate in the intima layer of blood vessels, where they become pro-inflammatory and immunogenic due to oxidative or other modifications. Circulating pro-inflammatory monocytes, attracted by chemokines, attach to adhesion molecules on activated ECs and ultimately differentiate into macrophages/ foam cells by binding to lipoprotein particles through scavenger receptors. Furthermore, resident SMCs, which are mainly present at sites prone to atherosclerotic plaque formation, migrate and proliferate into the intimal layer causing pathologic intimal thickening and fibrous cap atheroma, which is considered the progressive stage from early to advanced lesion formation. Advanced atherosclerotic lesions are characterized by plaque vulnerability due to an increased risk of plaque rupture and life-threatening thrombus formation (Libby et al., 2019).

Genetically modified apolipoprotein E (Apoe) knockout (*Apoe*$^{-/-}$) mice are the most widely used models to study atherosclerotic processes and inter-organ cross-talk *in vivo* (Oppi et al., 2019). The glycoprotein apolipoprotein E (Apoe), which is a component of all lipoproteins apart from low-density lipoproteins (LDL), is primarily synthesized in the liver and brain but also by monocytes and macrophages in vessels (Meir and Leitersdorf, 2004). Apoe acts as a ligand for receptors that degrade chylomicrons and remnants of very low-density lipoproteins (VLDL). In humans, distinct Apoe isoforms are related to altered lipid profiles and an elevated risk for cardiovascular mortality. For instance, individuals who carry the Apoe4 allele are more susceptible to developing cardiovascular risks by enhancing oxidative stress and inflammation than those with the Apoe2 and Apoe3 isoforms (Oppi et al., 2019). Importantly, Apoe genetic deletion in mice results in severe hypercholesterolemia and spontaneous atherosclerotic lesions occurring more frequently in the aortic root, carotid artery, and aortic arch/ branches (Meir and Leitersdorf, 2004; Oppi et al., 2019).

On the whole, atherosclerotic lesions tend to develop primarily in the proximal (closer to the heart) region of the aorta and become more prominent along the distal aorta as the disease progresses (Oppi et al., 2019).

In this study, exposure to ImP and HFD for 6 and 12 weeks increased atherosclerotic plaque formation in the ascending aorta (aortic arch). Atherosclerotic lesions were also observed to be distributed differently in the aortic arch and the aortic roots of *Apoe*$^{-/-}$ mice, demonstrating a more rapid plaque development in the aortic roots of ImP-treated mice after 12 weeks of HFD compared to short-term treatment for 6 weeks. Despite mild lesions being visible in both the aortic arch and aortic root area of SCD-fed mice, no significant differences were found. The spontaneous development of atherosclerotic lesions in *Apoe*$^{-/-}$ mice under SCD has been frequently reported due to hypercholesterolemia. An HFD accelerates the atherosclerotic process (Meir and Leitersdorf, 2004). Previous studies have shown that dietary compositions, including cholesterol and fat, can impact lipoprotein levels and the development of atherosclerosis. A standard protocol to induce atherosclerosis in animal models often involves a fat content ranging from 20% to 45% and a cholesterol level of 0.5% to 4% for a duration of about 8 to 16 weeks (Kolodgie et al., 1996; Gisterå et al., 2022). Among these components, dietary cholesterol has been identified as the main pro-atherogenic factor (Getz and Reardon, 2006). The typical composition of a normal SCD contains 4% to 6% fat and ≤0.03% cholesterol (Gisterå et al., 2022). In this study, the mice received an HFD with a crude fat content of 34.6% and cholesterol levels of 2.9%, whereas the control animals of the same age received a corresponding control (SCD) diet containing 4.2% of crude fat and 0.14% of cholesterol by weight. Other research on diets has shown that high-fat levels above 45% have diabetogenic effects contributing to dyslipidemia and metabolic syndromes, including glucose intolerance and insulin resistance (Liu et al., 2018). In most wild-type mice, HFD alone is insufficient to induce atherosclerosis, but it effectively promotes disease progression in atheroprone genetic mice (Oppi et al., 2019). Hence, the present study aimed to identify atherosclerotic plaque development and the extent of lesion formation in *Apoe*$^{-/-}$ mice in response to ImP treatment without exaggerating the pathological effects induced by dietary factors. Of note, only low histidine content was defined in both SCD (0.64%) and HFD (0.74%) foods (ssniff-Spezialdiäten GmbH, Germany), which can lead to minimal ImP production also in the control animals as indicated by the ImP

plasma measurements. Nevertheless, these data revealed increased ImP plasma levels in the intervention group without affecting urocanate concentrations, suggesting an effective drinking protocol during 6 and 12 weeks of ImP treatment. The comparable plasma levels of urocanate between both groups might suggest a resemblance in gut microbial composition and environment capable of generating ImP from urocanate during histidine degradation (Koh et al., 2018). In addition, the administration of HFD is more consistent with a well-defined atherogenic mouse model rather than a diabetogenic model contributing to gut dysbiosis and alternative histidine metabolism. However, the circadian rhythm in mice and food intake may influence plasma metabolite levels, and therefore, ImP levels introduce additional variability in the data. Furthermore, the age of the mice also plays a critical role in plaque progression, as histological and morphometric analyses show that increased elastic lamina fragmentation, arterial calcification and wall thinning occurred at 32 weeks of age, while macrophage accumulation and fibrous plaques were observed between 15 and 20 weeks of age (Meir and Leitersdorf, 2004). This assessment is aligned with the age of the mice used in this study, which was between 19 and 20 weeks old. In addition, CD68+ expression was also enhanced in murine atherosclerotic plaques in response to ImP treatment, indicative of increased macrophage infiltration to the lesion site. Notably, a recent study reported that administration of macrolide antibiotics in *Apoe*$^{-/-}$ mice demonstrated increased CD68-expressing foam cells and M1 polarization in atherosclerotic plaque content due to loss of microbial diversity and change in *Firmicutes*/ *Bacteroidetes* ratio, suggesting a link between specific microbial-related metabolites and atherosclerotic vascular disease (Gerhardt et al., 2021). Finally, lipid profiling of control and ImP-treated mice revealed no difference in plasma levels of total cholesterol, VLDL, LDL and HDL within the two groups. Previous studies have related high total plasma cholesterol above 1000 mg/dl as a major cause of more pronounced and accelerated progression of atherosclerosis in mice (Oppi et al., 2019). In this study, the cholesterol levels were predominantly below 1000 mg/dl, further highlighting the pro-atherogenic and pro-inflammatory specific effects of ImP, which is independent of blood lipoprotein levels in *Apoe*$^{-/-}$ mice, but rather on endothelial dysfunction or injury (Gotto, JR, 1995), characterized by impaired endothelial migration and angiogenic potential as well as inflammatory activation upon suppression of the intracellular PI3K/ AKT signaling (Figure 23).

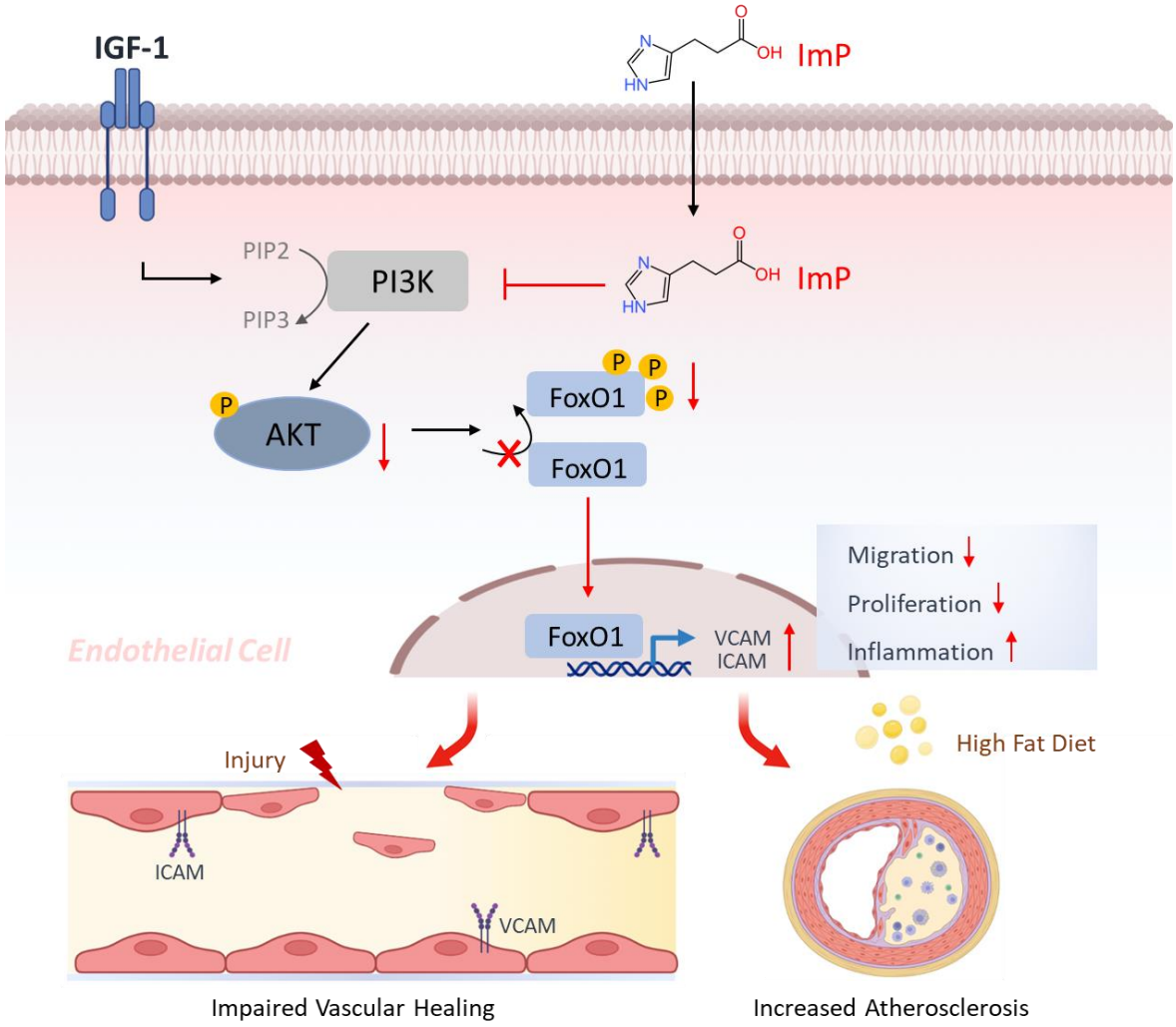

Figure 23: Novel cellular mechanism of Imidazole propionate involved in endothelial dysregulation.
The PI3K/ AKT signaling pathway regulates the transcriptional activity of FOXO1 in endothelial cells. Upon IGF-1 stimulation, PI3K is activated through the generation of phosphatidylinositol 4,5-bisphosphate (PIP2) to phosphatidylinositol (3,4,5)-trisphosphate (PIP3), thus resulting in subsequently AKT activation that directly phosphorylates and thereby inactivates FOXO1. Negative regulation of AKT prevents FOXO1 translocation to the nucleus and inhibits FOXO1 transcriptional activity. Upon imidazole propionate (ImP) treatment, the PI3K/ AKT signaling is significantly downregulated, leading to decreased phosphorylation and increased nuclear accumulation of FOXO1. Combined, these actions promote inflammation and inhibit both cell migration and proliferation of endothelial cells through FOXO1 downstream targets such as ICAM-1 and VCAM-1. Impaired vascular regeneration and endothelial wound healing after arterial injury ultimately increased atherosclerotic plaque formation *in vivo* (Nageswaran et al., 2024, *submitted*) (created with BioRender.com).

7. Limitations

A few limitations should be considered when interpreting these findings. Although the study used murine models and *in vitro* cell systems to study the underlying mechanism

of vascular complications, the data may not translate directly to the pathophysiology of atherosclerosis in humans. These models are performed in highly controlled and standardized conditions covering animal husbandry, dietary manipulations and defined treatment, which are limited in clinical trials. Compared to cell culture experiments, where the conditions of the cells cannot be replicated in a living organism, the mouse model considers the inter-organ crosstalk, including the gut microbiome and the vascular system. In addition, animal models are inherently different from human biology and may not fully reflect the complexity of human disease. Nonetheless, mouse models are more commonly used to study the pathophysiology of various human diseases due to their high genetic homology and resemblance to human vascular anatomy (Mehta and Vemuganti, 2014). Another concern applies to the sex differences in host behavior, as only male mice were used in this *in vivo* study. Men before age 50 are more likely at higher risk for CAD, but women experiencing acute coronary events tend to have a worse prognosis than men. Additionally, following the menopause transition, women have a higher incidence of CAD, which eventually exceeds that of men (Reue and Wiese, 2022). However, the study design did not incorporate a gender-specific analysis, which would have required a significantly higher number of animals conflicting with the animal ethics and the 3R (Replace, Reduce, Refine) principal guideline.

One further limitation involves the lack of ImP treatment in the control group of HAECs when considering that healthy subjects from clinical studies and control animals exhibit low plasma levels of ImP (Koh et al., 2018). Nevertheless, the study initially focused exclusively on ImP-mediated effects in ECs. Moreover, while the typical concentration of ImP in plasma falls within the tens of nanomolar range, the ImP-induced dysregulation of the PI3K/ AKT/ FOXO1 signaling pathway in HAECs ranged from 10 to 100 nM concentrations. Therefore, it would be valuable to investigate the extent to which ImP at physiological concentrations affects the regenerative potential of ECs. Whether ImP acts receptor-dependent or directly incorporates into the cells and translocates through the membranes also remains unclear. Further quantitative studies using fluorescence-based binding assay can provide more insight into the interaction between ImP and the receptor or cell membrane diffusion. Furthermore, in an *in vitro* rescue experiment, targeted gene knockdown of FOXO1 in ECs abrogated the pro-inflammatory phenotype of ImP, underscoring the negative impact on endothelial cell physiology. However, endothelial-specific FOXO1 knockout mice would allow a more

comprehensive mechanistic understanding of ImP and endothelial dysregulation to develop potential new therapeutic strategies.

8. Conclusion

The key findings have shown that the gut microbiota-derived metabolite imidazole propionate (ImP) significantly impairs insulin receptor signaling through aberration of PI3K/ AKT/ FOXO1 signaling pathway in ECs, thereby dysregulating their functional properties, including migratory, proliferative and angiogenic capacities. Additionally, ImP induces inflammatory activation of ECs, leading to enhanced expression of cellular adhesion molecules ICAM-1, VCAM-1, and E-selectin. This inflammatory response of ImP was accompanied by increased adhesion of monocytes to ECs. The ImP-mediated pro-inflammatory phenotype was rescued by targeted gene silencing of FOXO1 in endothelial cells. The exact mechanism for FOXO1 regulation *in vivo* is not yet clear. Therefore, it may be necessary to investigate the underlying molecular regulation and interaction between ImP-induced endothelial dysfunction and endothelial-specific FOXO1-knockout animal model.

In addition, ImP treatment in mice results in impaired vascular regeneration and endothelial wound healing after arterial injury and, ultimately, increased atherosclerosis in atheroprone *Apoe*$^{-/-}$ mice, linking gut microbiota-derived processes to various cardiovascular disease-related phenotypes, including endothelial dysfunction and chronic vascular inflammation. The interplay between the gut microbiota and these phenotypes highlights the significance of comprehending and targeting the gut microbiome and its metabolites to develop novel treatment or prevention strategies for CVDs. The advancement of non-lethal microbial inhibitors that selectively target specific bacterial enzymes involved in the ImP production while exhibiting limited systemic exposure in the host could be a promising therapeutic approach. However, dietary interventions, probiotics and lifestyle changes could be used to modulate the microbial community to prevent cardiovascular events and improve cardiovascular outcomes.

9. References

1. Aitsebaomo, J., Wennerberg, K., Der, C.J., Zhang, C., Kedar, V., Moser, M., Kingsley-Kallesen, M.L., Zeng, G.-Q., and Patterson, C. (2004). p68RacGAP is a novel GTPase-activating protein that interacts with vascular endothelial zinc finger-1 and modulates endothelial cell capillary formation. The Journal of biological chemistry *279*, 17963-17972.

2. Aki, S., Yoshioka, K., Okamoto, Y., Takuwa, N., and Takuwa, Y. (2015). Phosphatidylinositol 3-kinase class II α-isoform PI3K-C2α is required for transforming growth factor β-induced Smad signaling in endothelial cells. The Journal of biological chemistry *290*, 6086-6105.

3. Arnaoutova, I., and Kleinman, H.K. (2010). In vitro angiogenesis: endothelial cell tube formation on gelled basement membrane extract. Nature protocols *5*, 628-635.

4. Autiero, M., Waltenberger, J., Communi, D., Kranz, A., Moons, L., Lambrechts, D., Kroll, J., Plaisance, S., Mol, M. de, and Bono, F., et al. (2003). Role of PlGF in the intra- and intermolecular cross talk between the VEGF receptors Flt1 and Flk1. Nature medicine *9*, 936-943.

5. Battiprolu, P.K., Hojayev, B., Jiang, N., Wang, Z.V., Luo, X., Iglewski, M., Shelton, J.M., Gerard, R.D., Rothermel, B.A., and Gillette, T.G., et al. (2012). Metabolic stress-induced activation of FoxO1 triggers diabetic cardiomyopathy in mice. The Journal of clinical investigation *122*, 1109-1118.

6. Bentzon, J.F., Otsuka, F., Virmani, R., and Falk, E. (2014). Mechanisms of plaque formation and rupture. Circulation research *114*, 1852-1866.

7. Boal, F., Timotin, A., Roumegoux, J., Alfarano, C., Calise, D., Anesia, R., Parini, A., Valet, P., Tronchere, H., and Kunduzova, O. (2016). Apelin-13 administration protects against ischaemia/reperfusion-mediated apoptosis through the FoxO1 pathway in high-fat diet-induced obesity. British journal of pharmacology *173*, 1850-1863.

8. Boccitto, M., and Kalb, R.G. (2011). Regulation of Foxo-dependent transcription by post-translational modifications. Current drug targets *12*, 1303-1310.

9. Boukhalfa, A., Nascimbeni, A.C., Ramel, D., Dupont, N., Hirsch, E., Gayral, S., Laffargue, M., Codogno, P., and Morel, E. (2020). PI3KC2α-dependent and VPS34-independent generation of PI3P controls primary cilium-mediated autophagy in response to shear stress. Nature communications *11*, 294.

10. Brown, J.M., and Hazen, S.L. (2018). Microbial modulation of cardiovascular disease. Nature reviews. Microbiology *16*, 171-181.

11. Carter, M.E., and Brunet, A. (2007). FOXO transcription factors. Current biology : CB *17*, R113-4.

12. Caterina, R. de, Zampolli, A., Del Turco, S., Madonna, R., and Massaro, M. (2006). Nutritional mechanisms that influence cardiovascular disease. The American journal of clinical nutrition *83*, 421S-426S.

13. Catry, E., Bindels, L.B., Tailleux, A., Lestavel, S., Neyrinck, A.M., Goossens, J.-F., Lobysheva, I., Plovier, H., Essaghir, A., and Demoulin, J.-B., et al. (2018). Targeting the

gut microbiota with inulin-type fructans: preclinical demonstration of a novel approach in the management of endothelial dysfunction. Gut *67*, 271-283.

14. Chen, S., Shen, Y., Liu, Y.-H., Dai, Y., Wu, Z.-M., Wang, X.-Q., Yang, C.-D., Li, L.-Y., Liu, J.-M., and Zhang, L.-P., et al. (2021). Impact of glycemic control on the association of endothelial dysfunction and coronary artery disease in patients with type 2 diabetes mellitus. Cardiovascular diabetology *20*, 64.

15. Chiu, J.-J., and Chien, S. (2011). Effects of disturbed flow on vascular endothelium: pathophysiological basis and clinical perspectives. Physiological reviews *91*, 327-387.

16. Chong, Z.Z., Wang, S., Shang, Y.C., and Maiese, K. (2012). Targeting cardiovascular disease with novel SIRT1 pathways. Future cardiology *8*, 89-100.

17. Cook-Mills, J.M., Marchese, M.E., and Abdala-Valencia, H. (2011). Vascular cell adhesion molecule-1 expression and signaling during disease: regulation by reactive oxygen species and antioxidants. Antioxidants & redox signaling *15*, 1607-1638.

18. Ćurić, Ž.B., Masle, A.M., Kibel, A., Selthofer-Relatić, K., Stupin, A., Mihaljević, Z., Jukić, I., Stupin, M., Matić, A., and Kozina, N., et al. (2021). Effects of n-3 Polyunsaturated Fatty Acid-Enriched Hen Egg Consumption on the Inflammatory Biomarkers and Microvascular Function in Patients with Acute and Chronic Coronary Syndrome-A Randomized Study. Biology *10*.

19. De Meyer, Guido R Y, Grootaert, M.O.J., Michiels, C.F., Kurdi, A., Schrijvers, D.M., and Martinet, W. (2015). Autophagy in vascular disease. Circulation research *116*, 468-479.

20. Deepjyoti Paul, and Bhabatosh Das (2022). Chapter One - Gut microbiome in the emergence of antibiotic-resistant bacterial pathogens. In Human Microbiome in Health and Disease - Part B, Bhabatosh Das and Vijai Singh, eds. (Academic Press), pp. 1–31.

21. Dharaneeswaran, H., Abid, M.R., Yuan, L., Dupuis, D., Beeler, D., Spokes, K.C., Janes, L., Sciuto, T., Kang, P.M., and Jaminet, S.-C.S., et al. (2014). FOXO1-mediated activation of Akt plays a critical role in vascular homeostasis. Circulation research *115*, 238-251.

22. Döring, Y., Noels, H., van der Vorst, Emiel P C, Neideck, C., Egea, V., Drechsler, M., Mandl, M., Pawig, L., Jansen, Y., and Schröder, K., et al. (2017). Vascular CXCR4 Limits Atherosclerosis by Maintaining Arterial Integrity: Evidence From Mouse and Human Studies. Circulation *136*, 388-403.

23. Dudek, M., Lohr, K., Donakonda, S., Baumann, T., Lüdemann, M., Hegenbarth, S., Dübbel, L., Eberhagen, C., Michailidou, S., and Yassin, A., et al. (2022). IL-6-induced FOXO1 activity determines the dynamics of metabolism in CD8 T cells cross-primed by liver sinusoidal endothelial cells. Cell reports *38*, 110389.

24. Durst, R., Sauls, K., Peal, D.S., deVlaming, A., Toomer, K., Leyne, M., Salani, M., Talkowski, M.E., Brand, H., and Perrocheau, M., et al. (2015). Mutations in DCHS1 cause mitral valve prolapse. Nature *525*, 109-113.

25. Eelen, G., Treps, L., Li, X., and Carmeliet, P. (2020). Basic and Therapeutic Aspects of Angiogenesis Updated. Circulation research *127*, 310-329.

26. Farhan, M., Silva, M., Xingan, X., Huang, Y., and Zheng, W. (2020). Role of FOXO Transcription Factors in Cancer Metabolism and Angiogenesis. Cells *9*.

27. Feingold, K.R. (2000). Introduction to Lipids and Lipoproteins. In Endotext, K.R. Feingold, B. Anawalt, M.R. Blackman, A. Boyce, G. Chrousos, E. Corpas, W.W. de Herder, K. Dhatariya, K. Dungan and J. Hofland et al., eds. (South Dartmouth (MA)).

28. Fernández-Hernando, C., Ackah, E., Yu, J., Suárez, Y., Murata, T., Iwakiri, Y., Prendergast, J., Miao, R.Q., Birnbaum, M.J., and Sessa, W.C. (2007). Loss of Akt1 leads to severe atherosclerosis and occlusive coronary artery disease. Cell metabolism *6*, 446-457.

29. Gadecka, A., and Bielak-Zmijewska, A. (2019). Slowing Down Ageing: The Role of Nutrients and Microbiota in Modulation of the Epigenome. Nutrients *11*.

30. Gail A.M. Cresci, and Kristin Izzo (2019). Chapter 4 - Gut Microbiome. In Adult Short Bowel Syndrome, Mandy L. Corrigan, Kristen Roberts and Ezra Steiger, eds. (Academic Press), pp. 45–54.

31. Gallay, N., Dos Santos, C., Cuzin, L., Bousquet, M., Simmonet Gouy, V., Chaussade, C., Attal, M., Payrastre, B., Demur, C., and Récher, C. (2009). The level of AKT phosphorylation on threonine 308 but not on serine 473 is associated with high-risk cytogenetics and predicts poor overall survival in acute myeloid leukaemia. Leukemia *23*, 1029-1038.

32. Ganesh, D., Jain, P., Shanthamurthy, C.D., Toraskar, S., and Kikkeri, R. (2021). Targeting Selectins Mediated Biological Activities With Multivalent Probes. Frontiers in chemistry *9*, 773027.

33. Gao, Y., Moten, A., and Lin, H.-K. (2014). Akt: a new activation mechanism. Cell research *24*, 785-786.

34. GBD 2019 Stroke Collaborator (2021). Global, regional, and national burden of stroke and its risk factors, 1990-2019: a systematic analysis for the Global Burden of Disease Study 2019. The Lancet. Neurology *20*, 795-820.

35. Gerhardt, T., Haghikia, A., Stapmanns, P., and Leistner, D.M. (2021). Immune Mechanisms of Plaque Instability. Frontiers in cardiovascular medicine *8*, 797046.

36. Getz, G.S., and Reardon, C.A. (2006). Diet and murine atherosclerosis. Arteriosclerosis, thrombosis, and vascular biology *26*, 242-249.

37. Getzin, T., Krishnasamy, K., Gamrekelashvili, J., Kapanadze, T., Limbourg, A., Häger, C., Napp, L.C., Bauersachs, J., Haller, H., and Limbourg, F.P. (2018). The chemokine receptor CX(3)CR1 coordinates monocyte recruitment and endothelial regeneration after arterial injury. EMBO molecular medicine *10*, 151-159.

38. Ghigo, A., Laffargue, M., Li, M., and Hirsch, E. (2017). PI3K and Calcium Signaling in Cardiovascular Disease. Circulation research *121*, 282-292.

39. Gimbrone, M.A., JR, and García-Cardeña, G. (2016). Endothelial Cell Dysfunction and the Pathobiology of Atherosclerosis. Circulation research *118*, 620-636.

40. Gisterå, A., Ketelhuth, D.F.J., Malin, S.G., and Hansson, G.K. (2022). Animal Models of Atherosclerosis-Supportive Notes and Tricks of the Trade. Circulation research *130*, 1869-1887.

41. Gotto, A.M., JR (1995). Lipid lowering, regression, and coronary events. A review of the Interdisciplinary Council on Lipids and Cardiovascular Risk Intervention, Seventh Council meeting. Circulation *92*, 646-656.

42. Gross, D.N., Wan, M., and Birnbaum, M.J. (2009). The role of FOXO in the regulation of metabolism. Current diabetes reports *9*, 208-214.

43. Grossi, V., Fasano, C., Celestini, V., Lepore Signorile, M., Sanese, P., and Simone, C. (2019). Chasing the FOXO3: Insights into Its New Mitochondrial Lair in Colorectal Cancer Landscape. Cancers *11*.

44. Guarner, F., and Malagelada, J.-R. (2003). Gut flora in health and disease. Lancet (London, England) *361*, 512-519.

45. Gui, Y., Zheng, H., and Cao, R.Y. (2022). Foam Cells in Atherosclerosis: Novel Insights Into Its Origins, Consequences, and Molecular Mechanisms. Frontiers in cardiovascular medicine *9*, 845942.

46. Guinane, C.M., and Cotter, P.D. (2013). Role of the gut microbiota in health and chronic gastrointestinal disease: understanding a hidden metabolic organ. Therapeutic advances in gastroenterology *6*, 295-308.

47. Gurung, M., Li, Z., You, H., Rodrigues, R., Jump, D.B., Morgun, A., and Shulzhenko, N. (2020). Role of gut microbiota in type 2 diabetes pathophysiology. EBioMedicine *51*, 102590.

48. Haghikia, A., Zimmermann, F., Schumann, P., Jasina, A., Roessler, J., Schmidt, D., Heinze, P., Kaisler, J., Nageswaran, V., and Aigner, A., et al. (2022). Propionate attenuates atherosclerosis by immune-dependent regulation of intestinal cholesterol metabolism. European heart journal *43*, 518-533.

49. Harishkumar, R., Hans, S., Stanton, J.E., Grabrucker, A.M., Lordan, R., and Zabetakis, I. (2022). Targeting the Platelet-Activating Factor Receptor (PAF-R): Antithrombotic and Anti-Atherosclerotic Nutrients. Nutrients *14*.

50. He, Y., Sun, M.M., Zhang, G.G., Yang, J., Chen, K.S., Xu, W.W., and Li, B. (2021). Targeting PI3K/Akt signal transduction for cancer therapy. Signal transduction and targeted therapy *6*, 425.

51. Heinecke, J.W. (2006). Lipoprotein oxidation in cardiovascular disease: chief culprit or innocent bystander? The Journal of experimental medicine *203*, 813-816.

52. Hetherington, I., and Totary-Jain, H. (2022). Anti-atherosclerotic therapies: Milestones, challenges, and emerging innovations. Molecular therapy : the journal of the American Society of Gene Therapy *30*, 3106-3117.

53. Hou, K., Wu, Z.-X., Chen, X.-Y., Wang, J.-Q., Zhang, D., Xiao, C., Zhu, D., Koya, J.B., Wei, L., and Li, J., et al. (2022). Microbiota in health and diseases. Signal transduction and targeted therapy *7*, 135.

54. Huang, J.-P., Huang, S.-S., Deng, J.-Y., and Hung, L.-M. (2009). Impairment of insulin-stimulated Akt/GLUT4 signaling is associated with cardiac contractile dysfunction and aggravates I/R injury in STZ-diabetic rats. Journal of biomedical science *16*, 77.

55. Human Microbiome Project Consortium (2012). Structure, function and diversity of the healthy human microbiome. Nature *486*, 207-214.

56. Humphrey, J.D., and McCulloch, A.D. (2003). The Cardiovascular System — Anatomy, Physiology and Cell Biology. In Biomechanics of Soft Tissue in Cardiovascular Systems, G.A. Holzapfel and R.W. Ogden, eds. (Vienna: Springer Vienna), pp. 1–14.

57. Hwang, J.-w., Yao, H., Caito, S., Sundar, I.K., and Rahman, I. (2013). Redox regulation of SIRT1 in inflammation and cellular senescence. Free radical biology & medicine *61*, 95-110.

58. Jandhyala, S.M., Talukdar, R., Subramanyam, C., Vuyyuru, H., Sasikala, M., and Nageshwar Reddy, D. (2015). Role of the normal gut microbiota. World journal of gastroenterology *21*, 8787-8803.

59. Javadifar, A., Rastgoo, S., Banach, M., Jamialahmadi, T., Johnston, T.P., and Sahebkar, A. (2021). Foam Cells as Therapeutic Targets in Atherosclerosis with a Focus on the Regulatory Roles of Non-Coding RNAs. International journal of molecular sciences *22*.

60. Jayaraman, S. (2019). Of ethnicity, environment, and microbiota. Cellular & molecular immunology *16*, 106-108.

61. Jean, S., and Kiger, A.A. (2014). Classes of phosphoinositide 3-kinases at a glance. Journal of cell science *127*, 923-928.

62. Jian, D., Wang, Y., Jian, L., Tang, H., Rao, L., Chen, K., Jia, Z., Zhang, W., Liu, Y., and Chen, X., et al. (2020). METTL14 aggravates endothelial inflammation and atherosclerosis by increasing FOXO1 N6-methyladeosine modifications. Theranostics *10*, 8939-8956.

63. Jiramongkol, Y., and Lam, E.W.-F. (2020). FOXO transcription factor family in cancer and metastasis. Cancer metastasis reviews *39*, 681-709.

64. Jörg, S., Grohme, D.A., Erzler, M., Binsfeld, M., Haghikia, A., Müller, D.N., Linker, R.A., and Kleinewietfeld, M. (2016). Environmental factors in autoimmune diseases and their role in multiple sclerosis. Cellular and molecular life sciences : CMLS *73*, 4611-4622.

65. Kandula, V., Kosuru, R., Li, H., Yan, D., Zhu, Q., Lian, Q., Ge, R.-S., Xia, Z., and Irwin, M.G. (2016). Forkhead box transcription factor 1: role in the pathogenesis of diabetic cardiomyopathy. Cardiovascular diabetology *15*, 44.

66. Kaur, S., Leszczynska, K., Abraham, S., Scarcia, M., Hiltbrunner, S., Marshall, C.J., Mavria, G., Bicknell, R., and Heath, V.L. (2011). RhoJ/TCL regulates endothelial motility and tube formation and modulates actomyosin contractility and focal adhesion numbers. Arteriosclerosis, thrombosis, and vascular biology *31*, 657-664.

67. Khera, A.V., Emdin, C.A., Drake, I., Natarajan, P., Bick, A.G., Cook, N.R., Chasman, D.I., Baber, U., Mehran, R., and Rader, D.J., et al. (2016). Genetic Risk, Adherence to a Healthy Lifestyle, and Coronary Disease. The New England journal of medicine *375*, 2349-2358.

68. Kinross, J.M., Darzi, A.W., and Nicholson, J.K. (2011). Gut microbiome-host interactions in health and disease. Genome medicine *3*, 14.

69. Koch, P.A., Dornan, G.L., Hessenberger, M., and Haucke, V. (2021). The molecular mechanisms mediating class II PI 3-kinase function in cell physiology. The FEBS journal *288*, 7025-7042.

70. Koh, A., Mannerås-Holm, L., Yunn, N.-O., Nilsson, P.M., Ryu, S.H., Molinaro, A., Perkins, R., Smith, J.G., and Bäckhed, F. (2020). Microbial Imidazole Propionate Affects Responses to Metformin through p38γ-Dependent Inhibitory AMPK Phosphorylation. Cell metabolism *32*, 643-653.e4.

71. Koh, A., Molinaro, A., Ståhlman, M., Khan, M.T., Schmidt, C., Mannerås-Holm, L., Wu, H., Carreras, A., Jeong, H., and Olofsson, L.E., et al. (2018). Microbially Produced Imidazole Propionate Impairs Insulin Signaling through mTORC1. Cell *175*, 947-961.e17.

72. Kolodgie, F.D., Katocs, A.S., JR, Largis, E.E., Wrenn, S.M., Cornhill, J.F., Herderick, E.E., Lee, S.J., and Virmani, R. (1996). Hypercholesterolemia in the rabbit induced by feeding graded amounts of low-level cholesterol. Methodological considerations regarding individual variability in response to dietary cholesterol and development of lesion type. Arteriosclerosis, thrombosis, and vascular biology *16*, 1454-1464.

73. Kong, P., Cui, Z.-Y., Huang, X.-F., Zhang, D.-D., Guo, R.-J., and Han, M. (2022). Inflammation and atherosclerosis: signaling pathways and therapeutic intervention. Signal transduction and targeted therapy *7*, 131.

74. Krüger-Genge, A., Blocki, A., Franke, R.-P., and Jung, F. (2019). Vascular Endothelial Cell Biology: An Update. International journal of molecular sciences *20*.

75. La Cuesta-Zuluaga, J. de, Mueller, N.T., Corrales-Agudelo, V., Velásquez-Mejía, E.P., Carmona, J.A., Abad, J.M., and Escobar, J.S. (2017). Metformin Is Associated With Higher Relative Abundance of Mucin-Degrading Akkermansia muciniphila and Several Short-Chain Fatty Acid-Producing Microbiota in the Gut. Diabetes care *40*, 54-62.

76. Lee, J.M., Hammarén, H.M., Savitski, M.M., and Baek, S.H. (2023). Control of protein stability by post-translational modifications. Nature communications *14*, 201.

77. Lee, J.-W., Chen, H., Pullikotil, P., and Quon, M.J. (2011). Protein kinase A-alpha directly phosphorylates FoxO1 in vascular endothelial cells to regulate expression of vascular cellular adhesion molecule-1 mRNA. The Journal of biological chemistry *286*, 6423-6432.

78. Lee, M.Y., Gamez-Mendez, A., Zhang, J., Zhuang, Z., Vinyard, D.J., Kraehling, J., Velazquez, H., Brudvig, G.W., Kyriakides, T.R., and Simons, M., et al. (2018). Endothelial Cell Autonomous Role of Akt1: Regulation of Vascular Tone and Ischemia-Induced Arteriogenesis. Arteriosclerosis, thrombosis, and vascular biology *38*, 870-879.

79. Li, J., Lin, S., Vanhoutte, P.M., Woo, C.W., and Xu, A. (2016). Akkermansia Muciniphila Protects Against Atherosclerosis by Preventing Metabolic Endotoxemia-Induced Inflammation in Apoe-/- Mice. Circulation *133*, 2434-2446.

80. Li, K., Le Yang, Li, J., Guan, C., Zhang, S., Lao, X., Ouyang, D., Zheng, G., Gao, S., and Wang, D., et al. (2019). TGFβ induces stemness through non-canonical AKT-FOXO3a axis in oral squamous cell carcinoma. EBioMedicine *48*, 70-80.

81. Libby, P., Buring, J.E., Badimon, L., Hansson, G.K., Deanfield, J., Bittencourt, M.S., Tokgözoğlu, L., and Lewis, E.F. (2019). Atherosclerosis. Nature reviews. Disease primers *5*, 56.

82. Libby, P., and Everett, B.M. (2019). Novel Antiatherosclerotic Therapies. Arteriosclerosis, thrombosis, and vascular biology *39*, 538-545.

83. Lin, S., Zhang, Q., Shao, X., Zhang, T., Xue, C., Shi, S., Zhao, D., and Lin, Y. (2017). IGF-1 promotes angiogenesis in endothelial cells/adipose-derived stem cells co-culture system with activation of PI3K/Akt signal pathway. Cell proliferation *50*.

84. Liu, J., Xie, X., Yan, D., Wang, Y., Yuan, H., Cai, Y., Luo, J., Xu, A., Huang, Y., and Cheung, C.W., et al. (2020). Up-regulation of FoxO1 contributes to adverse vascular remodelling in type 1 diabetic rats. Journal of cellular and molecular medicine *24*, 13727-13738.

85. Liu, L., Huang, Y., Fang, C., Zhang, H., Yang, J., Xuan, C., Wang, F., Lu, H., Cao, S., and Wang, Y., et al. (2018). Chronic noise-exposure exacerbates insulin resistance and promotes the manifestations of the type 2 diabetes in a high-fat diet mouse model. PloS one *13*, e0195411.

86. Liu, Y., Liu, Y., Deng, J., Li, W., and Nie, X. (2021a). Fibroblast Growth Factor in Diabetic Foot Ulcer: Progress and Therapeutic Prospects. Frontiers in endocrinology *12*, 744868.

87. Liu, Y.-X., Yuan, P.-Z., Wu, J.-H., and Hu, B. (2021b). Lipid accumulation and novel insight into vascular smooth muscle cells in atherosclerosis. Journal of molecular medicine (Berlin, Germany) *99*, 1511-1526.

88. Long, H.-Z., Cheng, Y., Zhou, Z.-W., Luo, H.-Y., Wen, D.-D., and Gao, L.-C. (2021). PI3K/AKT Signal Pathway: A Target of Natural Products in the Prevention and Treatment of Alzheimer's Disease and Parkinson's Disease. Frontiers in pharmacology *12*, 648636.

89. Low Wang, C.C., Hess, C.N., Hiatt, W.R., and Goldfine, A.B. (2016). Clinical Update: Cardiovascular Disease in Diabetes Mellitus: Atherosclerotic Cardiovascular Disease and Heart Failure in Type 2 Diabetes Mellitus - Mechanisms, Management, and Clinical Considerations. Circulation *133*, 2459-2502.

90. Manning, B.D., and Cantley, L.C. (2007). AKT/PKB signaling: navigating downstream. Cell *129*, 1261-1274.

91. Marchelek-Mysliwiec, M., Nalewajska, M., Turoń-Skrzypińska, A., Kotrych, K., Dziedziejko, V., Sulikowski, T., and Pawlik, A. (2022). The Role of Forkhead Box O in Pathogenesis and Therapy of Diabetes Mellitus. International journal of molecular sciences *23*.

92. Margaria, J.P., Ratto, E., Gozzelino, L., Li, H., and Hirsch, E. (2019). Class II PI3Ks at the Intersection between Signal Transduction and Membrane Trafficking. Biomolecules *9*.

93. Maurya, M.R., Gupta, S., Li, J.Y.-S., Ajami, N.E., Chen, Z.B., Shyy, J.Y.-J., Chien, S., and Subramaniam, S. (2021). Longitudinal shear stress response in human endothelial cells to atheroprone and atheroprotective conditions. Proceedings of the National Academy of Sciences of the United States of America *118*.

94. Mehta, S.L., and Vemuganti, R. (2014). Mechanisms of Stroke Induced Neuronal Death: Multiple Therapeutic Opportunities. Advances in Animal and Veterinary Sciences *2*, 438-446.

95. Meir, K.S., and Leitersdorf, E. (2004). Atherosclerosis in the apolipoprotein-E-deficient mouse: a decade of progress. Arteriosclerosis, thrombosis, and vascular biology *24*, 1006-1014.

96. Mendez, P.-L., Obendorf, L., Jatzlau, J., Burdzinski, W., Reichenbach, M., Nageswaran, V., Haghikia, A., Stangl, V., Hiepen, C., and Knaus, P. (2022). Atheroprone fluid shear

stress-regulated ALK1-Endoglin-SMAD signaling originates from early endosomes. BMC biology *20*, 210.

97. Menghini, R., Casagrande, V., Cardellini, M., Ballanti, M., Davato, F., Cardolini, I., Stoehr, R., Fabrizi, M., Morelli, M., and Anemona, L., et al. (2015). FoxO1 regulates asymmetric dimethylarginine via downregulation of dimethylaminohydrolase 1 in human endothelial cells and subjects with atherosclerosis. Atherosclerosis *242*, 230-235.

98. Menon, R.T., Shrestha, A.K., and Shivanna, B. (2017). Hyperoxia exposure disrupts adrenomedullin signaling in newborn mice: Implications for lung development in premature infants. Biochemical and biophysical research communications *487*, 666-671.

99. Meyer, N., and Akdis, C.A. (2013). Vascular endothelial growth factor as a key inducer of angiogenesis in the asthmatic airways. Current allergy and asthma reports *13*, 1-9.

100. Molinaro, A., Bel Lassen, P., Henricsson, M., Wu, H., Adriouch, S., Belda, E., Chakaroun, R., Nielsen, T., Bergh, P.-O., and Rouault, C., et al. (2020). Imidazole propionate is increased in diabetes and associated with dietary patterns and altered microbial ecology. Nature communications *11*, 5881.

101. Molinaro, A., Nemet, I., Bel Lassen, P., Chakaroun, R., Nielsen, T., Aron-Wisnewsky, J., Bergh, P.-O., Li, L., Henricsson, M., and Køber, L., et al. (2023). Microbially Produced Imidazole Propionate Is Associated With Heart Failure and Mortality. JACC. Heart failure.

102. Morello, F., Perino, A., and Hirsch, E. (2009). Phosphoinositide 3-kinase signalling in the vascular system. Cardiovascular research *82*, 261-271.

103. Moro, J., Tomé, D., Schmidely, P., Demersay, T.-C., and Azzout-Marniche, D. (2020). Histidine: A Systematic Review on Metabolism and Physiological Effects in Human and Different Animal Species. Nutrients *12*.

104. Mountford, J.K., Petitjean, C., Putra, H.W.K., McCafferty, J.A., Setiabakti, N.M., Lee, H., Tønnesen, L.L., McFadyen, J.D., Schoenwaelder, S.M., and Eckly, A., et al. (2015). The class II PI 3-kinase, PI3KC2α, links platelet internal membrane structure to shear-dependent adhesive function. Nature communications *6*, 6535.

105. Nageswaran, V., Reinshagen, L., Ramezani Rad, P., Kränkel, N., Knaus, P., Landmesser, U., and Haghikia, A. (2022a). Imidazole propionate impairs endothelial cell function and vascular repair after injury: Implication for coronary heart disease. DGK Herztage. Clinical Research in Cardiology *111*, 1299.

106. Nageswaran, V., Reinshagen, L., Ramezani Rad, P., Kränkel, N., Knaus, P., Landmesser, U., and Haghikia, A. (2022b). The gut microbiota-derived metabolite imidazole propionate affects endothelial cell physiology and vascular regeneration after arterial injury. 88. Jahrestagung der Deutschen Gesellschaft für Kardiologie - Herz- und Kreislaufforschung e.V. Clinical Research in Cardiology *111*, 592.

107. Nageswaran, V., Reinshagen, L., Ramezani Rad, P., Strässler, E.T., Kränkel, N., Leistner, D., Knaus, P., Landmesser, U., and Haghikia, A. (2023). Microbial Imidazole propionate mediates pro-inflammatory effects in endothelial cells and promotes atherosclerosis in mice. 89. Jahrestagung der Deutsche Gesellschaft für Kardiologie - Herz- und Kreislaufforschung e.V. (German Cardiac Society). Clinical Research in Cardiology *112*, 1005.

108. Nicoli, S., Tobia, C., Gualandi, L., Sena, G. de, and Presta, M. (2008). Calcitonin receptor-like receptor guides arterial differentiation in zebrafish. Blood *111*, 4965-4972.

109. Nold-Petry, C.A., Nold, M.F., Zepp, J.A., Kim, S.-H., Voelkel, N.F., and Dinarello, C.A. (2009). IL-32-dependent effects of IL-1beta on endothelial cell functions. Proceedings of the National Academy of Sciences of the United States of America *106*, 3883-3888.

110. North, B.J., and Sinclair, D.A. (2012). The intersection between aging and cardiovascular disease. Circulation research *110*, 1097-1108.

111. Oellerich, M.F., and Potente, M. (2012). FOXOs and sirtuins in vascular growth, maintenance, and aging. Circulation research *110*, 1238-1251.

112. Oppi, S., Lüscher, T.F., and Stein, S. (2019). Mouse Models for Atherosclerosis Research-Which Is My Line? Frontiers in cardiovascular medicine *6*, 46.

113. Page, D.J., Thuret, R., Venkatraman, L., Takahashi, T., Bentley, K., and Herbert, S.P. (2019). Positive Feedback Defines the Timing, Magnitude, and Robustness of Angiogenesis. Cell reports *27*, 3139-3151.e5.

114. Papadopoulos, P.D., Tsigalou, C., Valsamaki, P.N., Konstantinidis, T.G., Voidarou, C., and Bezirtzoglou, E. (2022). The Emerging Role of the Gut Microbiome in Cardiovascular Disease: Current Knowledge and Perspectives. Biomedicines *10*.

115. Park, S.-H., Sakamoto, H., Tsuji-Tamura, K., Furuyama, T., and Ogawa, M. (2009). Foxo1 is essential for in vitro vascular formation from embryonic stem cells. Biochemical and biophysical research communications *390*, 861-866.

116. Paulin, N., Döring, Y., Kooijman, S., Blanchet, X., Viola, J.R., Jong, R. de, Mandl, M., Hendrikse, J., Schiener, M., and Hundelshausen, P. von, et al. (2017). Human Neutrophil Peptide 1 Limits Hypercholesterolemia-induced Atherosclerosis by Increasing Hepatic LDL Clearance. EBioMedicine *16*, 204-211.

117. Perbellini, F., Watson, S.A., Bardi, I., and Terracciano, C.M. (2018). Heterocellularity and Cellular Cross-Talk in the Cardiovascular System. Frontiers in cardiovascular medicine *5*, 143.

118. Potente, M., Urbich, C., Sasaki, K.-i., Hofmann, W.K., Heeschen, C., Aicher, A., Kollipara, R., DePinho, R.A., Zeiher, A.M., and Dimmeler, S. (2005). Involvement of Foxo transcription factors in angiogenesis and postnatal neovascularization. The Journal of clinical investigation *115*, 2382-2392.

119. Poznyak, A., Grechko, A.V., Poggio, P., Myasoedova, V.A., Alfieri, V., and Orekhov, A.N. (2020). The Diabetes Mellitus-Atherosclerosis Connection: The Role of Lipid and Glucose Metabolism and Chronic Inflammation. International journal of molecular sciences *21*.

120. Psenakova, K., Kohoutova, K., Obsilova, V., Ausserlechner, M.J., Veverka, V., and Obsil, T. (2019). Forkhead Domains of FOXO Transcription Factors Differ in both Overall Conformation and Dynamics. Cells *8*.

121. Puthanveetil, P., Wan, A., and Rodrigues, B. (2013). FoxO1 is crucial for sustaining cardiomyocyte metabolism and cell survival. Cardiovascular research *97*, 393-403.

122. Qin, Q., Yan, S., Yang, Y., Chen, J., Li, T., Gao, X., Yan, H., Wang, Y., Wang, J., and Wang, S., et al. (2021). A Metagenome-Wide Association Study of the Gut Microbiome and Metabolic Syndrome. Frontiers in microbiology *12*, 682721.

123. Rajendran, P., Rengarajan, T., Thangavel, J., Nishigaki, Y., Sakthisekaran, D., Sethi, G., and Nishigaki, I. (2013). The vascular endothelium and human diseases. International journal of biological sciences *9*, 1057-1069.

124. Reue, K., and Wiese, C.B. (2022). Illuminating the Mechanisms Underlying Sex Differences in Cardiovascular Disease. Circulation research *130*, 1747-1762.

125. Roessler, J., Leistner, D.M., Landmesser, U., and Haghikia, A. (2022). Modulatory role of gut microbiota in cholesterol and glucose metabolism: Potential implications for atherosclerotic cardiovascular disease. Atherosclerosis *359*, 1-12.

126. Rong, S.J., Yang, C.L., Wang, F.X., Sun, F., Luo, J.H., Yue, T.T., Yang, P., Yu, Q., Zhang, S., and Wang, C.-Y. (2022). The Essential Role of FoxO1 in the Regulation of Macrophage Function. BioMed research international *2022*, 1068962.

127. Ronnebaum, S.M., and Patterson, C. (2010). The FoxO family in cardiac function and dysfunction. Annual review of physiology *72*, 81-94.

128. Roth, G.A., Mensah, G.A., Johnson, C.O., Addolorato, G., Ammirati, E., Baddour, L.M., Barengo, N.C., Beaton, A.Z., Benjamin, E.J., and Benziger, C.P., et al. (2020). Global Burden of Cardiovascular Diseases and Risk Factors, 1990-2019: Update From the GBD 2019 Study. Journal of the American College of Cardiology *76*, 2982-3021.

129. Sanchez-Alcoholado, L., Castellano-Castillo, D., Jordán-Martínez, L., Moreno-Indias, I., Cardila-Cruz, P., Elena, D., Muñoz-Garcia, A.J., Queipo-Ortuño, M.I., and Jimenez-Navarro, M. (2017). Role of Gut Microbiota on Cardio-Metabolic Parameters and Immunity in Coronary Artery Disease Patients with and without Type-2 Diabetes Mellitus. Frontiers in microbiology *8*, 1936.

130. Schober, A., Nazari-Jahantigh, M., Wei, Y., Bidzhekov, K., Gremse, F., Grommes, J., Megens, R.T.A., Heyll, K., Noels, H., and Hristov, M., et al. (2014). MicroRNA-126-5p promotes endothelial proliferation and limits atherosclerosis by suppressing Dlk1. Nature medicine *20*, 368-376.

131. Schroeder, A., Mueller, O., Stocker, S., Salowsky, R., Leiber, M., Gassmann, M., Lightfoot, S., Menzel, W., Granzow, M., and Ragg, T. (2006). The RIN: an RNA integrity number for assigning integrity values to RNA measurements. BMC molecular biology *7*, 3.

132. Seo, H.-R., Jeong, H.E., Joo, H.J., Choi, S.-C., Park, C.-Y., Kim, J.-H., Choi, J.-H., Cui, L.-H., Hong, S.J., and Chung, S., et al. (2016). Intrinsic FGF2 and FGF5 promotes angiogenesis of human aortic endothelial cells in 3D microfluidic angiogenesis system. Scientific reports *6*, 28832.

133. Shiojima, I., and Walsh, K. (2002). Role of Akt signaling in vascular homeostasis and angiogenesis. Circulation research *90*, 1243-1250.

134. Singh, R.K., Chang, H.-W., Di Yan, Lee, K.M., Ucmak, D., Wong, K., Abrouk, M., Farahnik, B., Nakamura, M., and Zhu, T.H., et al. (2017). Influence of diet on the gut microbiome and implications for human health. Journal of translational medicine *15*, 73.

135. Sorokin, V., Vickneson, K., Kofidis, T., Woo, C.C., Lin, X.Y., Foo, R., and Shanahan, C.M. (2020). Role of Vascular Smooth Muscle Cell Plasticity and Interactions in Vessel Wall Inflammation. Frontiers in immunology *11*, 599415.

136. Sorrentino, S.A., Bahlmann, F.H., Besler, C., Müller, M., Schulz, S., Kirchhoff, N., Doerries, C., Horváth, T., Limbourg, A., and Limbourg, F., et al. (2007). Oxidant stress impairs in vivo reendothelialization capacity of endothelial progenitor cells from patients with type 2 diabetes mellitus: restoration by the peroxisome proliferator-activated receptor-gamma agonist rosiglitazone. Circulation *116*, 163-173.

137. Summerhill, V.I., Grechko, A.V., Yet, S.-F., Sobenin, I.A., and Orekhov, A.N. (2019). The Atherogenic Role of Circulating Modified Lipids in Atherosclerosis. International journal of molecular sciences *20*.

138. Tai-Nagara, I., Yoshikawa, Y., Numata, N., Ando, T., Okabe, K., Sugiura, Y., Ieda, M., Takakura, N., Nakagawa, O., and Zhou, B., et al. (2017). Placental labyrinth formation in mice requires endothelial FLRT2/UNC5B signaling. Development (Cambridge, England) *144*, 2392-2401.

139. Tang, W.H.W., Bäckhed, F., Landmesser, U., and Hazen, S.L. (2019a). Intestinal Microbiota in Cardiovascular Health and Disease: JACC State-of-the-Art Review. Journal of the American College of Cardiology *73*, 2089-2105.

140. Tang, W.H.W., Kitai, T., and Hazen, S.L. (2017). Gut Microbiota in Cardiovascular Health and Disease. Circulation research *120*, 1183-1196.

141. Tang, W.H.W., Li, D.Y., and Hazen, S.L. (2019b). Dietary metabolism, the gut microbiome, and heart failure. Nature reviews. Cardiology *16*, 137-154.

142. Thillai, K., Lam, H., Sarker, D., and Wells, C.M. (2017). Deciphering the link between PI3K and PAK: An opportunity to target key pathways in pancreatic cancer? Oncotarget *8*, 14173-14191.

143. Tian, R. (2005). Another role for the celebrity: Akt and insulin resistance. Circulation research *96*, 139-140.

144. Tsuchiya, K., and Ogawa, Y. (2017). Forkhead box class O family member proteins: The biology and pathophysiological roles in diabetes. Journal of diabetes investigation *8*, 726-734.

145. Tzivion, G., Dobson, M., and Ramakrishnan, G. (2011). FoxO transcription factors; Regulation by AKT and 14-3-3 proteins. Biochimica et biophysica acta *1813*, 1938-1945.

146. Vezain, M., Lecuyer, M., Rubio, M., Dupé, V., Ratié, L., David, V., Pasquier, L., Odent, S., Coutant, S., and Tournier, I., et al. (2018). A de novo variant in ADGRL2 suggests a novel mechanism underlying the previously undescribed association of extreme microcephaly with severely reduced sulcation and rhombencephalosynapsis. Acta neuropathologica communications *6*, 109.

147. Wang, H., Lazarovici, P., and Zheng, W. (2016a). Forkhead Box Protein O. In Encyclopedia of Signaling Molecules, S. Choi, ed. (New York, NY: Springer New York), pp. 1–16.

148. Wang, Z., Yu, T., and Huang, P. (2016b). Post-translational modifications of FOXO family proteins (Review). Molecular medicine reports *14*, 4931-4941.

149. Webb, A.E., and Brunet, A. (2014). FOXO transcription factors: key regulators of cellular quality control. Trends in biochemical sciences *39*, 159-169.

150. Werner, N., Junk, S., Laufs, U., Link, A., Walenta, K., Bohm, M., and Nickenig, G. (2003). Intravenous transfusion of endothelial progenitor cells reduces neointima formation after vascular injury. Circulation research *93*, e17-24.

151. WHO. WHO. Cardiovascular Diseases (CVDs). 2021. Available online: https://www.who.int/news-room/fact-sheets/detail/cardiovascular-diseases-(cvds) (accessed in Mai 2023).

152. Wilhelm, K., Happel, K., Eelen, G., Schoors, S., Oellerich, M.F., Lim, R., Zimmermann, B., Aspalter, I.M., Franco, C.A., and Boettger, T., et al. (2016). FOXO1 couples metabolic activity and growth state in the vascular endothelium. Nature *529*, 216-220.

153. Witkowski, M., Weeks, T.L., and Hazen, S.L. (2020). Gut Microbiota and Cardiovascular Disease. Circulation research *127*, 553-570.

154. Witkowski, M., Witkowski, M., Friebel, J., Buffa, J.A., Li, X.S., Wang, Z., Sangwan, N., Li, L., DiDonato, J.A., and Tizian, C., et al. (2022). Vascular endothelial tissue factor contributes to trimethylamine N-oxide-enhanced arterial thrombosis. Cardiovascular research *118*, 2367-2384.

155. Xin, Z., Ma, Z., Jiang, S., Wang, D., Fan, C., Di, S., Hu, W., Li, T., She, J., and Yang, Y. (2017). FOXOs in the impaired heart: New therapeutic targets for cardiac diseases. Biochimica et biophysica acta. Molecular basis of disease *1863*, 486-498.

156. Xu, H., Wang, X., Feng, W., Liu, Q., Zhou, S., Liu, Q., and Cai, L. (2020). The gut microbiota and its interactions with cardiovascular disease. Microbial biotechnology *13*, 637-656.

157. Xu, S., Ilyas, I., Little, P.J., Li, H., Kamato, D., Zheng, X., Luo, S., Li, Z., Liu, P., and Han, J., et al. (2021). Endothelial Dysfunction in Atherosclerotic Cardiovascular Diseases and Beyond: From Mechanism to Pharmacotherapies. Pharmacological reviews *73*, 924-967.

158. Yan, D., Cai, Y., Luo, J., Liu, J., Li, X., Ying, F., Xie, X., Xu, A., Ma, X., and Xia, Z. (2020). FOXO1 contributes to diabetic cardiomyopathy via inducing imbalanced oxidative metabolism in type 1 diabetes. Journal of cellular and molecular medicine *24*, 7850-7861.

159. Yan, J., Pan, Y., Shao, W., Wang, C., Wang, R., He, Y., Zhang, M., Wang, Y., Li, T., and Wang, Z., et al. (2022). Beneficial effect of the short-chain fatty acid propionate on vascular calcification through intestinal microbiota remodelling. Microbiome *10*, 195.

160. Yang, K., and Dong, W. (2021). SIRT1-Related Signaling Pathways and Their Association With Bronchopulmonary Dysplasia. Frontiers in medicine *8*, 595634.

161. Yang, X., Zhang, X., Yang, W., Yu, H., He, Q., Xu, H., Li, S., Shang, Z.'a., Gao, X., and Wang, Y., et al. (2021). Gut Microbiota in Adipose Tissue Dysfunction Induced Cardiovascular Disease: Role as a Metabolic Organ. Frontiers in endocrinology *12*, 749125.

162. Ye, J., Li, L., Wang, M., Ma, Q., Tian, Y., Zhang, Q., Liu, J., Li, B., Zhang, B., and Liu, H., et al. (2022). Diabetes Mellitus Promotes the Development of Atherosclerosis: The Role of NLRP3. Frontiers in immunology *13*, 900254.

163. Yin, G.N., Kim, D.-K., Kang, J.I., Im, Y., Lee, D.S., Han, A.-R., Ock, J., Choi, M.-J., Kwon, M.-H., and Limanjaya, A., et al. (2022). Latrophilin-2 is a novel receptor of LRG1 that rescues vascular and neurological abnormalities and restores diabetic erectile function. Experimental & molecular medicine *54*, 626-638.

164. Yoshioka, K., Yoshida, K., Cui, H., Wakayama, T., Takuwa, N., Okamoto, Y., Du, W., Qi, X., Asanuma, K., and Sugihara, K., et al. (2012). Endothelial PI3K-C2α, a class II PI3K, has an essential role in angiogenesis and vascular barrier function. Nature medicine *18*, 1560-1569.

165. Yu, W., Chen, C., and Cheng, J. (2020). The role and molecular mechanism of FoxO1 in mediating cardiac hypertrophy. ESC heart failure *7*, 3497-3504.

166. Zhang, N., Wang, Z., Lv, J., Zhang, S., Liu, Y., Liu, T., Li, W., Gong, L., Zhang, X., and El-Omar, E.M., et al. (2022a). Characterization of Gut Microbiota and Exploration of Potential Predictive Model for Hepatocellular Carcinoma Microvascular Invasion. Frontiers in medicine *9*, 836369.

167. Zhang, P. (2022). Influence of Foods and Nutrition on the Gut Microbiome and Implications for Intestinal Health. International journal of molecular sciences *23*.

168. Zhang, Q., Liu, H., and Yang, J. (2019). Regulation of TGF-β1 on PI3KC3 and its role in hypertension-induced vascular injuries. Experimental and therapeutic medicine *17*, 1717-1727.

169. Zhang, S., Liu, Y., Cao, Y., Zhang, S., Sun, J., Wang, Y., Song, S., and Zhang, H. (2022b). Targeting the Microenvironment of Vulnerable Atherosclerotic Plaques: An Emerging Diagnosis and Therapy Strategy for Atherosclerosis. Advanced materials (Deerfield Beach, Fla.) *34*, e2110660.

170. Zhao, Y., Wang, Y., and Zhu, W.-G. (2011). Applications of post-translational modifications of FoxO family proteins in biological functions. Journal of molecular cell biology *3*, 276-282.

171. Zheng, D., Liwinski, T., and Elinav, E. (2020). Interaction between microbiota and immunity in health and disease. Cell research *30*, 492-506.

172. Zheng, X., and Cartee, G.D. (2016). Insulin-induced Effects on the Subcellular Localization of AKT1, AKT2 and AS160 in Rat Skeletal Muscle. Scientific reports *6*, 39230.

173. Zimmermann, F., Roessler, J., Schmidt, D., Jasina, A., Schumann, P., Gast, M., Poller, W., Leistner, D., Giral, H., and Kränkel, N., et al. (2020). Impact of the Gut Microbiota on Atorvastatin Mediated Effects on Blood Lipids. Journal of clinical medicine *9*.

10. Acknowledgment

Foremost, I would like to express my sincere thanks of gratitude to PD Dr. Arash Haghikia, who gave me the opportunity to work on this grateful research topic, “The impact of gut microbial imidazole propionate on endothelial regeneration and the development of atherosclerosis”, here at the Department of Cardiology, Angiology and Intensive Care Medicine in Deutsches Herzzentrum der Charité (DHZC). I am grateful for his patience, motivation, and guidance during my doctoral study. Furthermore, I would like to express my special thanks to Prof. Dr. Petra Knaus for her constant support, encouragement and valuable suggestions that have enriched my understanding and improved the quality of my work. Working under both supervisors has exposed me to a wide range of expertise and knowledge in molecular biology and medical cardiology. This experience has enabled me to work confidently on various exciting projects. I would also like to extend my sincere gratitude to Prof. Dr. med. Landmesser, the clinic director of the Medical Clinic for Cardiology at Charité-Campus Benjamin-Franklin, for giving me the opportunity to do my doctorate and research at the Charité Universitätsmedizin Berlin. My appreciation also extends to my collaborators in Sweden (Department of Molecular and Clinical Medicine at the University of Gothenburg) and Amsterdam (Department of Experimental Vascular Medicine at the University Medical Centers) as well as the doctoral students in our lab for technical support, helpful discussions, and contributions to an exceptional working atmosphere.

Lastly, I would like to express my heartfelt gratitude to *my beloved family*, especially my dear mother (அம்மா) and sisters, who have been the biggest source of strength throughout my academic career. I am deeply grateful for their blessing, unconditional love, and belief in my potential, which has helped me overcome challenges, strive for success, and reach this stage in my life. Of course, I would also like to thank my adorable nieces, who bring me great joy and fulfillment. Their innocent smiles, laughter, and pure presence have enriched my journey and reminded me of the beauty and preciousness of life. I am truly blessed to have them by my side.

Thank you!

11. Publications

1) **Nageswaran, V***., Carreras, A., Reinshagen, L., Beck, K., Steinfeldt, J., Ståhlman, M., Raemzani Rad, P., Strässler, E.T., Verhaar, B., Döring, Y., Weber, C., König, M., Steinhagen-Thiessen, E., Demuth, I., Kränkel, N., Leistner, D. M., Nieuwdrop, M., Knaus, P., Ferrell, M., Hazen, S. L., Landmesser, U., Bäckhed, F., Haghikia, A. (2024). Gut microbial metabolite imidazole propionate impairs endothelial cell function and promotes the development of atherosclerosis (*submitted*).

2) Reinshagen, L.*, **Nageswaran, V***., Heidecke, H., Schulze-Forster, K., Wilde, A. B., Ramezani Rad, P., Poller, W., Asmus, E., Simmons, S., Kuebler, W. M., Witzenrath, M., Markó, L., Jakobs, K., Puccini, M., Leistner, D. M., Rauch-Kröhnert, U., Kränkel, N., Forslund, S. K., Landmesser, U., Müller, D. N., … Haghikia, A. (2023). Protease-Activated Receptor-1 IgG Autoantibodies in Patients with COVID-19. Thrombosis and haemostasis, 10.1055/a-2205-0014. Advance online publication. https://doi.org/10.1055/a-2205-0014. (***equally contributed as first authors**).

3) Verhaar, B. J. H, Wijdeveld, M., Wortelboer, K., Rampanelli, E., Levels J. H. M., Collard, D., Cammenga, M., **Nageswaran, V**., Haghikia, A., Landmesser, U., Li, X. S., DiDonato, J. A., Hazen, S. L., Garrelds, I. M., Danser, A. H. J., van den Born, B. H., Nieuwdrop, M., Muller, M. (2023). Oral sodium butyrate increases daytime systolic blood pressure in hypertensive patients: a randomized, placebo-controlled trial (*in submission*).

4) Haghikia, A., Zimmermann, F., Schumann, P., Jasina, A., Roessler, J., Schmidt, D., Heinze, P., Kaisler, J., **Nageswaran, V**., Aigner, A., Ceglarek, U., Cineus, R., Hegazy, A. N., van der Vorst, E. P. C., Döring, Y., Strauch, C. M., Nemet, I., Tremaroli, V., Dwibedi, C., Kränkel, N., … Landmesser, U. (2022). Propionate attenuates atherosclerosis by immune-dependent regulation of intestinal cholesterol metabolism. European heart journal, 43(6), 518–533. https://doi.org/10.1093/eurheartj/ehab644.

5) Mendez, P. L., Obendorf, L., Jatzlau, J., Burdzinski, W., Reichenbach, M., **Nageswaran, V**., Haghikia, A., Stangl, V., Hiepen, C., & Knaus, P. (2022). Atheroprone fluid shear stress-regulated ALK1-Endoglin-SMAD signaling originates from early endosomes. BMC biology, 20(1), 210. https://doi.org/10.1186/s12915-022-01396-y.

6) Gast, M.*, **Nageswaran, V.***, Kuss, A. W., Tzvetkova, A., Wang, X., Mochmann, L. H., Rad, P. R., Weiss, S., Simm, S., Zeller, T., Voelzke, H., Hoffmann, W., Völker, U., Felix, S. B., Dörr, M., Beling, A., Skurk, C., Leistner, D. M., Rauch, B. H., Hirose, T., … Poller, W. (2022). tRNA-like Transcripts from the NEAT1-MALAT1 Genomic Region Critically Influence Human Innate Immunity and Macrophage Functions. Cells, 11(24), 3970. https://doi.org/10.3390/cells11243970. (***equally contributed as first authors**).

7) Renikunta, H.V., Lazarow, K., Chandra Shukla, P., **Nageswaran, V.**, Giral, H., Kratzer, A., Opitz, L., Engel, F.B., Haghikia, A., Constantino, S., Paneni, F., von Kries, J.P., Streckfuss-Bömeke, K., Landmesser, U., Jakob, P. (2023). Large-scale microRNA functional high-throughput screening identifies miR-515-3p and miR-519e-3p as inducers of human cardiomyocyte proliferation. iScience, 26(5), 106593. https://doi.org/10.1016/j.isci.2023.106593.

8) Liberale, L., Akhmedov, A., Vlachogiannis, N. I., Bonetti, N. R., **Nageswaran, V**., Miranda, M. X., Puspitasari, Y. M., Schwarz, L., Costantino, S., Paneni, F., Beer, J. H., Ruschitzka, F., Montecucco, F., Lüscher, T. F., Stamatelopoulos, K., Stellos, K., & Camici, G. G. (2021). Sirtuin 5 promotes arterial thrombosis by blunting the fibrinolytic system. Cardiovascular research, 117(10), 2275–2288. https://doi.org/10.1093/cvr/cvaa268.

9) Liberale, L., Gaul, D. S., Akhmedov, A., Bonetti, N. R., **Nageswaran, V**., Costantino, S., Pahla, J., Weber, J., Fehr, V., Vdovenko, D., Semerano, A., Giacalone, G., Kullak-Ublick, G. A., Sessa, M., Eriksson, U., Paneni, F., Ruschitzka, F., Montecucco, F., Beer, J. H., Lüscher, T. F., … Camici, G. G. (2020). Endothelial SIRT6 blunts stroke size and neurological deficit by preserving blood-brain barrier integrity: a translational study. European heart journal, 41(16), 1575–1587. https://doi.org/10.1093/eurheartj/ehz712.

Poster presentations at congresses:

- 89th German Cardiac Society (DGK) – Annual Meeting, 12.-15.04.2023 in Mannheim, Germany. Microbial Imidazole propionate mediates pro-inflammatory effects in endothelial cells and promotes atherosclerosis in mice. Inter-organ cross-talk in CV disease session. (*Nominated for DGK-Poster price)* (Nageswaran et al., 2023).

- 5th German Centre for Cardiovascular Research (DZHK) Partner Site Retreat, 14.12.2022 in Berlin, Germany. *Young-DZHK poster session.*

- DGK Heart Days, 29.09-01.10.2022 in Bonn, Germany. Imidazole propionate impairs endothelial cell function and vascular repair after injury: Implication for coronary heart disease. Vascular pathophysiology session (Nageswaran et al., 2022a).

- 88th German Cardiac Society (DGK) – Annual Meeting, 20.-23.04.2022 in Mannheim, Germany. The gut microbiota-derived metabolite imidazole propionate affects endothelial cell physiology and vascular regeneration after arterial injury. Endothelial cell biology session (Nageswaran et al., 2022b).